TRANSPORT OF ADSORBING METAL IONS BETWEEN STREAM WATER AND SEDIMENT BED IN A LABORATORY FLUME

Thesis by

Hinrich Eylers

In Partial Fulfillment of the Requirements

for the Degree of

Doctor of Philosophy

California Institute of Technology

Pasadena, California

1994

(submitted April 7, 1994)

Disclaimer

This material is based upon work supported by the National Science Foundation under Grant No. BCS-9105965. The Government has certain rights in this material.

Any opinions, findings, and conclusions or recommendations expressed in this publication are those of the author and do not necessarily reflect the views of the National Science Foundation.

ACKNOWLEDGMENTS

Many people – professors, staff, and students alike – made my stay at Caltech an enjoyable and educative experience.

Many thanks to Norman Brooks, my advisor, and Jim Morgan, my co-advisor, for always being available and providing guidance and valuable feedback. Our discussions always lead to new ways to define, approach and solve problems. Thanks also to Bob Koh for helpful discussions and to John List, Mike Hoffmann and Chris Brennen for serving on my examination committees.

The secretaries, Fran, Jennifer, and Linda, as well as the librarians, Rayma, Susan, and Gunilla, were always willing to provide help, assistance and cheer. Very little could be accomplished in the hydraulics laboratory without the assistance of Joe, Rich, and Hai.

My fellow students were always fun to be with; they were also always willing to discuss problems and help out taking samples late at night. Thanks (in no particular order) Aaron, Selena, Susan, Mike, Nicola, Bruce, Kelly, Edye, Matt, Jeremy, Ralf, Tom, Ron, Axel, Amy, Catherine, Inez, Jerry, Talal, and all the others (I can't name you all ..)!

The financial support for this research was provided by the National Science Foundation under grant number BCS-9105965. Most of the analytical work necessary in my research would have be impossible without the ICP-MS in the Environmental Analysis Center. I am thankful to Peter Green for teaching me the use of this instrument and for being available whenever problems appeared (and being my carpool partner).

My wife Merrie Anne, our furry 'children' Thomas, Tessa and Baby, and my family – both in Germany and in the United States – have been my main pillar of support through the sometimes stressful years at Caltech. This thesis is dedicated to them – the people I love.

ABSTRACT

The transport of adsorbing metal ions (copper, zinc, calcium and magnesium) between the water column and the sand bed in a 5 meter long recirculating laboratory flume with bottom bedforms has been investigated. A non-adsorbing tracer, lithium, was used simultaneously to observe the exchange of water between bed and water column. The presence of bedforms and associated pumping increases the exchange rate by several orders of magnitude over molecular processes.

The concentrations of initially added metal ions were monitored both in the circulating overlying water and in the pore-water of the sediment bed. The sand used for the bed was composed of over 99% silica, with geometric means of 500 μm and 195 μm. Before each run, the sand was acid-washed at pH 3.5 to provide reproducible experimental conditions. The chemical composition of the recirculating water was controlled and steady flow conditions were maintained in the experiments.

Batch experiments were performed to investigate the chemical partitioning of the selected metal ions to the sand grain surfaces. The adsorption of zinc onto silica was modeled in detail and binding constants were determined. The observed adsorption of the metal ions in the flume experiments compared well with batch adsorption data.

The transfer of metal ions into and out of a bed covered with stationary bedforms is dominated by advective pumping caused by pressure fluctuations over the bed. A residence-time model based on pressure-driven advective flow and linear equilibrium partitioning of the pollutant to the sediment was developed and describes the observed metal ion exchange between sediment and water column well. Increased partitioning of

the metal ion onto the sediment leads to an increase of the amount of tracer stored within the sediment bed. Furthermore, the concentrations of metal ions released from the bed after passing of an initial pulse in the overlying water will be lower, but longer lasting for stronger partitioning, leading to tailing in the water column for long times.

For a bed with moving bedforms, the main mechanism for mass exchange is the trapping and release of overlying water by the traveling bedform. The transport of metal ions can be approximately described for the initial phase of the experiment, but large deviations from the model occur for long times.

The models do not require calibration since the parameters for transport into and out of the bed can be derived from flow conditions, sediment parameters, bedform dimensions and adsorption characteristics of the tracer on the sand. Criteria for the applicability of the models and appropriate scaling variables are identified. The experimental results are presented in nondimensional form.

CONTENTS

LIST OF TABLES

LIST OF FIGURES

NOTATION

A	area
A_s	specific surface area of sediment (dimension area/mass)
C_d	capacitance of double layer
C	solute concentration in overlying water column (dimension mass/volume)
C^*	normalized solute concentration (C/C_0)
C_0	initial solute concentration
d	mean water depth
d'	effective water depth in closed system (total water volume/bed area)
d^*	normalized water depth (kd')
d_g	geometric mean grain diameter
F	Faraday's constant
f	Darcy-Weisbach friction factor ($8grh_s/U^2$)
f_a	fraction of sorbent adsorbed to the surface
f_b	bed friction factor
g	acceleration of gravity
H	mean bedform height (crest to trough)
h	dynamic pressure head (dimension length)
h_m	amplitude of dynamic pressure head at bed surface
I	ionic strength of solution
K	coefficient of permeability (dimension velocity)

K	chemical equilibrium constant
k	bedform wavenumber ($2\pi/\lambda$)
k_p	partitioning (or distribution) coefficient (dimension volume/mass)
ℓ	volume unit 'liter'
L	length
m	accumulated mass transfer function (dimension length)
m^*	normalized accumulated mass transfer function (km)
M^*	approximated mass transfer function (m^*/C^*)
m_t	total mass of sediment
q	flow into sediment bed (flux of pollutant into bed divided by pollutant concentration in solution, dimension velocity)
q^*	normalized flow into sediment bed (q/u_m)
$\bar{q}$	spatially averaged flow into sediment bed (dimension velocity)
$\bar{q}^*$	normalized, spatially averaged flow into sediment bed ($\bar{q}/u_m$)
R	retardation coefficient
R_f	residence time function
$\bar{R}_f$	flux-averaged residence time function
Re	flow Reynolds number ($4Ur_h/\nu$)
r_h	hydraulic radius of flow ($(d \cdot w)/(2 \cdot d + w)$)
s	slope of water surface ≈ energy slope (uniform flow)
t	time
t^*	normalized time (k^2Kh_mt)
τ^*	normalized relative time

t_{ads}	adsorption time scale
t_p	pumping time scale ($t^*=1$)
t_t	turnover time scale (λ/u_b)
U	mean flow velocity in channel
u	pore-water Darcy velocity
u*	normalized pore-water Darcy velocity (u/u_m)
u^*_b	normalized bedform velocity ($\theta u_b/u_m$)
$u^*_{b,R}$	normalized partitioning-dependent bedform velocity ($R\theta u_b/u_m$)
u^*_u	normalized underflow velocity (u_u/u_m)
$u^*_{u,b}$	normalized modified underflow velocity for moving bedforms ($(u_u-\theta R u_b)/u_m$)
u_b	bedform velocity
u_m	pore-water scaling velocity (kKh_m)
u_u	pore-water underflow velocity due to hydraulic gradient
V	volume
V_t	total volume of solution
w	flume width (15.24 cm)
x*	normalized x coordinate (kx)
y*	normalized y coordinate (ky)
α	correction factor for group 'Kh_m' = (fitted Kh_m)/(calculated Kh_m)
ν	kinematic viscosity
λ	bedform wavelength
θ	porosity
σ	charge density on the double layer

Ψ_0	potential of the double layer
σ_g	geometric standard deviation of grain diameter
Σ	surface adsorption density (dimension moles/area)
Γ_p	nondimensional number for determination of equilibrium in pumping model
Γ_t	nondimensional number for determination of equilibrium in turnover model
$\equiv$	denotes surface group ($\equiv$SiOH)
τ	relative time ($t-t_0$)

1. INTRODUCTION

The transfer of pollutants between river water and the underlying sediment bed has important implications for the ultimate fate of these pollutants in an aqueous environment. Contaminants in the water column can be transported into the sediment bed of a stream or river, which becomes an important sink for contaminants. At a later time, the contaminants can eventually be again released to the water column. A large fraction of the total mass of pollutants can be captured within the sediment bed (i.e., taken out of the flowing overlying water), or released back to the stream from the bed. In the case of a short-term spill of a chemical, this effect can lead to an apparent 'tailing' of the observed concentration in the stream water as the chemical is still released from the stream bed after the initial spill has already passed by. This results in a relatively longer-lasting, low level pollution of the water that could not be expected if only dispersion and diffusion in the overlying water were considered. If a pollutant is present in the overlying water for a long time, the sediment can be subject to contamination down to large depths within the bed.

Many processes can contribute to the fate of solutes in a natural stream: flow of solutes into and out of the bed or the banks of the stream, adsorption onto particulates and subsequent deposition, chemical conversions, uptake or degradation by biological processes, and evaporation. The exchange of solutes between stream water and the stream bed has previously been modeled by box models that divide the bed of the stream into one or more layers. Appropriate exchange coefficients for the transfer of solutes between these layers and the water column were determined by fitting of field data.

Two processes were investigated to model the observed stream water/bed exchange of metal ions: in the case of stationary bedforms, pressure variations over the sediment bed induce flow of water into and out of the bed, a process referred to as "pumping." If the bedforms are moving downstream, pore-water pumping still occurs, but an additional process is active: interstitial water is released at the upstream side of a dune, and overlying water is trapped at the downstream side. This latter process is referred to as "turnover." The relative importance of these two processes depends on many parameters: flow velocity of the stream water, propagation velocity of the bedforms, hydraulic permeability of the bed sediment, bedform dimensions, and partitioning of the pollutant. In general, pumping is most important in streams with smaller, slow moving, relatively permeable stream beds. Turnover is dominant for large, fast moving dunes and/or less permeable beds.

The influence of bottom sediment forms on the interfacial exchange of pollutants is investigated here. Bedforms are wave-like variations of the surface of the sediment bed in a stream. They are caused by deposition and movement of sediment particles due to the flow of water in the stream channel. Depending on the flow velocity of the stream water and the characteristics of the sediment, bedforms can be stationary (after being created by previous higher flows) or moving downstream. Bedforms can be very small (length about 10 cm) or very large (lengths of about 100 m as reported in large rivers). Smaller bedforms with wavelengths of less than about 30 cm are usually called ripples, larger bedforms are called dunes (ASCE, 1975). The influence of other bed features like bars (large bedforms with length comparable to channel width, height comparable to flow depth), antidunes (wavy bed profile in phase with wavy water surface near critical flow conditions), or flat beds were not investigated in this work.

The purpose of the work presented in this thesis is to combine the physical understanding of the hydraulic and chemical processes that control the exchange of metal ions between stream water and a sediment bed covered with bedforms and, based on the actual processes, develop an exchange model that can be integrated into larger river system models. Such a model then relates the actual exchange mechanisms and surface adsorption to the net interfacial exchange of solutes. Because the parameters in this model can be derived from the known physical and chemical conditions in the problem, the need for calibration of the model in each individual application is eliminated. Nondimensional presentation of the data allows the application of the results to larger systems like streams and rivers. Furthermore, nondimensional presentation also makes it possible to apply the results to similar systems in coastal and deep oceans and in the atmosphere. Examples are the surface exchange of solutes into rippled permeable marine sediments driven by ocean currents or wave action, and the advection of air through the surface of snowfields or glaciers. The models developed in this thesis require that the bed does not change significantly over the period of the simulation; episodic events like the changes in composition and topography of the river bottom during a flood cannot be modeled in this manner. Thus, a spill of chemicals lasting a few hours or days can be simulated by the models developed in this thesis, but it is very difficult to describe ongoing pollution of the riverbed over many years using these models because of possible major changes in discharge, bedforms, and dependence on complete past history.

The possible influence of chemical kinetics on the interfacial exchange of solutes was investigated, and appropriate scaling parameters for the determination of kinetic equilibrium are given.

Both adsorbing and non-adsorbing metal ions were used in the experiments performed in this study. Concentration measurements of metal ions in the experiments are presented as the aqueous concentrations of the solutes in the water column or pore-water. The simultaneous use of a non-adsorbing metal ion allows the observation of the exchange of water between the pores of the sediment on the overlying solution to determine the hydraulic conditions existing in the experiment. Then, the influence of surface adsorption on the mass exchange of adsorbing metal ions can be studied by comparing the concentration time history of the adsorbing metal ions to that for the nonadsorbing ion.

Flume experiments were performed under simplified, well-controlled conditions in a 5 m long recirculating flume. Recirculation of the flume water from the downstream end to the upstream end of the flume avoids longitudinal concentration gradients in the overlying water. The recirculating water is well mixed at all times except during the initial few minutes after the start of an experiment. Because the solution in the flume is recirculated, small fluxes of solute into or out of the bed will lead to a measurable change of metal ion concentration in the overlying water as it passes the bed many times. Thus, the measurement of the net flux between water column and sediment is much more precise in a recirculating flume than a one-pass flume. Furthermore, there are only small losses of water during a run (which are made up), so that experiments can be performed over a long period of time without a constant new supply of water, solutes and sand. The flow in the overlying water column was always fully turbulent (Reynolds numbers larger than 10,000), but Darcy flow existed in the pore space of the sediment bed. The Peclet numbers for the flow of solution in the pore space are of the order of one or less.

The chemical composition of the flume water was controlled during the runs. Silica sands with well-defined surface adsorption groups were used to allow chemical

modeling of the adsorption processes. Uniform silica sand was used in the experiments, but mixtures of sediment or coated sediments were not investigated in this work. Thus, the entire physical and chemical composition of the experimental system could be controlled. However, the results obtained in this work can be directly applied to more complicated systems if the controlling parameters and processes in those systems are determined.

Naturally and artificially formed bedforms were used in this study. Artificially formed dunes were relatively uniform in height and length, whereas naturally formed dunes showed a much larger variation in both height and length. Experiments were performed for both stationary and moving bedforms.

For field applications, for example a chemical spill in a stream, it is desirable to make predictions of the partitioning that can be expected in the river sediment without having to conduct a complete flume experiment to simulate the spill. Therefore, small-scale laboratory experiments investigating the partitioning of the pollutant and sand were also performed and the data compared to adsorption values observed in the sediment bed of the flume.

Previous field work and modeling results by various authors investigating the interfacial exchange of solutes is reviewed in Chapter 2. Also surveyed is the literature describing the adsorption of metal ions onto solid surfaces.

In Chapter 3, the underlying principles of interfacial stream water exchange are presented. The stream water exchange models used in this thesis are developed and the chemical modeling of surface adsorption onto silica is discussed.

The experimental apparatus and the methods used in conducting the flume and batch experiments are described in Chapter 4.

The results from the batch adsorption experiments and the flume runs, as well as the experimental parameters for the flume runs, are presented in Chapter 5.

A summary of the experiments and a discussion of the results is presented in Chapter 6 of this thesis. Also discussed is the relevance of the studies to natural stream systems. Conclusions are given and possible future studies are discussed.

In the appendices, data for the titration experiments, sample data for the flume runs, and the tabulated nondimensional residence time function are given.

2. LITERATURE

2.1. EXCHANGE PROCESSES AT THE SEDIMENT-WATER INTERFACE

2.1.1. Compartment models

The problem of transport at the sediment-water boundary in a turbulent flow of water has been a subject of interest to many authors. Various models have been developed to describe the observed transport rate. The simplest of such models describe the sediment bed of a stream as a compartment, and the rate of pollutant exchange between bed and stream water is then described by an exchange coefficient multiplied by a concentration difference.

Onishi (1981) describes the FETRA model for the transport of sorptive substances in streams. This model includes terms for the adsorption of contaminants to suspended sediments and to the bed surface, but does not provide for a water/bed exchange mechanism. The model is expanded to include more than one type of sediment.

O'Connor et al. (1983) developed a model that allowed for the transport of pollutants both in aqueous solution and adsorbed to suspended sediments. They used two sediment bed compartments, an active transport layer and a deeper stationary bed. The exchange of pollutants and sediment between the two layers is described as a vertical mixing process. Instant equilibrium is assumed between all dissolved and adsorbed phases.

Bencala (1984) developed a similar model that describes the transport of tracers in a gravel bed river. The model has terms for storage in storage zones and sorption of tracers to the sediment bottom of the stream. The exchange rates are determined by

multiplying rate coefficients with the difference between measured and equilibrium concentrations,

$$R = \lambda_s (C_s - C_s^*) \tag{2.1}$$

where λ_s is a rate coefficient and C_s-C_s^* is the difference between actual and equilibrium sediment adsorption.

Basmadjian and Quan (1987) modeled the adsorption/desorption rate of pollutant between the overlying water similarly. They also include sorption kinetics and extend this model for transport, deposition and resuspension of sediments. Analytical solutions to the differential equations are given.

Richardson and Parr (1988) described the release of solute from interstitial water in a laboratory flume with glass bead bed by a Fickian diffusion process. An empirical relationship between the diffusion coefficient and the shear Peclet number is given, but no physical mechanism is proposed.

Three models for pollutant transport in rivers are supported by the EPA Center for Water Quality Modeling: EXAMS (Burns 1982), TOXIWASP (Ambrose 1983), and HSPF (Donigan 1978, Donigan 1976 and Onishi 1982). These models are compartment models and thus require calibration. Schnoor (1987) discussed and compared these models and their applicability, showed sample runs and also gave a number of chemical reaction rates and coefficients.

2.1.2. Pore-water advection – field observations

The advection of interstitial fluid (water or air) has been observed in river beds, ocean beds and snow dunes.

Webb and Theodor (1972) measured dye transported through sea-bed sand due to pumping induced by wave action. They observed a correlation between the pore-water velocity and the wave height.

Grimm and Fisher (1984) observed interstitial-surface water exchange by dye injection in a shallow creek. They recorded distance of travel and travel time of the dye injected into the stream bed, but did not describe the stream bed topography.

Clarke and Waddington (1991) investigated wind pumping of air through permeable snow surfaces on glaciers and developed a three-dimensional model of the penetration of pressure fluctuation into the snow.

2.1.3. Pore-water advection – laboratory experiments

The simulation of pore-water advection induced by pressure variations over the surface gives rise to a better physical understanding of the transfer of solute, allowing more descriptive modeling of the transport processes.

Savant et al. (1987) observed the flow of interstitial water in a flume with sand bed using dye injected into the bed through injection ports. A pore-water flow model based on pressure measurements over bedforms by Vittal (1977) described the observed pore-water trajectories well.

Shen et al. (1990) separately measured skin -, form - and total resistance of flow over rigid triangular bedforms. The pressure distribution over the bedform was measured using a Preston tube with 2 mm diameter. A formula is given to compute the pressure drag coefficient from bedform height and water depth. Fehlman's thesis (1985) is part of this work.

Nagaoka and Ohgaki (1990) investigated the mass transfer mechanism in experimental channels with flat porous beds composed of large (2 and 4 cm diameter) ceramic balls. They determine turbulent diffusion as the driving mechanism of mass exchange between bed and water column and large-scale eddies in the deeper regions of the bed.

Elliott (1990) performed extensive flume experiments and developed a contaminant exchange model for non-adsorbing tracers. This model incorporates the pore-water advection process by calculating the average flux into the sediment bed and utilizes a residence time approach. His model, which is the starting point for this work, is explained in Chapter 3.

2.2. ADSORPTION OF METAL IONS

Good discussions of basic surface complexation models can be found in Stumm and Morgan (1981), Stumm (1987) , Dzombak and Morel (1987) and Honeyman and Santschi (1988). A vast amount of literature exists covering the equilibrium adsorption of metal ions onto various materials. This nonwithstanding, relatively few researchers have studied metal ion adsorption onto silica. Other "pure" sorbates (iron oxides, aluminum oxides) have been subject of more thorough investigation. Dzombak and Morel (1990)

presented a thorough and critical compilation of metal ion adsorption onto hydrous ferric oxide.

2.2.1. Adsorption of metal ions onto natural sediments

Reece et al. (1978) studied the concentration of heavy metals on polluted river sediments and found high concentrations of cadmium, lead, manganese and zinc. They performed leaching of the metal ions from the sediments at different pH values and observed equilibrium concentrations and equilibration times.

Shukla and Mittal (1979) conducted experiments to measure zinc adsorption in soil samples. They observed dependence of the zinc adsorption on the soil type and successfully fitted Langmuir and Freundlich isotherms to the measured data.

Smith et al. (1989) observed and modeled copper, cadmium and zinc partitioning on sediments from a small mountain stream. They observed good agreement between model sorption predictions and experimental partitioning data. The existence of a significant organic carbon fraction did not appear to have influence on the adsorption of zinc and copper.

Msaky and Cavet (1990) measured the adsorption of copper and zinc in three different soils. There observed a pH-dependence of both shape of the adsorption isotherm and adsorbed amount. The initial adsorption time in the soil samples appeared to be less than an hour (90% after 20-30 minutes), but the remainder of the adsorbing fraction appeared to be tailing over a period of hours.

2.2.2. Adsorption of metal ions onto silica

Dugger et al. (1964) studied the adsorption of twenty metal ions onto silica gel. They observed a correlation between the free energy of the surface adsorption process and the hydrolysis constants of a metal ion.

Schindler et al. (1976) investigated the surface complex formation of iron(III), copper, cadmium and lead adsorbed to silica gel. The metal ions adsorbed to the silica gel in the order Cd < Cu < Pb < Fe. A strong correlation was observed between the hydrolysis constants and the surface adsorption constants for these metal ions.

Young (1981) studied the adsorption of nickel onto silica gel (12 nm diameter particles with 200 m^2/g surface area). He included outer-sphere adsorption of the background electrolyte in his model. Young observed that the adsorption of nickel was not limited by the availability of surface silanol groups, there appeared to be no upper bound to nickel adsorption because of surface precipitation.

2.2.3. Adsorption kinetics

Most researchers have chosen to describe the partitioning of pollutant and sediment as an equilibrium process, but the validity of this approach is also discussed in the literature.

The actual surface binding, as investigated in pressure jump experiments, appears to be relatively fast with a time scale of less than a second, but the time scale for surface adsorption from bulk solution appears to be dominated by diffusion of the pollutants through the interstitial medium and into the pores of the sediment. Thus, the apparent

time scale for the equilibration of a system appears to depend strongly on the micro-porosity of the sediment and ranges from minutes on larger particles like sand to days in fine aquifer soil.

Mikami et al. (1983) performed pressure-jump experiments to investigate the kinetics of uranyl ion adsorption onto aluminum oxide. The adsorption time scale was found to be of the order of 100 ms.

James and Rubin (1979) conducted column experiments with calcium and various soils at different flow rates. Their data suggests that the equilibrium adsorption assumption only applies when the ratio of the hydrodynamic dispersion coefficient to the molecular diffusion coefficient is smaller or equal unity.

Goltz and Roberts (1986) model the subsurface transport of organic solutes in field experiments. Extended tailing of the breakthrough curves was observed for both sorbing and nonsorbing solutes and is explained by diffusion of the solutes into and out of zones of immobile water and fine pores and cracks in the sediment. Chemical adsorption equilibrium is assumed in the model.

Fuller and Davis (1987) characterized the adsorption of cadmium onto calcareous aquifer sand by two reaction steps. In the first step, the ion adsorbs to the surface and diffuses into the particles. This step appears to be completed in less than 24 hours, with a very rapid initial adsorption process. In the second step, continuing for days, surface co-precipitation occurs and a solid solution of $CdCO_3$ in $CaCO_3$ forms.

2.3. TRANSPORT OF ADSORBING POLLUTANTS IN AQUEOUS SYSTEMS

Kudo and Gloyna (1971) studied the uptake and release of ^{137}Cs in flumes 61 m and 17 m long. Natural lake sediment was used in these experiments. At higher flow rates, significant sediment transport and increased ^{137}Cs uptake were observed. Desorption experiments were performed by treating the bed with ^{137}Cs before the run. Very low desorption rates were observed. In this study, no information is given about sediment properties and possible bed forms.

Jackman et al. (1984) observed the transport of a number of metal ions in a small cobble bed stream, modeling the bed-stream exchange by diffusion processes. The model includes an underflow channel and partitioning for adsorbing species. The stream was divided into segments and a large number of parameters were then fitted for every reach.

Bencala (1984) uses a model incorporating one-dimensional transport, dead zone storage, first-order mass transfer into the bed and linear partitioning of sorbants. This model also requires fitting of a number of parameters in every reach.

Kuwabara et al. (1984) also used a one-dimension advection-dispersion model to describe chlorine and copper transport in a mountain stream. They included a kinetic submodel for sediment uptake of copper. Again, most parameters in the model required fitting.

Bencala (1993) and Harvey and Bencala (1993) investigated the recharging flow of streamwater into and out of the surrounding alluvium beneath and under the stream channel. Measurements of the flux of water from the subsurface to the stream by tracer injection lead to the conclusion that localized stream-subsurface water exchange does significantly influence solute transport in the stream.

A number of solute exchange models describing the exchange of pollutants at the sediment-water boundary have been developed in previous studies. Exchange parameters for those models were usually obtained by calibration to specific natural streams or flumes and were thus not transferable to other systems. Only recently, the pressure-driven flow field within a rippled sediment bed has been modeled. The models for solute exchange with adsorption presented in this thesis are based on the actual exchange mechanisms occurring in the sediment bed and at the interface and do not require calibration of parameters. Thus, these processes can be modeled for streams or rivers of various sizes.

3. THEORY

3.1. INTRODUCTION TO MODELING STREAMBED CONTAMINANT EXCHANGE

To be able to develop a model that describes the physical processes leading to the exchange of chemically reactive tracers between the overlying water column and the sediment bed of a stream, both the hydraulic and the chemical processes involved must be incorporated.

Observations of mass exchange between water column and stream beds in natural rivers have mostly been described by introducing one or more subsurface compartments (see Chapter 2). The contaminant exchange between compartment(s) and overlying water was then modeled by diffusive processes and the required physical parameters were usually fitted.

Alexander Elliott (1990) developed models that describe the exchange of conservative tracers between a stream bed covered with bed forms and the overlying water. In the case of stationary bedforms, the model is based on the advection of solute through the sediment bed due to pressure variations over the bed surface. These pressure variations are caused by the disturbance of the shear flow above the bed by the bedforms. If the bedforms are moving, the model describes how solution from the overlying water column is being covered up by the downstream front of a migrating bedform and released after the bedform has passed by. Because Elliott's models describe the actual physical processes taking place in the water/bed system, fitting of the parameters is not necessary. Figure 3.1 shows the underlying principles of modeling streambed exchange processes.

On the basis of Elliott's work, a model was developed to predict the exchange of adsorbing tracers between the sediment bed and overlying water. This model incorpo-

rates partitioning of the adsorbing tracers onto the sediment in the stream bed by making use of the retardation concept. The partitioning of the pollutant to the sediment, measured in separate batch experiments, can be used in combination with a pore-water advection model to describe the observed pollutant exchange in the flume. The modeling process is depicted in Figure 3.2.

Streambed exchange models were developed for the cases of both stationary and moving bedforms.

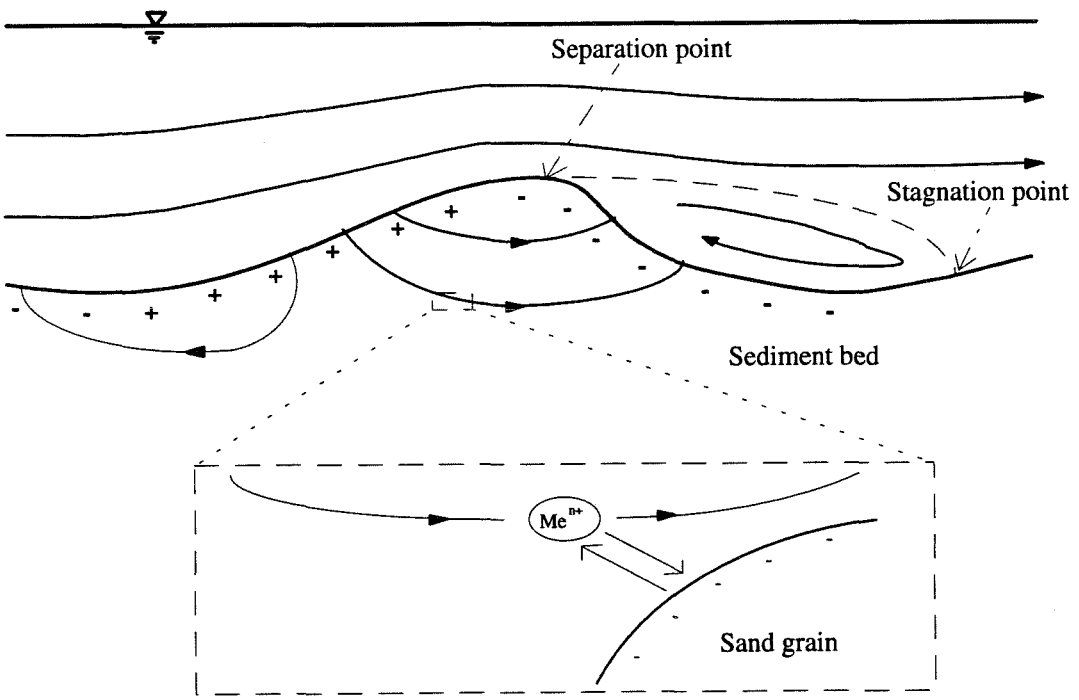

Figure 3.1. Principles of streambed exchange processes. Transport of pollutant by advective pumping and reversible adsorption to sediment grains.

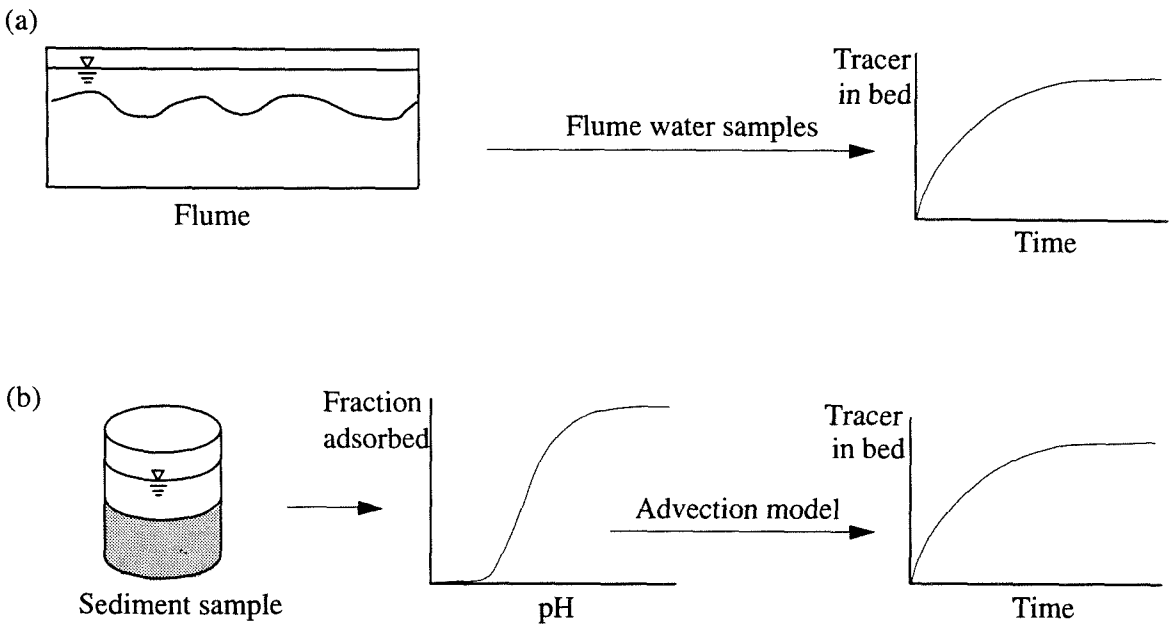

Figure 3.2. Modeling of the streambed exchange process. Flume experiments (a) and numerical simulation incorporating batch adsorption results (b).

3.2. PUMPING MODEL FOR STATIONARY BEDFORMS

3.2.1. Conservative mass transfer

Alexander Elliott, in his thesis (Caltech, 1990), developed a model for the transport of conservative tracers into and out of the sediment bed of a river on the basis of pore-water advection caused by pressure variations over the bed. In this section, an outline of Elliott's model will be given and the model will be extended to include equilibrium partitioning of tracers. For detailed information, the reader should consult Elliott's thesis.

The bedforms on the bottom of the stream are assumed to be periodic with wavelength λ, and the surface topography is assumed to only vary in the longitudinal direction. Furthermore, it is assumed that the advective flux dominates over diffusive flux. This

assumption also seems justified by experimental pore-water concentration profiles that show a very small concentration gradient, indicating that the effect of diffusion on the tracer transport in the bed is small.

3.2.1.1. *Interstitial flow field and scaling variables*

The interstitial flow field in the sediment bed can be predicted using continuity of flow and Darcy's law. It is assumed that the sediment bed is infinitely deep with constant coefficient of permeability and that the bedform topography varies only in longitudinal direction. However, the analysis shown here could be expanded for lateral variations in the topography and for nonperiodic surfaces.

The pressure and interstitial flow velocity can be related by Darcy's law,

$$\vec{v} = -K\nabla h, \tag{3.1}$$

where h is the dynamic pressure head and K the coefficient of permeability of the sediment bed. $\vec{v}$ is the Darcy velocity, the pore-water advection velocity multiplied by the porosity of the sediment θ.

Applying the equation of continuity to Equation 3.1 and assuming a constant coefficient of permeability K leads to Laplace's equation,

$$\nabla^2 h = 0. \tag{3.2}$$

Using measurements of the actual pressure distribution over triangular bedforms (Fehlman, 1985), Elliott showed that it is acceptable to assume a sinusoidal pressure dis-

tribution with wavelength λ over the bed. The pressure head with amplitude h_m and wavenumber k at the surface (approximated by y = 0 for the seepage calculation) is then

$$h|_{y=0} = h_m \sin(kx), \tag{3.3}$$

where

$$k = \frac{2\pi}{\lambda}. \tag{3.4}$$

Assuming an infinitely deep bed (e.g., $h(y \rightarrow -\infty) = 0$), solving Laplace's equation (Equation 3.2) leads to

$$h(x,y) = h_m \sin(kx) e^{ky}. \tag{3.5}$$

Then, applying Darcy's law (Equation 3.1), the resulting pore-water Darcy velocities are

$$\begin{aligned} u_x(x,y) &= -Kkh_m \cos(kx) e^{ky} \\ u_y(x,y) &= -Kkh_m \sin(kx) e^{ky} \end{aligned} \tag{3.6}$$

The amplitude of the pressure head h_m is estimated from an empirical formula that is based on Fehlman's measurements of the pressure distribution over bedforms (Fehlman 1985 and Shen et al. 1990):

$$h_m = 0.28 \frac{u^2}{2g} \begin{cases} \left(\frac{H/d}{0.34}\right)^{3/8} & H/d \le 0.34 \\ \left(\frac{H/d}{0.34}\right)^{3/2} & H/d \ge 0.34 \end{cases}, \tag{3.7}$$

where u is the flow velocity in the channel, d the channel depth, g the acceleration of gravity and H the bedform height (crest to trough). In the experiments in this work (Chapter 5), the actual value of the term Kh_m, containing the pressure head fluctuation h_m and the sediment permeability K, was determined by the initial flux of tracer into the bed

(in the experiments with lithium, lithium was used as the indicator). The values for Kh_m determined by the estimating formula and the initial flux agreed well (within a factor of two) for all experiments, indicating that Equation 3.7 allows a reasonable estimate of the pressure head over the bedforms.

As Equation 3.6 shows, the maximum pore-water Darcy velocity, a characteristic velocity for the pumping process, is

$$u_m = Kkh_m \quad . \tag{3.8}$$

The normalization of length, time and velocity will be performed as follows:

$$\begin{aligned} &\text{length:} && x^* = kx \\ &\text{time:} && \frac{t^*}{\theta} = k^2 Kh_m \frac{t}{\theta} \\ &\text{velocity:} && u^* = \frac{dx^*}{d\left(t^*/\theta\right)} = \frac{u}{kKh_m} = \frac{u}{u_m} \end{aligned} \quad . \tag{3.9}$$

The scaling length is 1/k and the scaling velocity is u_m. The resulting scaling time $1/(k^2Kh_m)$ is a measure of the time it takes the pore-water to travel a distance 1/k, or $\lambda/2\pi$, in the bed at the maximum pore-water Darcy velocity u_m.

3.2.1.2. Residence time model

To determine the net interfacial flux occurring due to pore-water advection, a model based on the residence time approach was developed. The residence time function $R_f(t, t_0, x_0)$ gives the probability that a particle that entered the sediment bed at time t_0 at position x_0 is still in the bed at time t.

The local flow of solution into the bed surface q (the flux of pollutant into the bed divided by the concentration of pollutant in solution) is given by the advective velocity of the pore-water perpendicular to the surface. The average value of the flow into the sediment bed $\bar{q}$ is then determined by integration over a bedforms wavelength λ along the bed surface (which is assumed to be flat in this calculation):

$$q = \begin{cases} \vec{v} \cdot \vec{n} & \text{if } \vec{v} \cdot \vec{n} \geq 0 \\ 0 & \text{if } \vec{v} \cdot \vec{n} < 0 \end{cases} \tag{3.10}$$

$$\bar{q} = \frac{1}{\lambda} \int_{x=0}^{x=\lambda} q \, dx \tag{3.11}$$

where $\vec{v}$ is the Darcy velocity vector at, and $\vec{n}$ the unit normal vector into, the surface. The total amount of mass transferred into the bed over the length L (where $L >> \lambda$) of a reach is thus $\bar{q}C(t)L$, where C(t) is the concentration of solute in the water.

If the flow conditions are constant ($d\bar{q}/dt = 0$), the residence time function R is not dependent on the time t but only on the time difference $\tau = t - t_0$, so

$$R_f(t, t_0, x_0) = R_f(\tau, x_0). \tag{3.12}$$

To remove the dependency on x_0, the flux weighted average $\bar{R}_f(\tau)$ can be obtained by integrating over the length of a bedform,

$$\bar{R}_f(\tau) = \frac{\overline{qR_f}}{\bar{q}} = \frac{\frac{1}{\lambda} \int_{x=0}^{x=\lambda} q(x) R_f(\tau, x) \frac{ds}{dx} dx}{\bar{q}} \tag{3.13}$$

For very short times τ, every particle that is swept into the bed will remain there, so $\bar{R}_f = 1$. This fact can also be used to determine the pore-water advection velocity (see Chapter 3.2.1.1). For time $\tau \rightarrow \infty$, all particles will eventually leave the bed, so $\bar{R}_f \rightarrow 0$.

The residence time function can generally be obtained by tracking the solute through the bed. In the case of sinusoidal pressure distribution over the bedforms, an implicit formula for $\bar{R}_f$ can be found:

$$\frac{t^*}{\theta} = \frac{2\cos^{-1}\bar{R}_f}{\bar{R}_f} \tag{3.14}$$

The residence time function in the case of a sinusoidal pressure distribution is shown in Figure 3.3. A table of values for the residence time function is given in Appendix C.

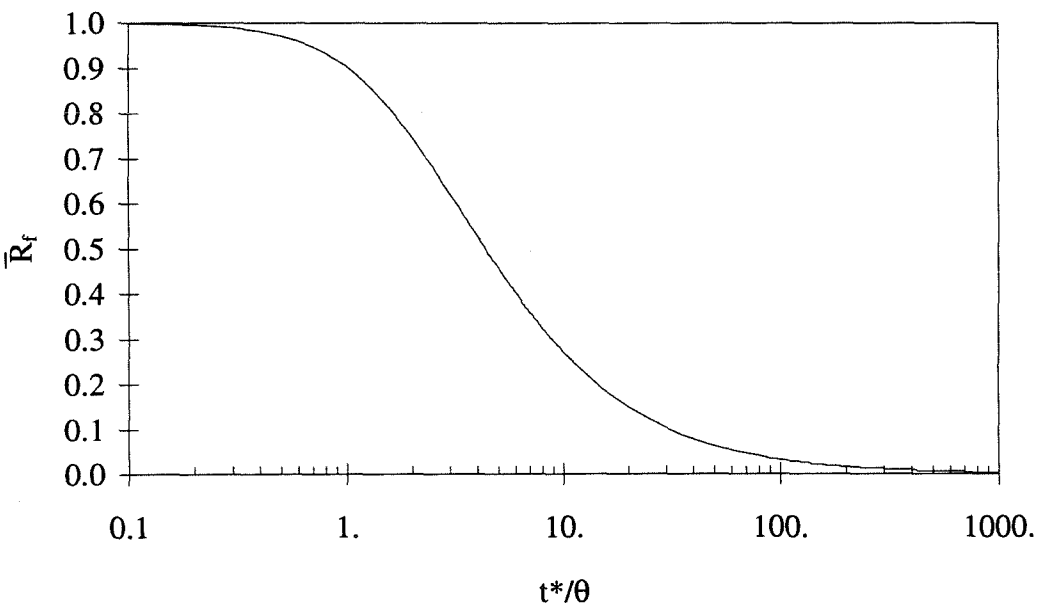

Figure 3.3. Pore-water residence time function $\bar{R}_f$ for sinusoidal pressure distribution over the bedforms. See text for definition of variables.

In the case of constant flux into the bed, the time dependent mass transfer into the bed can be obtained simply by temporal integration over the residence time function without having to perform any additional numerical calculations in the spatial dimensions. Thus, the residence time function approach greatly reduces the computational effort required to calculate the simulations.

The incremental contribution (per unit length) to the mass in the bed at time t from the mass that entered the bed at the past time t-τ over a period dτ is

$$\bar{q}\bar{R}_f(\tau)C(t-\tau)d\tau \tag{3.15}$$

The concentration C is normalized by a reference concentration C_0, for example the initial concentration in the water. Thus, the normalized concentration is

$$C^* = \frac{C}{C_0} \tag{3.16}$$

and the accumulated mass transfer m(t) can be determined as

$$m(t) = \bar{q} \int_{\tau=0}^{\tau=\infty} \bar{R}_f(\tau)C^*(t-\tau)d\tau \tag{3.17}$$

The accumulated mass transfer m(t) is defined as the accumulated mass (per unit area) divided by the reference concentration C_0 and has the dimension of a length. It can be understood as a measure of the penetration depth into the bed. In general, it is necessary to know the concentration of the inflowing solution over all past times to compute m(t).

Only the interfacial flow $\bar{q}$, the residence time function $\bar{R}_f(\tau)$, the physical experiment parameters (bedform size, water depth, flow velocity) and the concentration history

is needed for the calculation of pollutant exchange with the bed. The model does not contain any fitting parameters.

If the initial concentration of solute in the bed at the start of the flume experiment or spill is zero, Equation 3.17 can be simplified to

$$m(t) = \bar{q} \int_{\tau=0}^{\tau=t} \bar{R}_f(\tau) C^*(t-\tau) d\tau. \tag{3.18}$$

3.2.1.2.1. Application to a closed system

The experimental system in the flume used in this work is closed, so there are no losses from the water/sediment system. If the area of the sediment bed in the flume is A and the total volume of solution above the sediment bed V, an effective water depth d' can be defined as

$$d' = \frac{V}{A}, \tag{3.19}$$

and it follows that

$$\frac{dm}{dt} = -\frac{V}{A}\frac{dC^*}{dt} = -d'\frac{dC^*}{dt}. \tag{3.20}$$

With $m(0) = 0$ and $C(0) = C_0$,

$$C^*(t) = 1 - \frac{m(t)}{d'}. \tag{3.21}$$

Thus, the system of the two coupled Equations 3.18 and 3.21 must be solved to predict the mass transfer occurring in the closed flume system.

Applying the previously developed scaling variables to the system of two coupled equations that describe the mass transfer into the bed in a closed system (Equations 3.18 and 3.21) yields

$$m^*(\frac{t^*}{\theta}) = \bar{q}^* \int_0^{t^*/\theta} C^*(\frac{t^*}{\theta} - \frac{\tau^*}{\theta})\bar{R}_f(\frac{\tau^*}{\theta})d(\frac{\tau^*}{\theta})$$
$$C^*(\frac{t^*}{\theta}) = 1 - \frac{m^*(\frac{t^*}{\theta})}{d'^*} \qquad (3.22)$$

3.2.1.2.2. Approximation for a closed system

Under certain circumstances, the system of coupled equations (Equations 3.22) can be approximated: if it is assumed that the concentration of solute in the pore-water is at all times equal to the concentration of solute in the overlying water, then

$$m^*(\frac{t^*}{\theta}) = \bar{q}^* \int_0^{t^*/\theta} C^*(\frac{t^*}{\theta} - \frac{\tau^*}{\theta})\bar{R}_f(\frac{\tau^*}{\theta})d(\frac{\tau^*}{\theta}) = \bar{q}^* C^*(\frac{t^*}{\theta}) \int_0^{t^*/\theta} \bar{R}_f(\frac{\tau^*}{\theta})d(\frac{\tau^*}{\theta}) \qquad (3.23)$$

is valid and the expression M*(t), defined as

$$M^*(t) = \frac{m^*(t)}{C^*(t)}, \qquad (3.24)$$

can be used to describe the mass exchange. The advantage of this approximation of convolution is that the mass exchange in experiments with different values of d' can be compared to just one theoretical curve. However, this approximation only holds when the change in concentration C* is small and the tracers do not remain in the bed for very long times. These assumptions are not true for most of the experiments performed with adsorbing tracers: Figures 3.4 and 3.5 are test calculations (for d'*=kd'=4, a typical value in the flume used) and show that the approximation holds for nonadsorbing tracers

(Figure 3.4), but is not very good for an adsorbing tracer with a retardation coefficient of R=10 (Figure 3.5, see Chapter 3.4.1 for discussion of retardation coefficient R). Thus, in the case of adsorbing solutes one must solve the system of coupled equations (3.22).

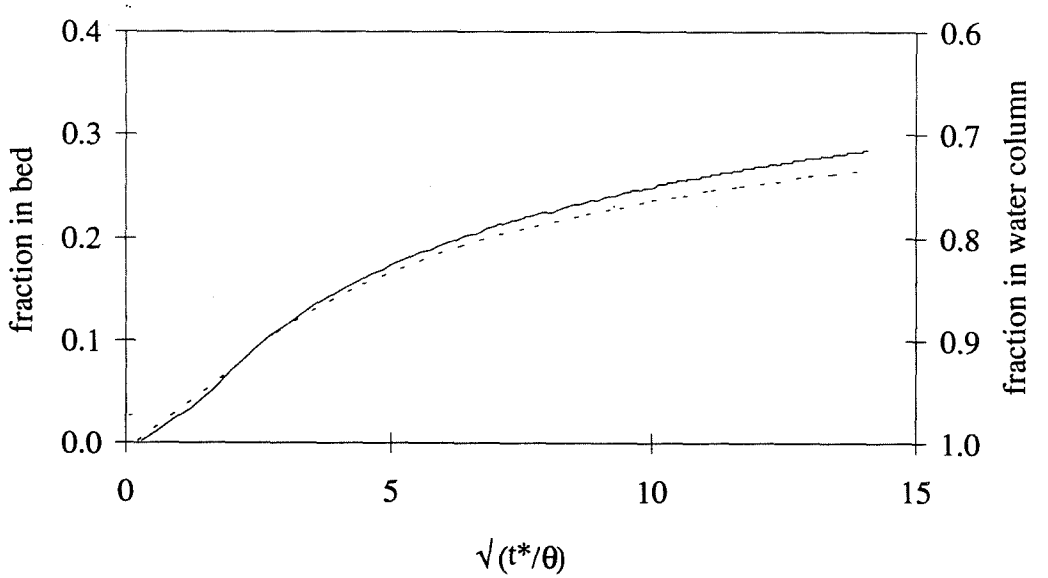

Figure 3.4. Validity of the approximation of convolution for nonadsorbing tracer.
——— exact solution – – – – approximate solution.

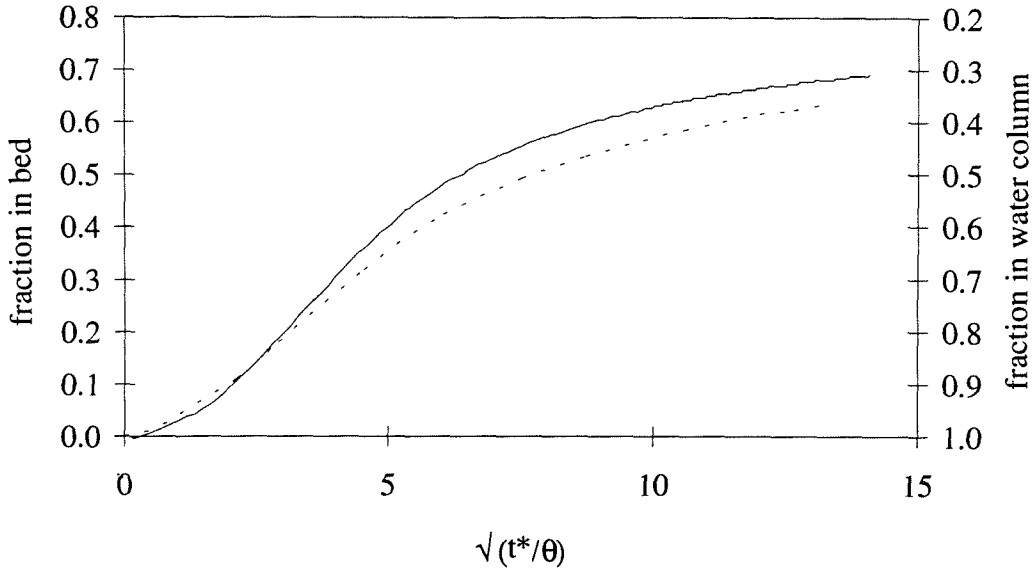

Figure 3.5. Validity of the approximation of convolution for sorbing tracer, R=10.
——— exact solution – – – – approximate solution.

3.2.1.3. Subsurface underflow

The hydraulic gradient of a natural river induces a flow of pore-water down the slope of the river bed. The magnitude of the underflow is given by the slope s of the channel and the coefficient of permeability K of the sediment as

$$u_u = K\, s, \tag{3.25}$$

normalized

$$u_u^* = \frac{K\, s}{k K h_m} = \frac{s}{k h_m}. \tag{3.26}$$

The effect of the underflow is that it causes fluid particles to be swept from regions with downward flux to regions with upward flux, thus limiting the residence time of a tracer in the bed. The main effect of the underflow is thus limitation of the total mass

exchange between stream water and the river bed for longer times. Underflow can be incorporated into the advective pumping model by modifying the equation for the pore-water velocities (Equation 3.6) to

$$\begin{aligned} u_x(x,y) &= -Kkh_m \cos(kx)e^{ky} + u_u \\ u_y(x,y) &= -Kkh_m \sin(kx)e^{ky} \end{aligned}, \tag{3.27}$$

normalized

$$\begin{aligned} u_x^*(x,y) &= -\cos(x^*)e^{y^*} + u_u^* \\ u_y^*(x,y) &= -\sin(x^*)e^{y^*} \end{aligned}. \tag{3.28}$$

Because the interstitial velocity field changes with u_u, a separate residence time function must be computed for all values of u^*_u.

3.3. SURFACE ADSORPTION MODELING

3.3.1. Equilibrium adsorption from solution

In a simplified approach, the adsorption of a solute molecule onto the surface of a solid can be treated analogously to reactions between molecules in solution. In this case, the reactive group of the surface is treated like any other molecule. The surface of the solid can exhibit acid-base chemistry, meaning that protons can be adsorbed to and desorbed from the surface (the symbol ≡ denotes a surface group, for example silica: ≡SiOH):

$$\equiv SiOH_2^+ \leftrightarrow \equiv SiOH + H^+ \tag{3.29}$$

$$\equiv SiOH \leftrightarrow \equiv SiO^- + H^+. \tag{3.30}$$

The distribution of surface groups between their differently charged species is described by equilibrium constants, here

$$K_{a1}^{s} = \frac{[\equiv SiOH][H^+]}{[\equiv SiOH_2^+]} \tag{3.31}$$

$$K_{a2}^{s} = \frac{[\equiv SiO^-][H^+]}{[\equiv SiOH]} \tag{3.32}$$

Similarly, the adsorption of a bivalent metal ion (Me^{2+}) onto silica can be written as

$$\equiv SiOH + Me^{2+} \leftrightarrow \equiv SiOMe^+ + H^+ \tag{3.33}$$

$$\equiv SiOH + Me^{2+} \leftrightarrow \equiv SiOHMe^{2+}, \tag{3.34}$$

where

$$K_1 = \frac{[\equiv SiOMe^+][H^+]}{[\equiv SiOH][Me^{2+}]} \tag{3.35}$$

$$K_2 = \frac{[\equiv SiOHMe^{2+}]}{[\equiv SiOH][Me^{2+}]} \tag{3.36}$$

are the equilibrium constants for the metal ion adsorption processes.

Basic models like the one above omit the influence of a charge distribution on the surface of the solid. This surface charge can arise from lattice imperfections in the crystalline structure or result from chemical reactions taking place at the surface. To preserve electroneutrality in the interface region, a layer of counterions forms in the solution next to the surface. The result is an electrochemical double layer at the solid-solution interface that has significant effect on the adsorption of ions to the solid surface.

To incorporate the effect of surface charges into the equations for the adsorption equilibrium, a number of models describing the nature of the electric double layer have been developed (see Stumm and Morgan 1981, Stumm 1987 or Dzombak and Morel 1987). The simplest model, the *Helmholtz* model, consists of a single sheet of charges in solution, neutralizing the charges on the surface. The *Gouy-Chapman* model allows for the sheet of charges in solution to diffuse due to thermal movement and form a diffused layer. The *Stern* model introduces a second layer of ions adsorbed to the surface inside the diffused Gouy layer. These models are depicted in Figure 3.6.

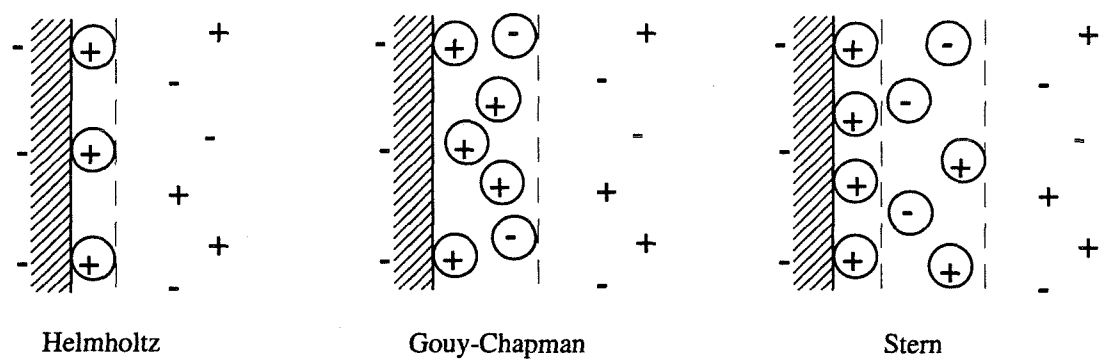

Figure 3.6. Surface double layer models (Stumm and Morgan 1981).

A potential Ψ, a charge density σ and a capacitance C_d are associated with each of the individual layers. The extent of the electrochemical double layer is strongly dependent on the ionic strength I of the solution.

The effect of changes in the electrokinetic double layer on the equilibrium constants is expressed by the Boltzmann factor $e^{F\Delta\Psi/RT}$, where R is the gas constant, T the temperature, F the Faraday constant and $\Delta\Psi$ the potential difference between the charged planes. The potential difference between the surface and the bulk solution is denoted as

Ψ_0. Equilibrium constants incorporating the electrokinetic effect are called intrinsic constants. For the adsorption and desorption of proton to the surface these are

$$K_{a1}^{int} = \frac{[\equiv SiOH][H^+]}{[\equiv SiOH_2^+]} e^{-\frac{F\Psi_0}{RT}} \tag{3.37}$$

$$K_{a2}^{int} = \frac{[\equiv SiO^-][H^+]}{[\equiv SiOH]} e^{-\frac{F\Psi_0}{RT}} \tag{3.38}$$

and the equilibrium constants for the adsorption of a metal ion to the surface are

$$K_1^{int} = \frac{[\equiv SiOMe^+][H^+]}{[\equiv SiOH][Me^{2+}]} e^{\frac{F\Psi_0}{RT}} \tag{3.39}$$

$$K_2^{int} = \frac{[\equiv SiOHMe^{2+}]}{[\equiv SiOH][Me^{2+}]} e^{\frac{2F\Psi_0}{RT}} \tag{3.40}$$

The surface acidity constants for silica are, dependent on the surface adsorption model, approximately

$$\log K_{a1}^{int} = 2.5 \tag{3.41}$$

$$\log K_{a2}^{int} = -6.5. \tag{3.42}$$

It is important to note the values of the equilibrium constants depend on the parameters Ψ_0, σ and C as well as the choice of double layer model.

Using any of the electrokinetic models, the equilibrium constants for metal ion adsorption can be determined by fitting the system of adsorption equations to the experimental data. Here, this was accomplished using the chemical equilibrium computation model HYDRAQL (Papelis et al. 1988).

In principle, the strength of adsorption of a metal ion onto the silica surface depends on the size and charge of the ion and the ability of the ion to form covalent bonds.

3.3.2. Quantification of adsorbed mass

A number of different choices are possible to express the equilibrium quantity of a tracer adsorbed to a surface. The most frequently used expressions are:

Adsorption density:	$\Sigma = \frac{\text{moles adsorbed}}{\text{surface area}}$	$\left[\frac{\text{moles}}{\text{area}}\right]$
Fraction adsorbed:	$f_a = \frac{\text{moles adsorbed}}{\text{total moles}}$	[dimensionless]
Retardation coefficient:	$R = \frac{1}{\text{fraction in solution}}$	[dimensionless]
Partitioning coefficient:	$k_p = \frac{\text{moles adsorbed per mass sediment}}{\text{moles per volume solution}}$	$\left[\frac{\text{volume}}{\text{mass}}\right]$

The origin of these different expressions lies in the type of experiment originally performed to observe the adsorption of tracers. Surface chemists, who usually perform beaker experiments with fixed small amounts of solid particles and sorbate, often express the amount of adsorbed tracer as an *adsorption density*. Expressing surface adsorption as adsorption density is the best choice to analyze and compare experimental data from experiments performed with different size particles, different concentrations, or different amounts of solid and solution. The calculation of the adsorption density requires knowledge of the surface area of the sorbents used. Especially in earlier chemistry papers, investigators have also tended to express the amount of adsorbed tracer as a *fraction ad-*

sorbed f_a (or *percent adsorbed*) in the observed system. The adsorption density can be computed from the fraction adsorbed as

$$\Sigma = \frac{\text{total moles adsorbed}}{\text{total surface area}} = \frac{f_a C_0 V_t}{A_s m_t}, \tag{3.43}$$

where C_0 is the initial concentration of sorbate and V_t the total volume of solution. A_s is the specific surface area and m_t the total mass of sorbent.

Hydraulic engineers who are concerned with the transport of an adsorbing substance through soil or other sediments often use the *retardation coefficient* R (see Chapter 3.4.1) of a tracer, a directly observable parameter in field experiments. Alternatively, the *partitioning coefficient* k_p is sometimes used. It also can be easily measured and directly inserted into the advection-diffusion equation.

Fraction adsorbed and retardation coefficient are nondimensional, the partitioning coefficient is expressed in units of volume per mass. All three parameters are calculated for specific conditions, their magnitude for the adsorption of pollutants to different materials is only comparable if all necessary sorbate and sediment parameters are also known.

If the porosity θ and bulk density ρ of the sediment are known, the coefficients can be easily converted (see Equation 3.44 and Figure 3.7).

$$\begin{aligned} f_a &= \frac{R-1}{R} = \frac{\rho k_p}{\rho k_p + \theta} \\ R &= 1 + \frac{\rho k_p}{\theta} = \frac{1}{1-f_a} \\ k_p &= \frac{\theta}{\rho} \frac{f_a}{1-f_a} = \frac{\theta}{\rho}(R-1) \end{aligned} \tag{3.44}$$

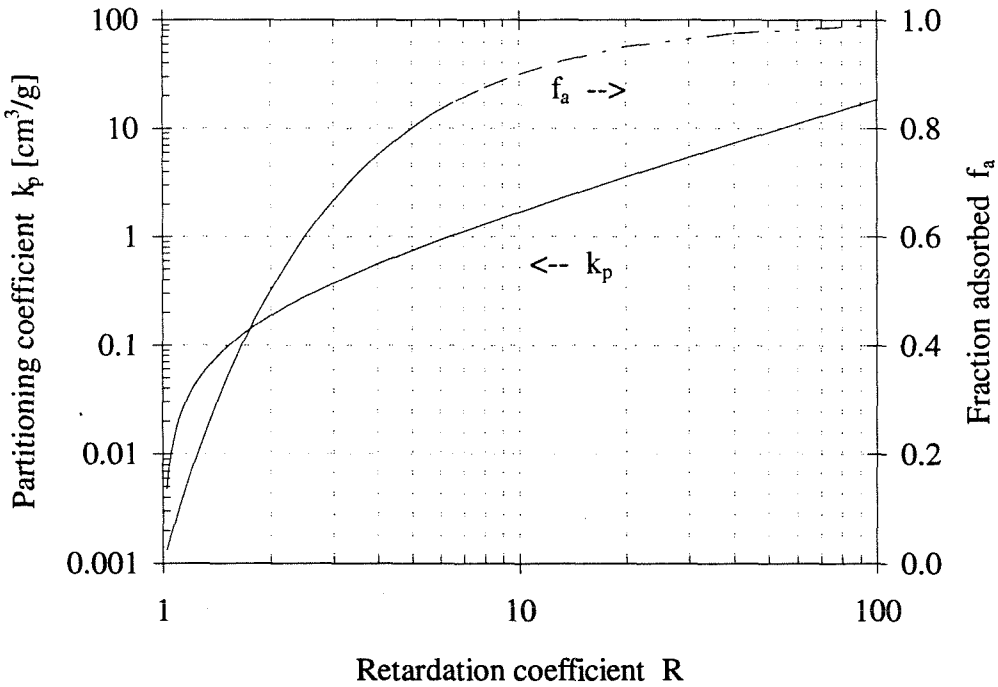

Figure 3.7. Graphical conversion of k_p, R, and f_a in quantifying adsorption onto Ottawa 30 sand used in this study.

3.4. TRANSFER OF ADSORBING POLLUTANTS

3.4.1. Retardation

For the purpose of this investigation, the contaminant exchange model needed to be extended to incorporate the effects of partitioning of the observed pollutant to the sediment.

Equilibrium partitioning of the contaminant to the sediment as the pore-water is driven through the bed by the pressure field causes retardation of the contaminant, similar

to the retardation of chemicals in ground water flow. A mass balance for a unit volume of sediment gives

$$\theta\frac{\partial C}{\partial t}+\theta u\frac{\partial C}{\partial x}=\theta\frac{\partial^2 C}{\partial x^2}-\rho\frac{\partial C_{ads}}{\partial t}, \tag{3.45}$$

where C is the concentration of pollutant in the pore-water (in moles/unit volume) and C_{ads} the adsorbed mass of pollutant per unit mass of bulk sediment (in moles/unit mass sediment). θ is the porosity and ρ the density of the sediment.

The partition coefficient k_p describes the relationship between C and C_{ads} as $C_{ads}= k_pC$. Because the mass of sediment in a unit volume of pore-water is ρ/θ, the mass of adsorbed sediment per unit volume of pore-water is $\rho k_p/\theta$. The advection-diffusion equation for the pollutant in the pore-water can then be simplified to

$$(1+\frac{\rho}{\theta}k_p)\frac{\partial c}{\partial t}+u\frac{\partial c}{\partial x}=\frac{\partial^2 c}{\partial x^2} \tag{3.46}$$

with the retardation factor

$$R=1+\frac{\rho}{\theta}k_p. \tag{3.47}$$

Thus, the addition of partitioning to the advection-diffusion equation results in two modifications: the advective velocity of the sorbate in the pore volume is effectively reduced by R, and the total mass of contaminant in a unit volume of the sediment bed increases by R.

The transport of adsorbing materials through the pore space of the sediment bed can thus be described by the advective transport model (pumping model) by reducing the time scale by a factor of 1/R. Therefore, the introduction of surface adsorption leads to a longer residence time of the tracer in the bed, while the flux into the bed stays the same.

The result is a larger amount of tracer being contained within a unit volume of the bed. The modified residence time function for adsorbing tracers is shown in Figure 3.8. Figure 3.8 is the same as Figure 3.3 except for changing the time scale from t^*/θ to $t^*/(\theta R)$. The scaling of length, velocity and time are now:

$$\begin{aligned} &\text{length:} && x^* = kx \\ &\text{time:} && \frac{t^*}{\theta R} = \frac{k^2 K h_m}{R}\frac{t}{\theta} \\ &\text{velocity:} && u^* = \frac{u/R}{kKh_m/R} = \frac{u}{u_m} \end{aligned} \tag{3.48}$$

The coupled system of equations describing the mass transfer into the sediment bed (Equation 3.22) then becomes

$$\begin{aligned} m^*\left(\frac{t^*}{\theta R}\right) &= \overline{q}^* \int_0^{\frac{t^*}{\theta R}} C^*\left(\frac{t^*}{\theta R} - \frac{\tau^*}{\theta R}\right)\overline{R}_f\left(\frac{\tau^*}{\theta R}\right)d\left(\frac{\tau^*}{\theta R}\right) \\ C^*\left(\frac{t^*}{\theta R}\right) &= 1 - \frac{m^*\left(\frac{t^*}{\theta R}\right)}{d'^*} \end{aligned} \tag{3.49}$$

To illustrate the effect of retardation on the mass exchange between stream water and the bed, Figures 3.9 and 3.10 show an example ($d'/\lambda = 0.75$) of the mass exchange between water column and the sediment bed in a closed system after an increase in tracer concentration in the overlying water. Initially ($t^*/\theta < 1$), advective flux into the bed dominates. At these small times, the flux into the bed is essentially independent of R, and the initial concentration decrease in the water column is therefore identical for all tracers. After entering the bed at the upstream side of a dune, the tracers are advected through the bed by the pumping process. Since the pumping velocity of the tracer is dependent on the

retardation coefficient, nonadsorbing tracers are advected faster than the adsorbing tracers and will thus reach the downstream side of the dunes faster than the adsorbing tracers. It can be seen from Figure 3.3 that, at $t^*/\theta \cong 1$, over 90% of the tracers that entered the sediment bed at $t^* = 0$ are still contained within the bed. Significant release of the nonadsorbing tracer begins at the downstream side of dunes at about $t^*/\theta \cong 1$ and the rate of concentration decrease for the nonadsorbing tracer begins to decrease. The adsorbing tracers, moving at a slower velocity through the pore space of the sediment, are still being transported through the bed and will reach the downstream side of the dunes later. Significant release of tracer at the downstream side begins at $t^*/\theta \cong 3$ for the tracer with retardation R = 3 and finally at $t^*/\theta \cong 10$ for the stronger adsorbing tracer (R = 10). Generally, significant release of tracer at the downstream end of the dunes begins at about $t^*/(\theta R) = 1$ (see Figure 3.8, 90% of tracer is still within the bed at $t^*/(\theta R) = 1$).

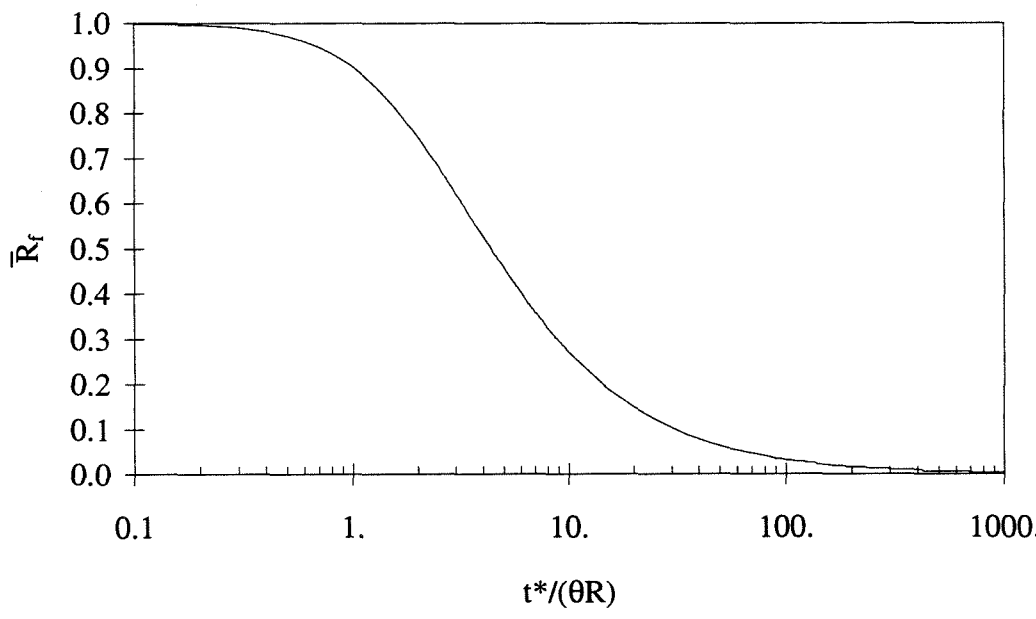

Figure 3.8. Residence time function $\bar{R}_f$ for adsorbing tracers. R is the retardation coefficient.

The net flux of tracer into the bed (advective flow into the dune at the upstream side minus release at the downstream side) can be determined by using the residence time function. For longer times (Figure 3.10), it can be seen that the amount of metal ions removed from the water column is larger for stronger adsorbing tracers. The amount of tracer remaining in the water column decreases more slowly at later times because the flux out of the bed increases as pollutant has traveled through the bed and is released into the water column again.

The reduced flow of pollutant out of the bed due to the smaller advection velocity for adsorbing tracers after an initial pulse input into the bed from $t^*/\theta = 0$ to $t^*/\theta = 1$ (see inset) is illustrated in Figures 3.11 and 3.12. The fraction released/unit time (as t^*/θ) is calculated by differentiating $\bar{R}_f$ with respect to t^*/θ. The amount of tracer released per unit time becomes smaller, but the duration of contaminant release increases as the retardation coefficient increases. This results in a long, tailing flow of tracer from the bed for adsorbing tracers.

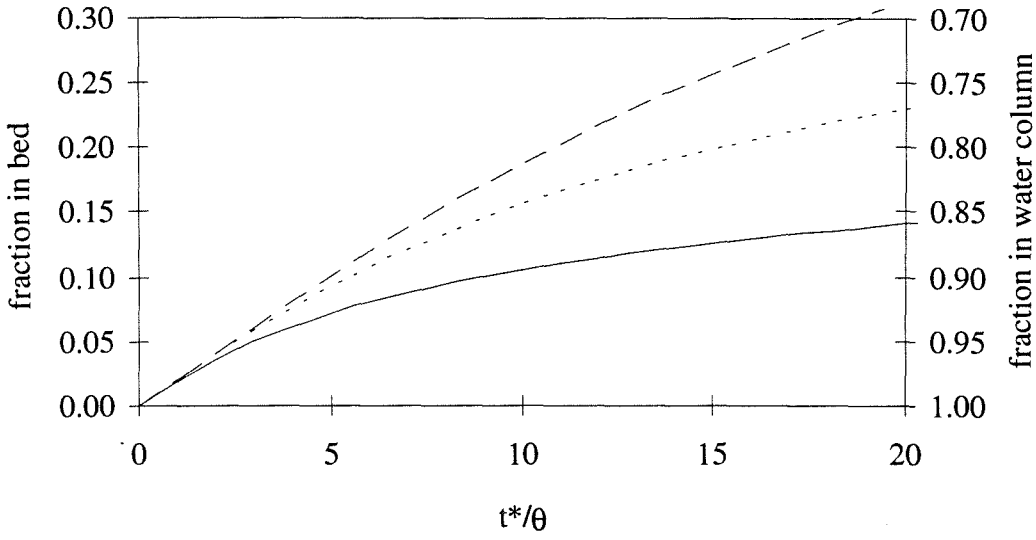

Figure 3.9. Effect of increasing retardation coefficient on mass exchange between stream water and sediment bed (short times).

—— no adsorption; - - - R=3; — — R=10.

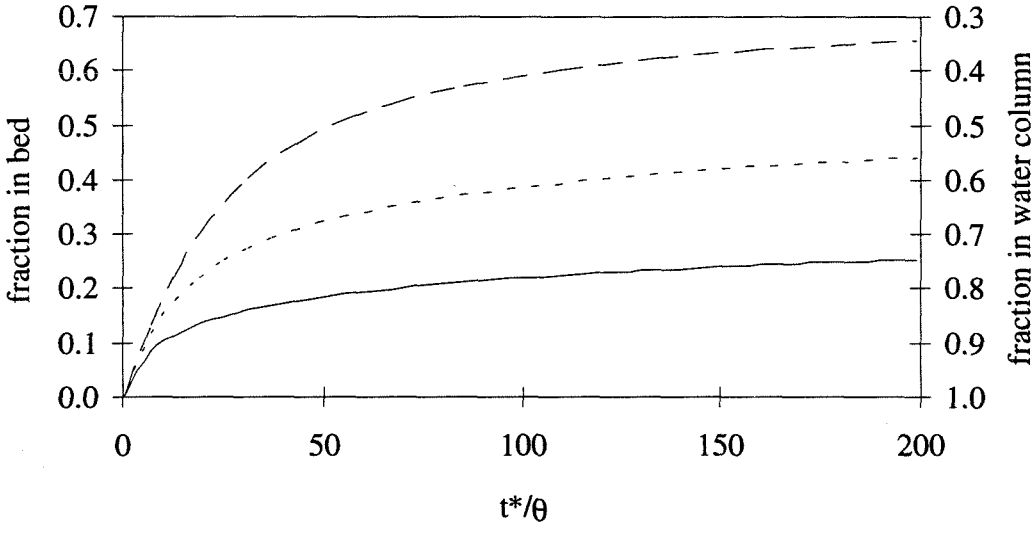

Figure 3.10. Effect of increasing retardation coefficient on mass exchange between stream water and sediment bed (long times).

—— no adsorption; - - - R=3; — — R=10.

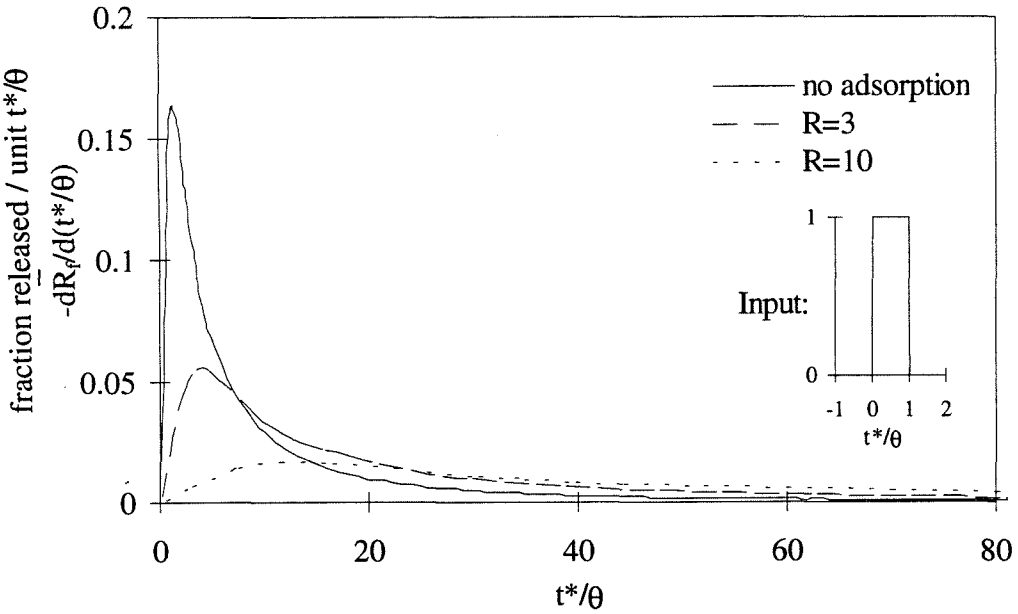

Figure 3.11. Release of nonadsorbing (R = 1) and adsorbing (R = 3 and R = 10) tracer from bed after pulse input.

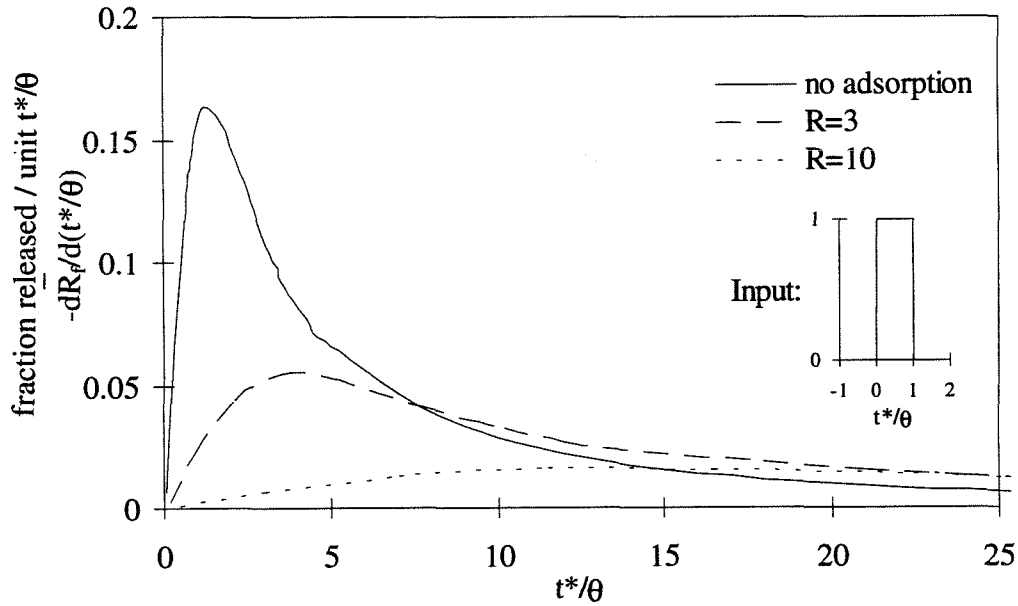

Figure 3.12. Release of nonadsorbing (R = 1) and adsorbing (R = 3 and R = 10) tracer from bed after pulse input (short times).

3.4.2. Adsorption kinetics and equilibrium assumption

3.4.2.1. Adsorption kinetics

Every chemical reaction takes place over a certain period of time. In the case of surface adsorption of metal ions, a number of steps is required for the metal ion to reach the surface:

a) Diffusion through the interstitial solution to the electrokinetic double layer.

b) Possibly, diffusion into pores in individual sediment grains.

c) Diffusion through the double layer.

d) Attachment to the surface.

When performing batch experiments, the individual processes cannot easily be observed separately.

Simple dimensional analysis can be performed to estimate roughly the time scale required for the diffusion of sorbents through the interstitial solution to the double layer (step a): Assuming a grain spacing of $L \approx 100$ μm in sand and a molecular diffusion coefficient of $D_m = 10^{-5}$ cm^2/s, the estimated time required for a molecule to diffuse from the middle of the pore to the electrokinetic double layer around a sand grain is of the order of $(L/2)^2/D_m \approx 2.5$ seconds. A measure of the relative time scale of pore diffusion compared to that for pore advection (with velocity u) in the pore space is the Peclet number, $Pe = ud_g/D_m$, where d_g is the grain size. The Peclet number in the experiments performed in this work ranges from about 10 (near the surface of the sediment bed) to values smaller than 0.1 (deep in the bed). This means that the attachment to grain surfaces is not generally limited by diffusion in the pore water towards the grain surfaces.

Diffusion into the pores of individual sediment grains (step b) is sometimes modeled by using a pore-scale (Lyklema 1980) or partitioning-dependent (Wu and Gschwend 1986) molecular diffusion coefficient. Because these diffusion coefficients decrease as the pores become smaller or the partitioning coefficient increases, the diffusion time required can be relatively large even though distances within the pores are small.

The thickness of the double layer, κ^{-1}, depends on the ionic strength I of the medium. Stumm and Morgan (1982) approximate the double layer thickness in water as

$$\kappa^{-1} \cong \frac{3 \cdot 10^{-8}}{\sqrt{I}}, \quad \kappa^{-1} \text{ in cm} \tag{3.50}$$

The double layer thickness in fresh water is typically in the range of 5 to 20 nm. Molecular diffusion through the double layer (step c) will thus occur very rapidly ($t \cong 10^{-8}$ s).

Pressure-jump studies (Mikami 1983) indicate that the actual attachment to the surface (step d) occurs rapidly, with a time scale of some 100 μsec. However, it is not entirely clear if the actual surface adsorption step or other processes are measured during these experiments.

The above analysis indicates that diffusion through the interstitial solution and into the pores of the sediment grains, not the actual surface binding, are rate limiting.

3.4.2.2. Equilibrium adsorption assumption for pumping model

Adsorption kinetics can be neglected and equilibrium partitioning can be assumed if the time a tracer remains in the bed is long compared to the adsorption time scale for this tracer. The time pore water remains within the sediment bed (the pumping time scale

t_p) can be approximated by the time at which the nondimensional time t^* (Equation 3.9) equals one, thus $t_p = 1/(k^2 Kh_m)$. At $t^* = 1$, $t^*/\theta \cong 3$ (for $\theta \cong 0.33$), and the value of $\bar{R}_f$ is approximately 0.5.

Comparing this time scale to the adsorption time scale t_{ads} (which needs to be determined experimentally) yields a nondimensional number, Γ_p:

$$\Gamma_p = \frac{t_{ads}}{t_p} = t_{ads} k^2 Kh_m . \tag{3.51}$$

The equilibrium assumption then holds if the time that the tracer remains in the bed is large compared to the adsorption time t_{ads}, i.e., Γ_p is small. Thus,

$$\begin{aligned} &\text{if } \Gamma_p << 1 \quad \text{implies equilibrium; and} \\ &\text{if } \Gamma_p >> 1 \quad \text{implies non - equilibrium.} \end{aligned} \tag{3.52}$$

Note that this criterion does not necessarily imply local equilibrium at every point in the bed. Also, because of the choice of velocity (maximum velocity) and length scale (only $1/(2\pi) = 1/6$ of the bedform length), the applicability of the equilibrium partitioning model is likely underestimated. This is especially true at later times in the experiment, because the deeper penetration into the bed leads to much longer distances for the metal ions, to be traveled at much lower velocities. In the experiments with stationary bedforms, the value of Γ_p was between 0.1 and 0.6, indicating equilibrium adsorption.

3.5. MOVING BEDFORMS

3.5.1. Models for moving bedforms

The propagation velocity u_b of the bedforms is normalized using the pore-water scaling velocity u_m (Equation 3.53):

$$u_b^* = \frac{\theta u_b}{kKh_m} = \frac{\theta u_b}{u_m}. \tag{3.53}$$

The factor θ is included because u_m is the pore-water Darcy velocity, whereas the actual pore-water advection velocity is u_m/θ. Thus, the parameter u^*_b is the ratio of the bedform propagation velocity to the maximum pore-water velocity (for a non-adsorbing tracer) and is a measure of the relative importance of the bedform turnover compared to the advective pore-water pumping. A small value of u^*_b corresponds to negligible turn-over, a large u^*_b corresponds to negligible pore-water pumping.

If the tracer partitions to the sediment, the apparent velocity of the tracer in the pore-water due to pumping is reduced by a factor of 1/R. However, the bedform velocity is independent of the surface adsorption. Thus, for the same bedform velocity and pore-water scaling velocity, the bedform velocity for adsorbing tracers appears to be R times faster relative to the transport velocity of the tracer in the bed. Therefore, a net effect of partitioning to the surface is a larger relative bedform velocity. A partitioning-dependent normalized bedform velocity, $u^*_{b,R}$, can then be defined as

$$u^*_{b,R} = \frac{R\theta u_b}{kKh_m} = \frac{R\theta u_b}{u_m}. \tag{3.54}$$

The partitioning-dependent normalized bedform velocity can be used to determine the applicability of either the pumping or the turnover model. The experiments performed in this thesis indicate that:

$$\begin{array}{ll} \text{if } u^*_{b,R} > 5 & \text{turnover} \\ \text{if } u^*_{b,R} < 0.5 & \text{pumping} \end{array} \qquad (3.55)$$

In the intermediate range ($0.5 < u^*_{b,R} < 5$), both processes are significant. No general model could be developed because the two processes depend on different scaling parameters as well as the partitioning of the pollutant. Thus, a simulation must be performed on a case-by-case basis if the value of $u^*_{b,R}$ is between 0.5 and 5.

Because $u^*_{b,R}$ depends also on R, it is possible that turnover is the dominating process for a strongly adsorbing pollutant, whereas pumping is dominating for an only weakly adsorbing pollutant under the same hydraulic conditions.

3.5.1.1. Slowly moving bedforms

If the bedforms are moving very slowly ($u_{b,R}{}^* << 1$), the pore-water pumping process still dominates the exchange of pollutant between water column and sediment bed. In this case, the propagation of the bedforms can be modeled equivalent to a 'backward' underflow of the pore-water (see Section 3.2.1.3). Then, the pore-water pumping model with a modified underflow can be used to simulate mass exchange in the case of slowly moving bedforms. The underflow velocity, $u^*_{u,m}$, now used in the model is given by the velocity of the underflow due to the hydraulic gradient minus the effective bedform propagation velocity:

$$u^*_{u,m} = u^*_u - u^*_{b,R}. \qquad (3.56)$$

3.5.1.2. Simple turnover model

If the bedform velocity is fast enough so that the pore-water pumping model does not apply any more ($u_{b,R}^{*} >> 1$), the mass exchange between sediment and water column is dominated by turnover. Elliott (1990) describes the effective depth of mixing (the average penetration depth of the mixed pore-water or a nonadsorbing pollutant) for a bed of moving regular bedforms of height H and wavelength λ moving at a bedform velocity u_b (see Figure 3.13) as

$$m(t) = \begin{cases} \frac{\theta H}{2}\left(1-\left(\frac{\lambda - u_b t}{\lambda}\right)^2\right) & u_b t < \lambda \\ \frac{\theta H}{2} & u_b t > \lambda \end{cases} \qquad (3.57)$$

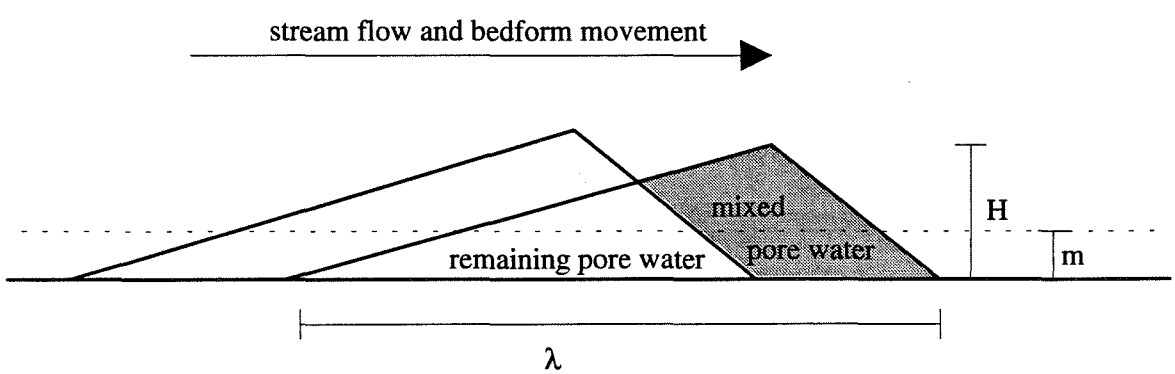

Figure 3.13. Average mixing depth for moving regular ripples (Elliott 1990).

The time-dependent apparent flow velocity (flux into the bed divided by the aqueous concentration) of solute into the bed due to bedform movement is then given by

$$\bar{q}_m(t) = \frac{dm(t)}{dt} = \begin{cases} \frac{u_b \theta H}{\lambda}\left(1 - \frac{u_b t}{\lambda}\right) & u_b t < \lambda \\ 0 & u_b t > \lambda \end{cases}. \tag{3.58}$$

After the bedforms have moved by their own length, the pore-water is mixed to the maximum depth H and no further mixing will occur.

3.5.2. Adsorption kinetics in moving bedforms

A characteristic time scale for the turnover process is the time required for a dune to move its own length, λ, at the propagation velocity u_b:

$$t_t = \frac{\lambda}{u_b}. \tag{3.59}$$

A nondimensional number, Γ_t, can be defined as the ratio of the adsorption time scale, t_{ads}, and the turnover time scale:

$$\Gamma = \frac{t_{ads}}{t_t} = \frac{t_{ads} u_b}{\lambda}. \tag{3.60}$$

Adsorption equilibrium for moving bedforms can then be expected if the adsorption time scale is small compared to the turnover time scale, or Γ_t is small:

$$\begin{array}{ll} \text{if } \Gamma_t >> 1 & \text{non-equilibrium} \\ \text{if } \Gamma_t << 1 & \text{equilibrium} \end{array}. \tag{3.61}$$

Thus, kinetic considerations can be of importance in the case of moving bedforms. The value of Γ_t in the flume experiments with moving bedforms ranged from 0.1 to 10.

3.5.2.1. No adsorption equilibrium

If the bedforms move very fast, the adsorption time scale is very long, or the dunes are very short, partitioning of the pollutant between pore-water and sediment inside the dunes may not reach equilibrium. In this case, the kinetics of the adsorption process must be incorporated into the simulation.

3.5.2.2. Very fast adsorption kinetics - adsorption equilibrium at the bed surface

On the other hand, for very fast adsorption kinetics, equilibrium partitioning between sediment and solution may already be reached before the solution is covered up by the moving dune. In other words, the pollutant is always in equilibrium with the overlying water column. Then, the effective flow velocity of a tracer with partitioning coefficient R into the bed is given by

$$\bar{q}_m(t) = \begin{cases} \dfrac{Ru_b\theta H}{\lambda}\left(1-\dfrac{u_b t}{\lambda}\right) & u_b t < \lambda \\ 0 & u_b t > \lambda \end{cases} \qquad (3.62)$$

However, the conditions for this case will likely only exist in extreme cases: if the bedform movement was slow enough to allow equilibration of the pollutants with the surface of the sediment bed, the value of u^*_b would probably be very small, and pressure-driven advection would be the dominating process over turnover for mass exchange between water column and bed. Only if the hydraulic permeability of the sediment also is very small (very slow pore-water movement by pumping), turnover could be the dominating exchange process. These conditions are only likely to occur in a stream with very muddy or silty bottom sediment and slow bedform propagation.

3.5.2.3. Adsorption equilibrium inside the bedforms

Unless the bedforms are moving very rapidly or adsorption is very fast, the adsorption time scale and the bedform propagation time scale will be comparable and the mass transfer into the bed will initially follow Equation 3.58, but continue after $t = \lambda/u_b$: as a bedform moves, water from the water column is covered up by the sediment. The pore-water inside the bed can be assumed to be in local equilibrium with the sediment in the bedform and the pollutant will partition to the surfaces. After the time required for one bedform to move a distance equal to its own length, the pore-water will be released back into the water column. Because of partitioning, the concentration of pollutant in the released pore-water will be lower than the initial concentration of water originally covered up. The concentration of pollutant in the water column will be gradually reduced as many bed forms pass by a given point in the bed until the equilibrium concentration of pollutant in the pore-water equals the concentration of pollutant in the overlying water. Because the equilibrium concentration and the number of bedforms required to pass for equilibrium are functions of the pollutant concentration in the overlying water, a generalizing simplified simulation model equivalent to the pore-water pumping residence time model could not be developed for the cover-up model. Flux into the bed will be identical to the flux given in Equation 3.58 for $t < \lambda/u_b$, but numerical simulations must be performed on a case-by-case basis using local equilibrium assumptions inside the bedforms after the bedforms have moved more than one wavelength. This model is referred to as the cover-up model.

4. APPARATUS AND PROCEDURE

4.1. FLUME

To investigate the transport of adsorbing metal ions between flume water and the sand bed in the laboratory, experiments were conducted in a recirculating, tilting laboratory flume with a total length of 533 cm, a width of 15.24 cm and a depth of 50 cm. The flume walls were straight and impermeable. To keep the volume of water inside the return system small and avoid sediment buildup, the return pipes had a diameter of only 4.04 cm. The flume is illustrated in Figures 4.1 and 4.2.

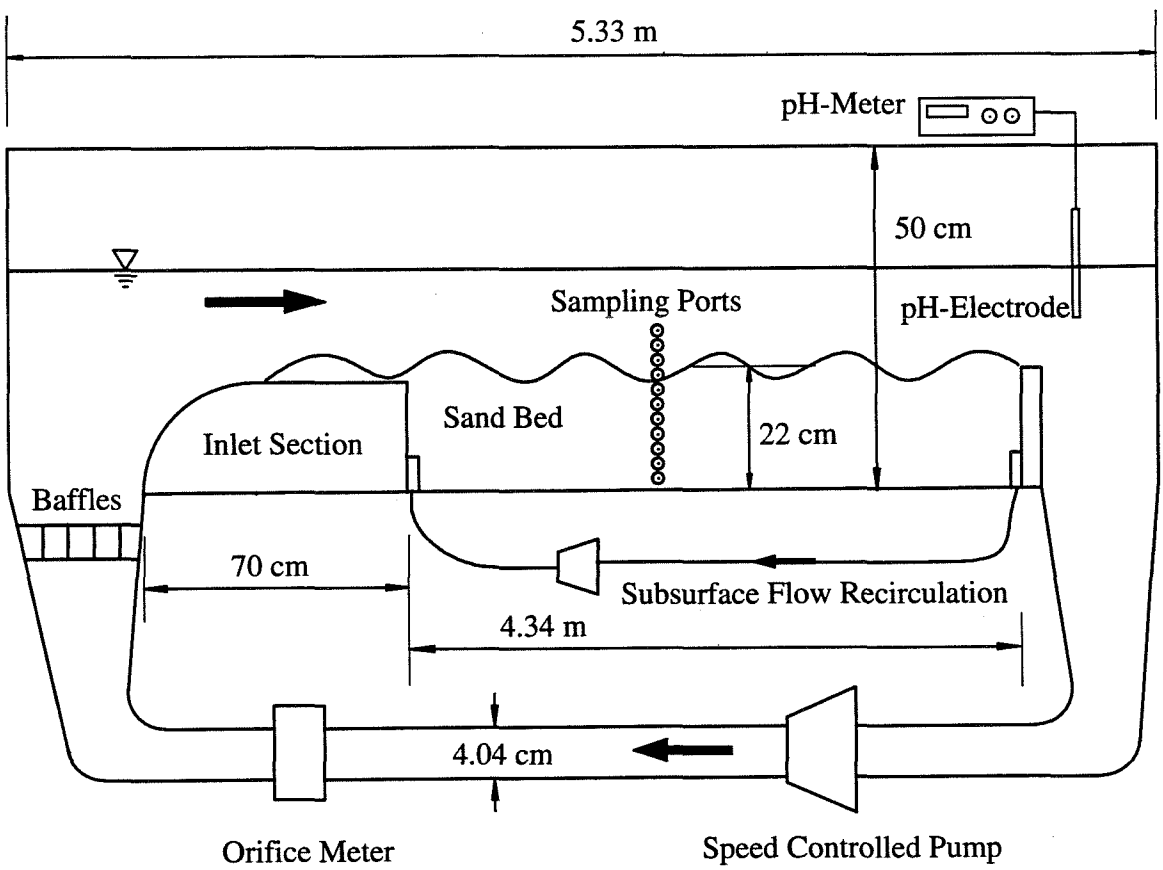

Figure 4.1. Schematic of flume used in experiments (not to scale).

In a recirculating flume, the same volume of water is flowing over the bed many times. Consequently, in contrast to a reach of a natural river, the flume constitutes a closed system. Performing the experiments in a recirculation flume has several advantages:

1. If the flowing water passes over the sediment bed only once, changes in concentration of pollutant in the flowing water are very small. In a recirculating system, concentration changes are amplified because the solution passes over the bed many times. This allows a more accurate investigation of the exchange process.
2. It is uncomplicated to run experiments over long periods of time (longer than a week) because it is not necessary to constantly supply a flow of water, sand and chemicals to the upstream end of the flume. Only evaporation losses need to be replaced.
3. A much smaller volume of waste water is produced in the experiments, allowing uncomplicated disposal of the solution in the flume after each run.

To allow turbulence generated in the return pipe and the diverging section of the return system to dissipate, baffles were placed in the diverging part of the return system and a 70 cm long inlet section, constructed of a lucite box with curved upstream side, was placed at the upstream end of the flume. This inlet box also provided an impermeable boundary at the upstream end of the sand bed, avoiding solute transport into the bed other than through the horizontal interface. Similarly, the downstream end of the sediment bed was sealed by a vertical end plate.

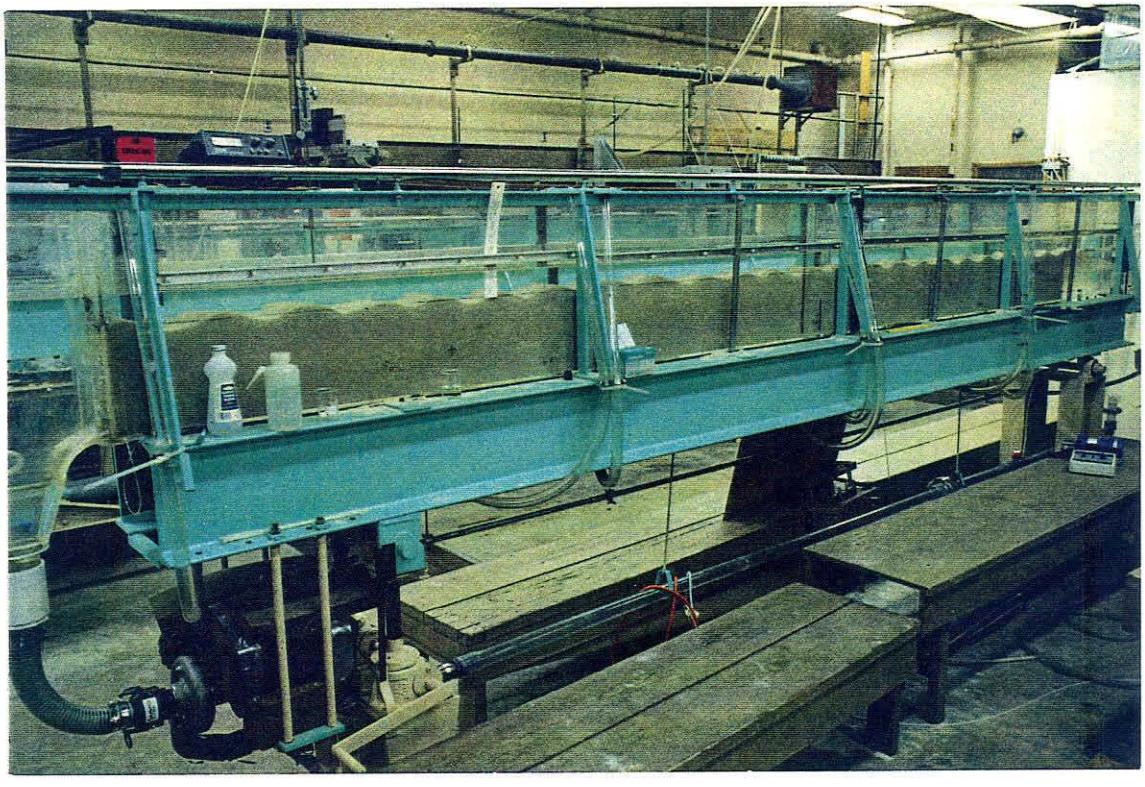

Figure 4.2. Photograph of flume apparatus.

The entire flume was constructed out of clear lucite and polyvinyl chloride (PVC) for four reasons:

1. To observe the shape of the bedforms in the flume.
2. To observe buildup of sediment in the return pipes.
3. To avoid sorption of tracers to the walls of the flume.
4. To avoid contamination of the system by desorbing pollutants from the walls of the flume.

The only component of the flume not made of plastic was the stainless steel pump.

To draw pore-water samples from the bed, a vertical row of sampling ports in the sidewall of the flume was used. The ports were spaced in 1 cm intervals. Pore-water was

withdrawn with a 1 ml syringe through a 30-gauge Hamilton needle of 5 cm length. The volume of pore-water withdrawn was 500 µl, a small enough volume to keep disturbances of the hydraulic conditions inside the bed minimal.

To allow measurement of the water level and bed surface in the flume, rails parallel to the flume bottom, carrying an instrument carriage with a point gauge, were mounted over the entire length of the flume. A portable pH-meter (Radiometer, Copenhagen) connected to a glass combination electrode was placed on top of the flume to allow continuous monitoring of the solution pH.

The sediment bed in the flume was 434 cm long and 22 cm deep. This was deep enough to avoid transport of tracers close to the bottom of the flume, so that the sand bed could be considered infinitely deep. The total mass of sand used in the experiments was about 250 kg. Typically, about 20 individual bed forms were formed over the length of the bed, a large enough number to allow averaging of possible local concentration differences in the bed.

The depth of the water column in the experiments performed was about 6 to 10 cm, leading to a total solution volume in the flume above bed level of about 75 to 110 ℓ. About 28 ℓ of this volume were contained in the recirculation system (return pipe, diverging sections) below the sediment bed level. About an additional 45 ℓ of water were contained in the pore space of the sediment bed.

The circulation time of the solution in the flume was of the order of minutes, assuring that the recirculating solution was well mixed and no longitudinal concentration variations existed during the cause of every experiment run. To determine the flow rates in the experiments, an orifice meter, installed in the return pipe of the circulation system

and connected to a mercury manometer, was used. The orifice was sharp with a diameter of 2.83 cm, the ratio of the orifice diameter to the pipe diameter was 0.70.

The hydraulic gradient of a natural river induces flow a of pore-water down the slope of the river bed. This underflow, which can potentially influence the mass exchange between the sediment bed and the overlying water, also existed in the flume utilized. However, because both ends of the sediment bed were sealed off, the volume of water required for the underflow is instead driven into the bed at the upstream end and back out of the bed on the downstream end of the flume (see Figure 4.3).

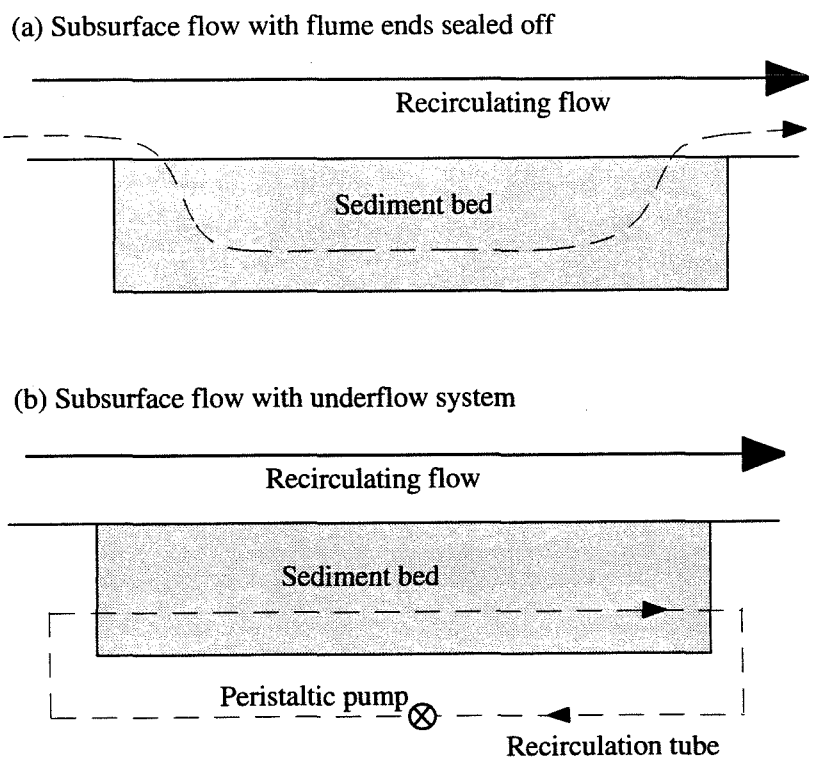

Figure 4.3. Underflow of pore-water in flume without (a) and with (b) underflow system.

To prevent this advective flow of water into and out of the bed, a recirculation system, driven by a peristaltic pump, was used to substitute for the flow of pore-water down the stream bed that would occur in an infinitely long sediment bed. The magnitude of the underflow was set to match the required flow which equals the product of the coefficient of permeability of the sediment bed, the cross sectional area of the bed and the energy slope of the flow.

4.2. CHOICE OF SEDIMENT, SORBATE AND CHEMICAL PARAMETERS

Because of the large amounts of sand and water that were used in the flume for each run and the particular environmental conditions in the hydraulics laboratory, a variety of experimental parameters needed to be considered in the process of planning the design of this experiment.

For reasons of cost and simplicity, it was desired to discard the water used in the runs (about 150 ℓ) and the water used to wash the sand (about 300 ℓ) into the sewer system.

To achieve reproducibility of experiment results, it was necessary to clean the entire mass of sand (about 250 kg) before a new experiment by acid-washing the sand in washing tubes and then transferring it into the flume. This treatment of the sand required the sediment to resist both mechanical and chemical abrasion in order to assure reproducibility of the results.

Furthermore, the environment in the hydraulics lab was somewhat less clean then could be expected if the experiment would have been performed at a smaller scale in a chemistry lab. An effort was made to keep the conditions in the experiment as close to

the conditions in a natural environment as possible while designing the experiment simply enough to be able to understand the processes in the flume. Once the basic hydraulic and chemical processes are understood, other relevant factors (colloids in the system, metal oxide and organic coatings of the surfaces, biological activity) can be added to the experimental design in future work.

4.2.1. Sediment

Because of ready availability and relative chemical purity, Ottawa and other silica sands have been used in research investigating transport processes in sediments. In an effort to more closely simulate natural river bed sediments, metal oxide coating of the sediment in the flume was considered (Edwards and Benjamin 1989 and Stahl and James 1991), but the technological requirements necessary in such a process (ability to collect developing acid fumes while heating the sand to about 100 °C) prohibit the reproducible preparation of the large amounts of sand required for this experiment. Coating of the sediment with humic materials (Burris et al. 1991) was also investigated, but the coating was found to be only partially adherent.

4.2.1.1. Physical and chemical composition

Two silica sands with different mean grain size were used in the experiments. They were supplied by Scott Sales Co., Huntington Park, CA. The chemical composition of the sands, as reported by the manufacturers (U.S. Silica, Ottawa, IL for Ottawa 30 sand, Simplot Silica Products, Overton, NV for Nevada 70 sand), is given in Table 4.1. Both sands consist mostly of SiO_2, with very small amounts of other metal oxides.

Table 4.1. Chemical composition of sediments used in this study.

Mineral	Ottawa 30 sand	Nevada 70 sand
SiO_2	99.81 %	99.04 %
Fe_2O_3	0.015 %	0.047 %
Al_2O_3	0.042 %	0.43 %
TiO_2	0.013 %	0.03 %
CaO	< 0.01 %	0.04 %
MgO	< 0.01 %	0.01 %
Na_2O	< 0.01 %	0.40 %

The sieve analyses of the sands used are shown in Figure 4.4. The coarse sand, Ottawa 30 Flintshot blasting sand, is the same sand as used by Elliott (1990). It has a geometric mean diameter of d_g = 500 μm and a geometric standard deviation of σ_g = 1.25, computed for the middle 80 % of the size distribution. Compared to a log-normal distribution, the smaller size fractions (less than about 200 μm diameter) appear to be larger than expected. Nevada 70 sand has a geometric mean diameter of d_g = 195 μm and a geometric standard deviation of σ_g = 1.54. Its distribution follows the log-normal distribution closely.

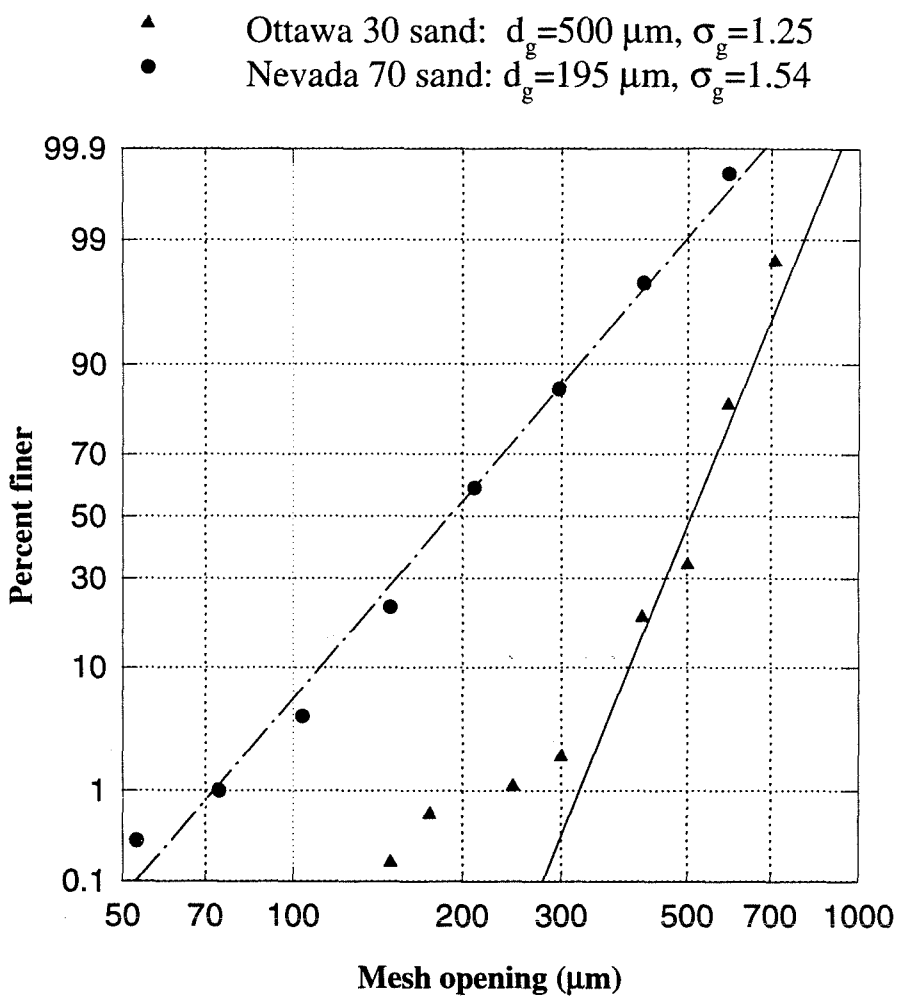

Figure 4.4. Sieve analyses of Ottawa 30 and Nevada 70 sands.

4.2.1.2. Properties in the sediment bed

Using the same procedures as Elliott (1990), the porosity and hydraulic permeability of the two sediments were determined. The porosity, θ, of the sand was determined by measuring the volume of water required to fill the pore space of 2 ℓ sediment. Dried sand was placed in a glass measuring cylinder. Then a measured volume of

water was added and the mixture was stirred and shaken vigorously to remove air bubbles from the volume. The volume of excess water was measured to determine the remaining volume of water within the pore spaces. The porosity was found to be $\theta = 0.325$ for both sands.

A falling head permeability test (Bear 1972) resulted in values of $K \cong 0.15$ cm/s for Ottawa 30 sand and $K \cong 0.04$ cm/s for Nevada 70 sand, in reasonable agreement with the empirical value given by Bear,

$$K = 6.5 \cdot 10^{-4} \frac{d_g^2 g}{\nu}, \tag{4.1}$$

which yields $K = 0.14$ cm/s for Ottawa 30 and $K = 0.025$ for Nevada 70 sand. The coefficient of permeability was found to be rather strongly dependent on the packing of the sediment.

The bulk density of the sediments was $\rho = 1.79$ g/cm^3, computed from the porosity of the sediment and the mineral density of $\rho = 2.65$ g/cm^3. These values lead to a sediment load of 5500 g/ℓ in the pore-water of the sediment bed.

The specific surface area of the sediment used in the experiments is very small. An estimate can be made by computing the surface area of spheres with a mean diameter of 500 µm. For the Ottawa 30 sand, this calculation yields a specific surface area of only 45 cm^2/g. To allow for additional surface area due to irregular grain size and pores, a larger value of 70 cm^2/g was used in all calculations. This correction is supported by dye-adsorption experiments performed by Kotronarou (1989). This value corresponds to a surface area of 4 m^2/ℓ pore-water and, using a surface density of 6 SOH-groups per nm^2, a concentration of surface groups in the pore-water of 0.4 mM.

The corresponding values for Nevada 70 sand are 120 cm^2/g specific surface area, a surface area of about 10 m^2/ℓ pore-water and a concentration of surface groups of 10 mM.

For comparison, most of the available data for metal ion adsorption onto silica was obtained by using silica gels with surface areas of 100-500 m^2/g and concentrations (sediment load) of the order of 1 mg/ℓ to 1 g/ℓ.

4.2.2. Choice of metal ions

The sorbate used in this experiment had to be relatively non-toxic in order to allow easy disposal of the large volume of waste water after each run. Organic sorbates were considered, but this approach was not pursued further because of volatility and toxicity problems. Also, the use of radiolabeled tracers was considered, but was rejected due to waste disposal problems and safety considerations.

Because metal ions are important pollutants in many rivers, mono-, bi- and trivalent metal ions were considered. Monovalent metal ions display very weak adsorption to silica surfaces, while trivalent metal ions sorb very strongly to silica. The adsorption characteristics of bivalent metal ions, ranging from relatively weak to strong, were found to be satisfactory for the purposes of this experiment. Additionally, it was desired to choose metal ions that only exist in a single oxidation state to avoid complication of the chemical processes in the system due to oxidation and reduction reactions.

The metal ions used in the experiments were chosen to exhibit a range of adsorption behavior from non-adsorbing to strongly adsorbing to the sand. Selected were lithium, calcium, magnesium, zinc and copper:

Lithium (Li^+) does not adsorb to sand under the conditions of the experiments. Lithium was used as a nonadsorbing tracer to measure the exchange of solution between the water column and the sediment bed. The hydraulic parameters of each experiment run could thus be determined by the changes in lithium concentration in the water column. Lithium serves the same purpose in the experiments in this thesis as dyes did in Elliott's experiments (1990).

Calcium (Ca^{2+}) adsorbs weakly onto sand. Magnesium (Mg^{2+}) also adsorbs weakly to sand, but somewhat stronger than calcium. Calcium and magnesium are both abundant in natural aquatic systems.

Zinc (Zn^{2+}) adsorbs rather strongly to sand. Zinc is an important metallic pollutant in many aquatic systems in the environment.

Copper (Cu^{2+}) is the most strongly adsorbing metal ion used in this study. Copper also is an important pollutant in the environment. It is the only metal ion used that can form a solid (malachite, $Cu_2(OH)_2CO_3 \cdot s$) under some of the experimental conditions in this work. All other bivalent metal ions used will form a solid (carbonate, $MeCO_3 \cdot s$) only at pH greater than about 7.5 to 8.

The distribution of the dissolved species of copper, zinc, magnesium and calcium at total concentrations of 10 μM in an aqueous system open to the atmosphere is shown in Figures 4.5 through 4.8.

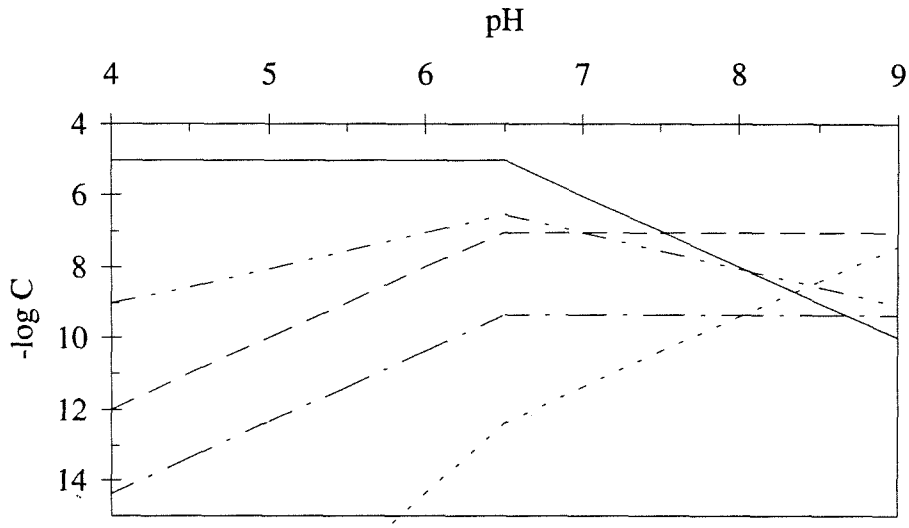

Figure 4.5. Aqueous copper species in a system open to the atmosphere.
Solid precipitation due to formation of malachite begins at pH ≅ 6.5.
— Cu^{2+} —·— $CuOH^{+}$ — — $CuCO_3$ —·— $Cu(OH)_2$ ··· $Cu(CO_3)_2^{2-}$

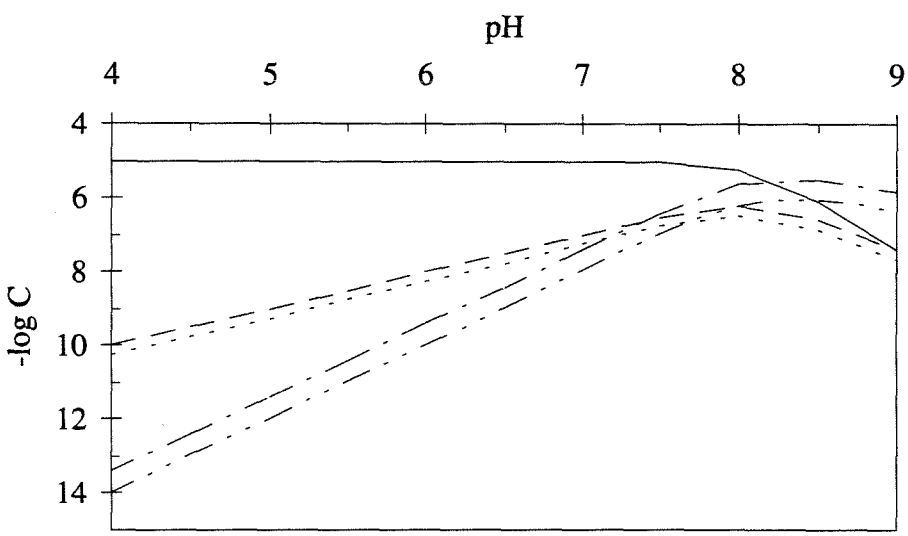

Figure 4.6. Aqueous zinc species in a system open to the atmosphere.
Solid precipitation due to formation of zinc carbonate begins at pH ≅ 7.5.
— Zn^{2+} —·— $ZnHCO_3^{+}$ — — $ZnOH^{+}$ —·— $ZuCO_3$ ··· $Zn(OH)_2$

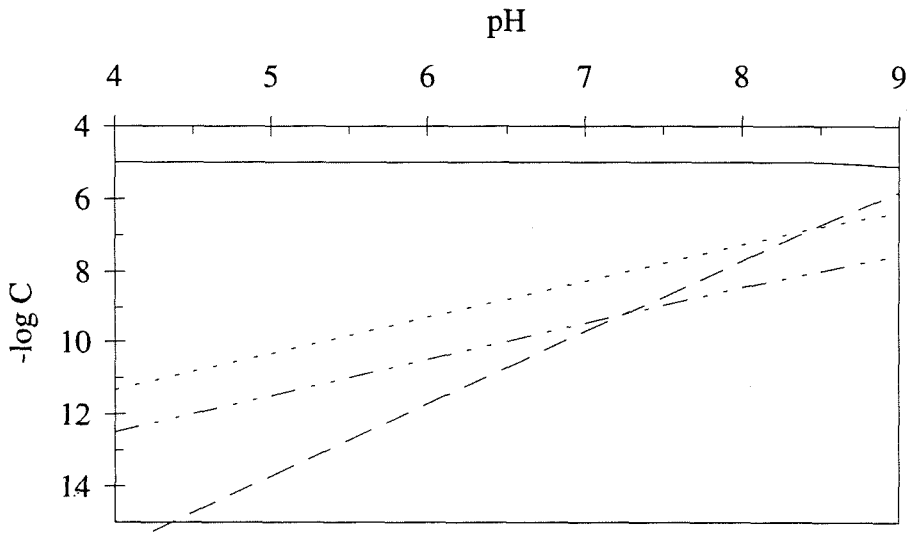

Figure 4.7. Aqueous magnesium species in a system open to the atmosphere.

— Mg^{2+} — - - — $MgHCO_3^+$ — — $ZnCO_3$ - - - $MgOH^+$

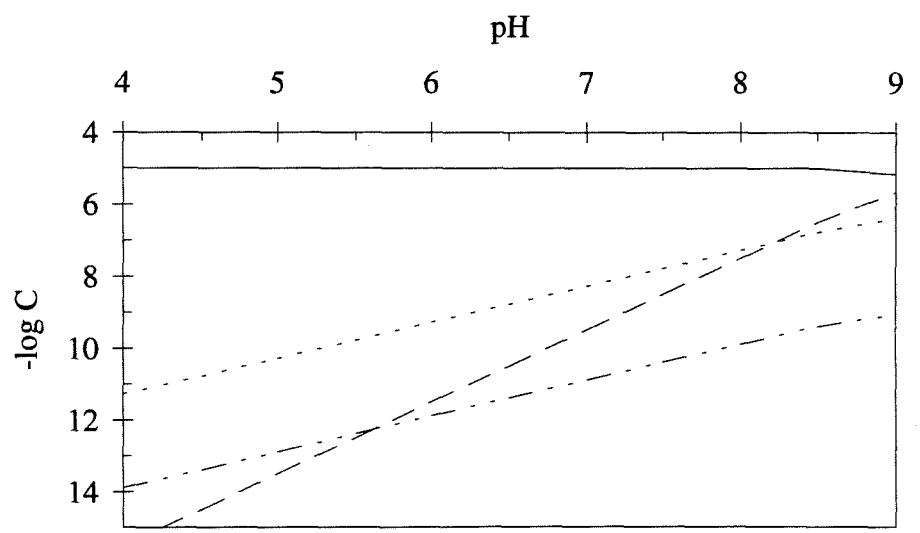

Figure 4.8. Aqueous calcium species in a system open to the atmosphere.

— Ca^{2+} — - - — $CaHCO_3^+$ — — $CaCO_3$ - - - $CaOH^+$

To verify that the metal ions do not sorb to the walls of the flume and to check for possible sources of contamination in the flume, a solution of the metal ions used in the sorption experiments was circulated in the flume for 5 days without a sand bed (see Figure 4.9). The concentrations of the tracers in the water column were chosen to be within the range of concentrations used in the flume experiments with sand bed. The aqueous concentrations remained constant within the analytical error (except for copper at pH 7 due to the precipitation of malachite), indicating that no sorption/desorption from the flume walls took place. Copper did not precipitate at pH 6.

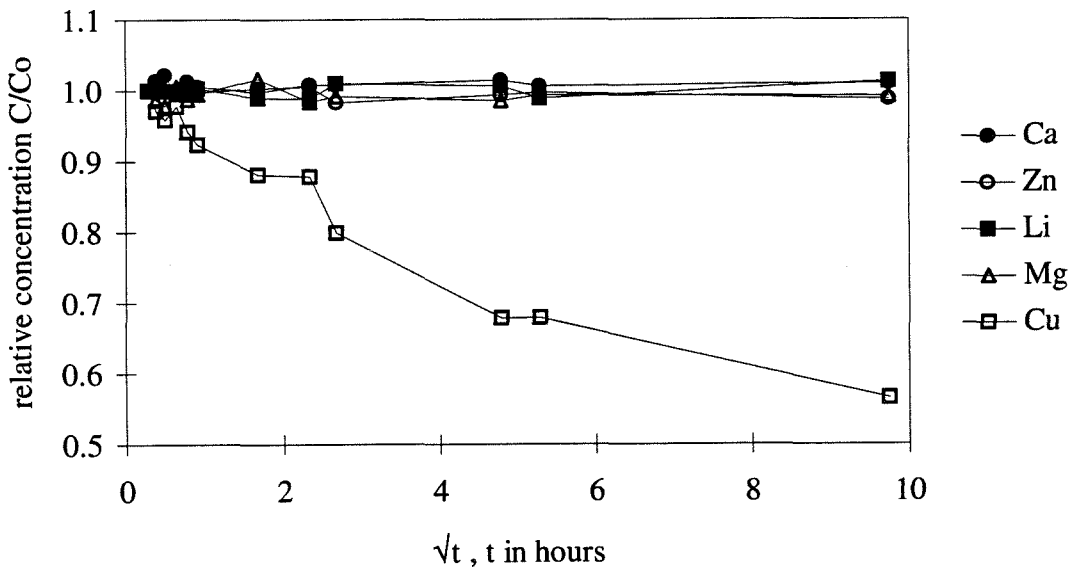

Figure 4.9. Conservation of metal ion concentrations without sand in flume (pH 7). Initial concentration of all metal ions C_0 = 10 μM.

4.2.3. Chemical composition of the system

To assure reproducibility of results, the chemical composition of the solution in all adsorption experiments needs to be controlled. The values of all controlled parameters were chosen to be within the range of naturally occurring freshwater environments. Deionized water was used in all experiments, and ionic strength electrolyte, buffer medium and adsorbing metal ions were then added to create the desired chemical conditions.

4.2.3.1. Ionic strength

The magnitude of the ionic strength influences the electrostatic conditions of the adsorption process, so that changes of I will have effects on the partitioning of the metal ions. The ionic strength of the solution (1 mM using NaCl) was chosen to be within the range of the ionic strength of most natural river and groundwater systems (0.1 to 10 mM).

4.2.3.2. Buffering

The pH of the solution has a very large influence on the fraction of the metal ion adsorbed to the sand. At pH of less than 4, the metal ions present will be in aqueous solution. The amount adsorbed will increase with increasing pH, and a large fraction of the bivalent metal ions will be adsorbed to the sediment at about pH 8.

Virtually every natural water system is buffered. In the presence of a buffer, a solution expresses a certain resistance to pH changes as chemical reactions in the system take up or release protons. For example, during the adsorption of metal ions at silica sur-

faces, protons are released which would lower the pH of a solution if no buffer was present.

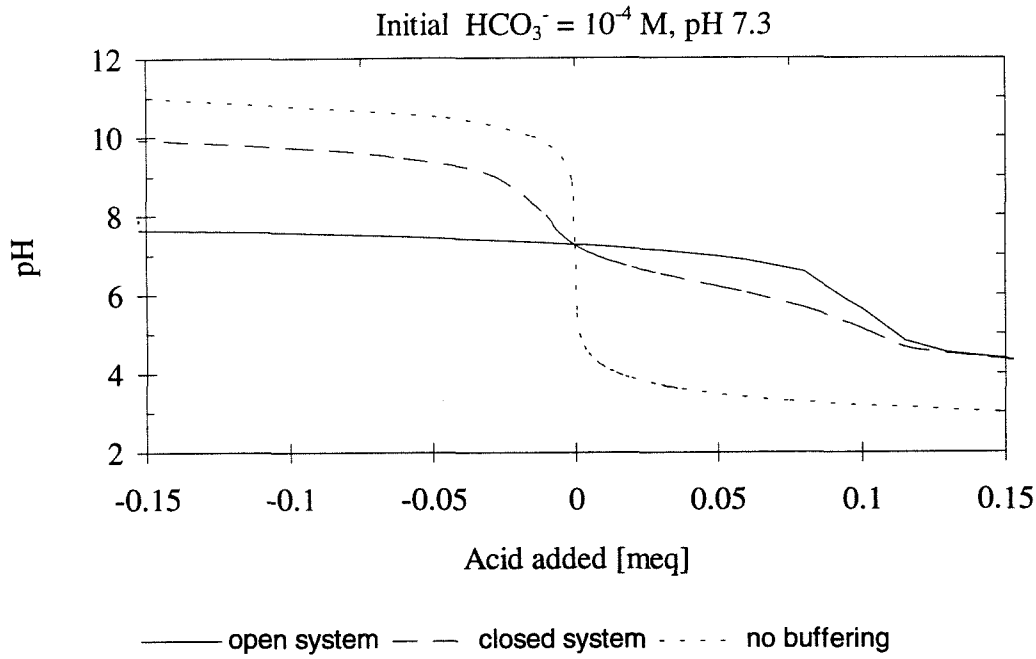

Figure 4.10. Titration curves of bicarbonate solutions in open and closed systems. In this plot, a smaller slope of the titration curve indicates higher buffering capacity.

The most common buffer in natural aquatic systems is bicarbonate (HCO_3^-). Therefore, this was also the buffer chosen for this experiment (as $NaHCO_3^-$). While a bicarbonate buffer works best in a system open to the atmosphere (like the water column), its buffering capacity is still very significant in a closed system (like the sediment bed). The buffering of a bicarbonate solution in open and closed systems compared to an aqueous system without any added buffer is shown in Figure 4.10.

4.3. BEAKER EXPERIMENTS

To quantify the surface adsorption of the metal ions onto sand, a series of experiments was conducted on a much smaller scale. The experiments were initially performed in beakers which were placed on a shaker table to keep the system well mixed. The mixing of overlying and pore-water in these experiments was found to be very slow.

Improved mixing with more consistent results was accomplished by using a plastic bottle which was kept at about 45^{o} angle and rotated around its axis at about 4 rpm, a design similar to a concrete mixer. The sand in the bottle was constantly turned over, allowing rapid exchange of pore-water and overlying water. The volume of solution used in these experiments was about 500 mℓ, the sand mass was about 300 g.

4.4. ANALYSIS

Concentration measurements of the aqueous zinc concentration for the first four runs were performed with the flame atomic absorption spectrometer in the Keck environmental chemistry laboratory (Varian Techtron AA6). The flame AA is especially sensitive for zinc. While this instrument only allows the analysis of one element at a time, a large number of samples can be analyzed in a short period. This allows samples to be analyzed even during the process of an experiment. Concentration values are reproducible with deviations of less than 10% in repeated analyses. The optimal working range for zinc is 1 μM to 30 μM (60 ppb to 2 ppm), sufficient for the zinc concentrations in the experiments (about 1 ppm at the beginning of a run).

In the experiments beginning with Run 5, the metal ion concentrations were measured using an inductively coupled plasma mass spectrometer (ICP-MS, Perkin-Elmer Elan 5000). Because of the ability to measure concentrations of many metal ions simultaneously with the ICP-MS, the utilization of this instrument allowed the use of more than one sorbate in the experiments. Concentration measurements using the ICP-MS are also reproducible with deviations of less than 10%. The sensitivity of the ICP-MS is very high for zinc, copper, magnesium and lithium (1 ppb or lower) and about 100 ppb for calcium, in all cases sufficient for the desired concentrations in the experiment. Reference concentration standards were prepared from commercial 1000 ppm atomic absorption standards.

4.5. SEDIMENT PREPARATION

Before each experiment (except Run 2), metal ions adsorbed to the sediment in the previous run were removed from the surfaces. This was accomplished by washing the sand in acid solution (pH $\cong$ 3.5) for a period of about 12 hours. A pH of 3.5 was found to be sufficiently acidic to desorb the metal ions used in the experiments from the sand without causing modifications to the surface of the sand.

A special washing apparatus, consisting of four lucite tubes of 20 cm diameter and 180 cm height, was used for this purpose (Figures 4.11 and 4.12). The sediment was loaded into the tubes using a scoop. Hydrochloric acid was added to deionized water in a reservoir, then pumped through a cartridge filter to remove fines (pore diameter 5 μm), and upward through the washing tubes, fluidizing the sand. Flow straightening cones on the bottom of the washing tubes prevented the development of preferential flow patterns in the tubes, ensuring that the entire volume of sand was fluidized. The sand bed was ex-

panded by about 50%, keeping the top of the fluidized sand below the outlet at the top of the tubes. The acid solution exiting at the top of each washing tube was drained back into the reservoir. A volume of about 300 ℓ acid solution was used to clean about 120 kg of sand.

To assure that there were no metal ions adsorbed to the sand and to remove the fines from the sediment, both Ottawa 30 and Nevada 70 sands were treated initially by repeated acid washing at pH 3 for one day, alternated with sodium bicarbonate rinses. Four such cycles were done for the Ottawa 30 sand, six cycles for the Nevada 70 sand. Much more fines were removed from the Nevada 70 sand.

After acid washing the sediment, an overnight rinse with deionized water and bicarbonate buffer was performed to return the surface of the sand to the charge conditions in a neutral aqueous system. The sand was then dumped into storage bins or put back into the flume.

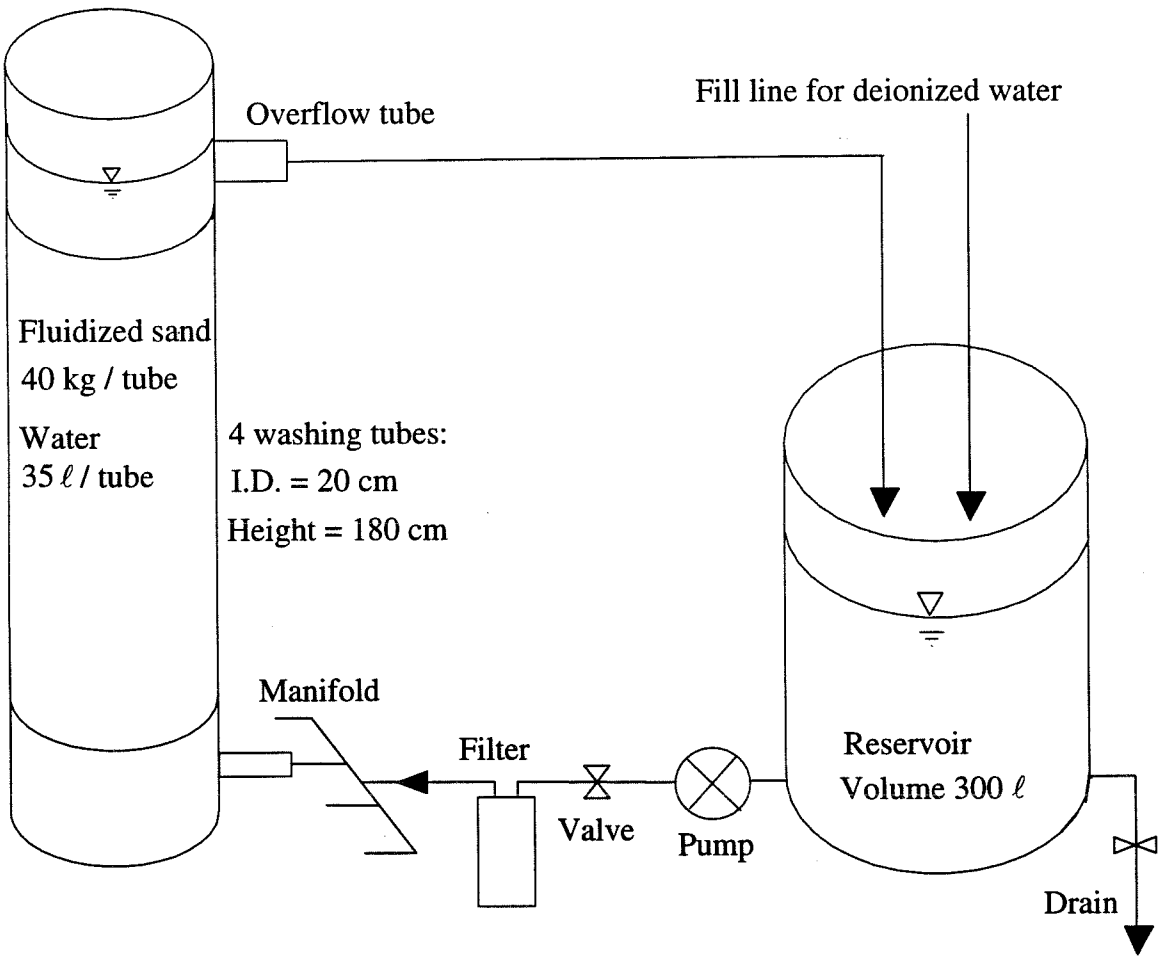

Figure 4.11. Schematic of washing apparatus.

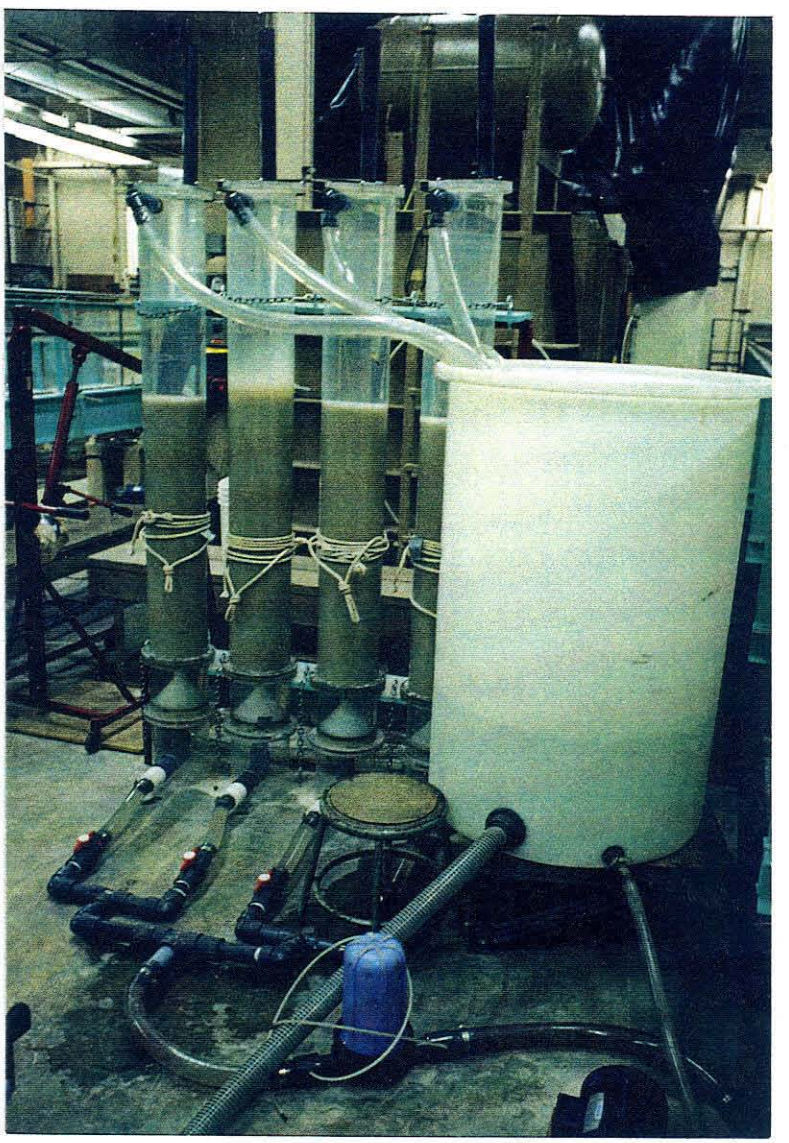

Figure 4.12. Photograph of washing apparatus. The pump is only partially visible.

4.6. EXPERIMENTAL PROTOCOL

4.6.1. Flume experiments

4.6.1.1. Experiment preparation

Before each run, the sediment was twice acid washed in the cleaning apparatus (pH 3.5) to remove potentially adsorbed metal ions from the sand. After each washing cycle, a rinse with a sodium bicarbonate solution followed. After cleaning, the sand was dumped into storage containers and later scooped into the flume using a plastic scoop.

To prepare the flume experiment, deionized water was put into the flume to about bed level. The ionic strength was adjusted to 1 mM using sodium chloride. Then, the pH of the system was adjusted to the desired value for the following experiment using sodium bicarbonate.

After adjusting the chemical parameters in the water, the sand was scooped into the flume. Because of the water already in the flume, relatively little air was contained in the sediment bed. To remove the remaining air, the sand was manually swirled with the flume running a low speed. After swirling, the sand bed was leveled to the mean bed surface level and compacted by manually thumping the side walls of the flume.

The bedforms in the flume were then created. For runs with naturally formed bedforms, the flume was run until the bedforms created by the flow had developed fully and did not change statistically with time. For runs with artificially created bedforms, the flume was run at a speed just below the initiation of motion of the sand. Then, the flow in the flume was increased locally by lowering a plastic plate into the water and thus reducing the area of the flow. The increased flow velocity caused scour in the bed, the sand

was transported a distance downstream and a dune was formed. Bedform height and length could be controlled by raising and lowering the plate in the flow. Variations in bedform height and wavelength were much smaller for artificially created bedforms then for naturally formed bedforms, especially when Ottawa 30 sand was used. For this reason, most experiments were performed with artificially formed ripples.

Then, the water in the flume was drained to bed level and refilled with deionized water to remove possible fines created by the addition of the sand, the following swirling, the creation of the bedforms, and to assure as small as possible metal ion background in the experiment. With the flume running slowly to allow mixing, the ionic strength and pH were then readjusted to the previous values.

The slope of the flume was then adjusted so that the surface of the water was parallel to the mean bedform level, assuring constant depth over the full length of the flume. The slope of the flume was determined by measuring the water surface level at several points with the flume both running and stopped. Then, the difference between these two measurements was calculated to determine the slope of the experiment run. The energy slope was assumed to be equal to the water surface slope. Because of end effects in the inlet and outlet sections and the relatively short length of the flume, the slope measurements were only accurate to about a factor of 2. The flow in the flume was measured using an orifice meter and a calibrated mercury manometer, the measurement error for flow measurements was about 2%.

Using the calculated slope and the sediment permeability, the required underflow volume was determined as the underflow velocity times three quarter of the bed depth. Concluding the preparation of an experiment run, the underflow system was then started.

4.6.1.2. Flume adsorption experiments

The basic approach in conducting the flume runs is to first establish the desired experimental conditions (flow, bedforms, and chemical parameters). Then, measured quantities of metal ion stock solutions (10 mM concentrations of Zn, Cu, Ca, Mg and Li at low pH) were prepared and the desired quantities added to the recirculation system (defined as t = 0). To aid initial mixing and achieve uniform initial concentration in the flume, the metal ion solution was slowly added to the flume over the period of one full circulation of the solution in the flume, typically about one minute.

To compensate for evaporation losses, deionized water was added to the flume daily. The amount of water typically added was about 750 mℓ/day, less than 1% of the volume of water above the bed level.

Water samples from the overlying solution were taken by dipping test tubes into the overlying water in the flume. Initially (in the first 10-15 minutes) samples were taken at three or four positions over the length of the flume to determine the state of mixing in the water column. After the initial period, samples were taken at two positions in the flume. The measured concentrations between these sample varied only by a few percent. The period between sampling times increased from a few minutes (in the beginning of the experiment) to once or twice daily (at the end of a run).

Pore-water samples were taken by inserting a 30-gauge Hamilton needle through the rubber ports in the side wall of the flume at various depths and times and drawing 500 μℓ of pore-water into a plastic syringe. The vertical row of ports (see Figure 4.1) was located about 2 m from the beginning of the deep sand bed. The pore-water samples were then diluted by adding 6 parts deionized water to 1 part of pore-water to obtain an analyzable volume of solution.

Every water sample was acidified with nitric acid to preserve the samples until measurement on the ICP-MS (or flame AA in the first 4 runs). All samples were measured at one time to reduce errors. Standards of known concentrations were measured frequently to detect and correct for possible changes in the calibration and drift of the instrument.

After ending a run, the bedform parameters in all runs were determined by measuring the crest-to-crest distance between neighboring dunes and crest-to-trough height of every dune through the transparent sidewalls of the flume. However, the results obtained by this method were verified by taking bedform profiles in the centerline of the flume in three runs. Using a point gauge, the bedform profile was measured every centimeter over the middle section of the flume. The bedform heights and wavelengths obtained by the profile method were identical to the values measured through the sidewall of the flume.

4.6.1.3. Flume desorption experiments

Desorption experiments were performed after the end of the adsorption phase for some of the runs. The overlying water was drained slowly and replaced with deionized water. Only the solution in the pore space remained in the flume. Then, pH and ionic strength in the water column were readjusted to the values of the previous experiment. Mixing of ionic strength and buffering media in the solution was achieved by running the flume slowly for a short time. The desorption run was then started by bringing the flume to the speed of the previous run. Samples from the water column were taken as in all other runs.

The bedform shape, water depth, slope and flow velocity were identical to the previous run to allow easy comparison of the results from the adsorption run and the following desorption run.

4.6.2. Batch experiments

Batch experiments were performed in an open, tilted 1 ℓ plastic bottle that was rotated at a 45^{o} angle. The sand used in batch experiments was treated in the same manner as the sand used in flume experiments. The mass of sand used was weighed dry on an electronic balance, the volume of solution in the batch experiments was determined using a graduated cylinder. Small volumes of stock solutions were measured using a calibrated pipettor.

The experiments were conducted in the following way: Deionized water was filled into the bottle and the desired chemical composition of the solution was created. Then, a measured mass of sand was added to the bottle and the rotation motor was started.

Initial concentrations of the solutions were determined before adding the sand to the beaker. In the titration experiments, the sand was added and the solution was acidified to pH 3. After equilibration time, a sample was taken. The concentration of this sample was used as initial concentration.

The experimental results are presented in the following chapter.

5. EXPERIMENTAL RESULTS AND DISCUSSION

In this chapter, the results of the batch experiments and flume runs are presented and discussed. First, the results of the batch experiments investigating partitioning and adsorption time scale are presented, then the experimental data for the flume runs are summarized, and finally the results of the individual runs are given.

5.1. BATCH EXPERIMENTS

5.1.1. Batch adsorption experiments

The adsorption of the metal ions (copper, zinc, magnesium, calcium, and lithium) was studied in batch adsorption experiments. The adsorption of zinc onto silica was investigated thoroughly, and partitioning experiments were also performed with the other metal ions. The fraction adsorbed to the sand surface, the corresponding retardation coefficients derived form the adsorption of the metal ions onto Ottawa 30 sand in the batch experiments, and the calculated adsorption densities are given in Figure 5.1 for the pH values used in this study.

Lithium did not display any adsorption to the sand used in this work, justifying its use as a conservative tracer. The adsorption of the other metal ions increased in the order $Ca^{2+} < Mg^{2+} < Zn^{2+} < Cu^{2+}$. The same order of adsorption strength was observed in the flume experiments.

In the runs with more than one bivalent metal ion, competition between the adsorbing metal ions is possible and can lead to changes in the observed partitioning

coefficients. This effect was indeed observed in Run 12. The effects of competition on the adsorption kinetics of the metal ions is discussed in Section 5.1.3.

Table 5.1. Fraction adsorbed, f_a, retardation coefficient, R, and adsorption density, Σ, for metal ion adsorption onto Ottawa sand as observed in batch experiments.

	pH 7.2			pH 6.2		
	f_a [%]	R	Σ [moles/m^2]	f_a [%]	R	Σ [moles/m^2]
Copper	(precipitates)			94	$\cong 16$	$\cong 3.3 \cdot 10^{-6}$
Zinc	90 ± 3	11 ± 2	$\cong 3.1 \cdot 10^{-6}$	80 ± 10	5 ± 2	$\cong 2.7 \cdot 10^{-6}$
Magnesium	$\cong 75$	$\cong 4$	$\cong 2.6 \cdot 10^{-6}$	$\cong 66$	$\cong 3$	$\cong 2.2. \cdot 10^{-6}$
Calcium	$\cong 66$	$\cong 3$	$\cong 2.2 \cdot 10^{-6}$	$\cong 50$	$\cong 2$	$\cong 1.7 \cdot 10^{-6}$
Lithium	< 5	< 1.05	$< 1.7 \cdot 10^{-7}$	< 5	< 1.05	$< 1.7 \cdot 10^{-7}$

5.1.2. Titration experiments

To determine the pH-dependency of zinc adsorption onto the flume sediment, a series of titrations was performed. Figure 5.1 shows the results of four separate titration experiments at zinc concentrations between 5 and 25 μM, and the fit of a Stern model using the surface complexation program HYDRAQL (Papelis et al. 1988).

The constants (see Chapter 3) used in Figure 5.1 fit are:

$$K_{a1}^{int} = \frac{[\equiv SiOH][H^+]}{[\equiv SiOH_2^+]} e^{-\frac{F\Psi_0}{RT}}, \log K_{a1}^{int} = 2.5 \tag{5.1}$$

$$K_{a2}^{int} = \frac{[\equiv SiO^-][H^+]}{[\equiv SiOH]} e^{-\frac{F\Psi_0}{RT}}, \log K_{a2}^{int} = -6.5 \tag{5.2}$$

$$K_{1,Zn}^{int} = \frac{[\equiv SiOZn^+][H^+]}{[\equiv SiOH][Zn^{2+}]} e^{\frac{F\Psi_0}{RT}}, \log K_{1,Zn}^{int} = -6.8 \tag{5.3}$$

$$K_{2,Zn}^{int} = \frac{[\equiv SiOHZn^{2+}]}{[\equiv SiOH][Zn^{2+}]} e^{\frac{2F\Psi_0}{RT}}, \log K_{2,Zn}^{int} = 0.0 \tag{5.4}$$

Also included in the model is the adsorption of sodium ions to the surface. The adsorption constant for sodium binding weakly in the outer adsorption plane is very small (Young 1982, and Dugger et al. 1964):

$$K_{1,Na}^{int} = \frac{[\equiv SiONa^+][H^+]}{[\equiv SiOH][Na^+]}, \log K_{1,Na}^{int} = -9.0 \tag{5.5}$$

Other parameters required in the Stern model are the double layer capacity and the surface area of the sorbent per unit volume solution. The values used are:

$$\begin{aligned} &\text{Double layer capacity: } C_d = 1 \text{ F/m}^2 \\ &\text{Surface area of sorbent: } A_s = 40 \text{ m}^2/\ell. \end{aligned} \tag{5.6}$$

A sensitivity analysis was performed by varying the constants and parameters in the model by an order of magnitude in both directions. The relative effect of the magnitude of the constants and parameters on the zinc adsorption isotherm was found as:

Very small effect:	$K^{int}_{1,Na}, K^{int}_{a1}$
Little effect:	$K^{int}_{1,Zn}$, C_1
Some effect:	K^{int}_{a2}, A_1
Strong effect:	$K^{int}_{2,Zn}$

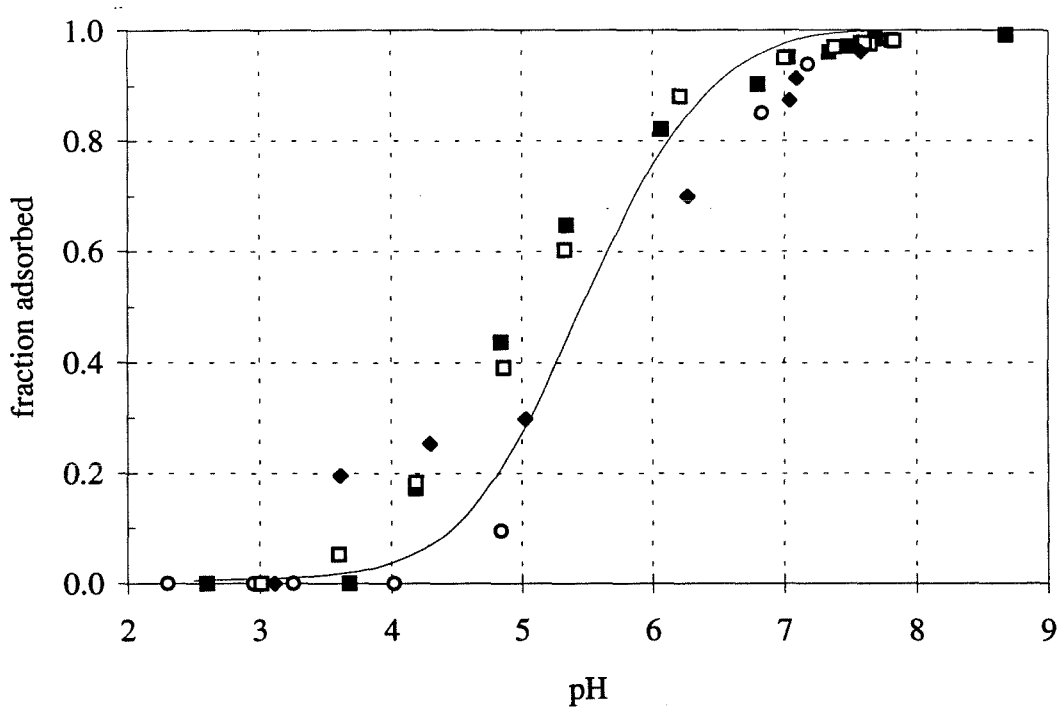

Figure 5.1. Zinc adsorption onto sand. Stern model (C_1 = 1 F/m^2) fitted to data.

■ Zn^{2+}, concentration 5 μM

□ Zn^{2+}, concentration 10 μM

○, ◆ Zn^{2+}, concentration 20 μM.

Thus, the adsorption to the surface without proton release appears to be the most important adsorption process of zinc adsorption to sand, with the proton exchange reaction playing only a minor role. A similar observation was made by Dzombak and Morel (1987) for calcium adsorption onto hydrous ferric oxide (HFO).

The raw data obtained in the titration experiments is shown in Appendix A.

5.1.3. Adsorption kinetics

To investigate the adsorption kinetics of zinc and calcium, batch kinetic experiments were performed. The results are shown in terms of the relative partitioning coefficient $k_{p_{rel}}$, the partitioning coefficient at the observed time divided by the final equilibrium partitioning coefficient.

Figure 5.2 shows the adsorption kinetics of zinc and calcium onto Ottawa 30 sand with only the ionic strength medium and buffer medium present. The equilibrium time scale (90% value) in these experiments was of the order of 10 minutes.

In Figure 5.3, the adsorption kinetics of copper ions in the presence of zinc ions is shown. The adsorption time scale for copper in the presence of zinc ions adsorption is about 30 minutes. The reverse case, the adsorption of zinc in the presence of copper is shown in Figure 5.4. It was found that the adsorption kinetics of zinc is more than 10 times slower due to the presence of the copper ions in solution, since the equilibrium time scale is now of the order of 140 minutes. This effect is likely due to competition at the surface.

Thus, adsorption kinetics of a metal ion can be influenced by the presence of another competing metal ion. However, even at the longer equilibration time scales, the equilibrium partitioning model appeared to be appropriate to describe the observed results.

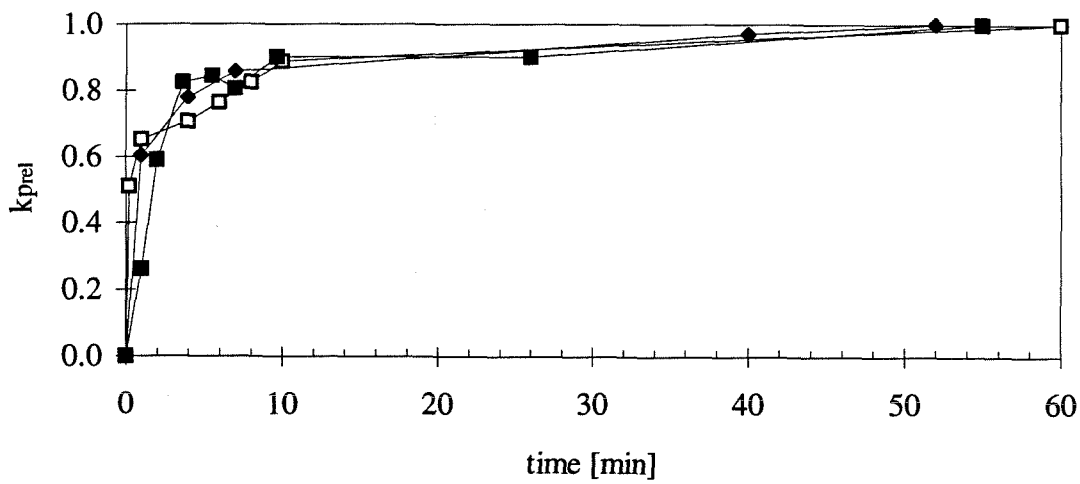

Figure 5.2. Adsorption kinetics of zinc and calcium onto silica.

- ■ Zn^{2+}, concentration 22 µM
- □ Zn^{2+}, concentration 18 µM
- ◆ Ca^{2+}, concentration 35 µM.

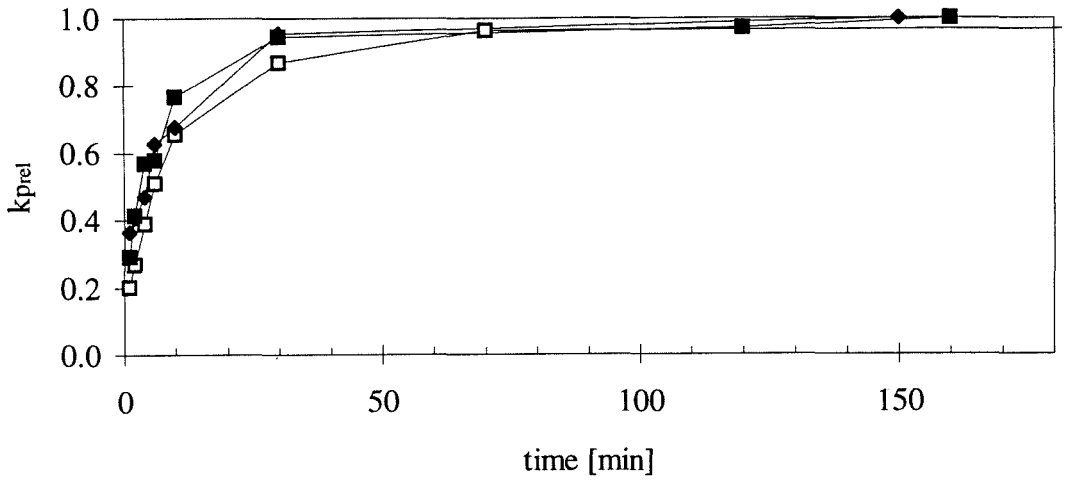

Figure 5.3. Adsorption kinetics of copper onto silica with zinc competition.
□, ■, ◆: 11 μM Cu^{2+} in 12 μM Zn^{2+} background.

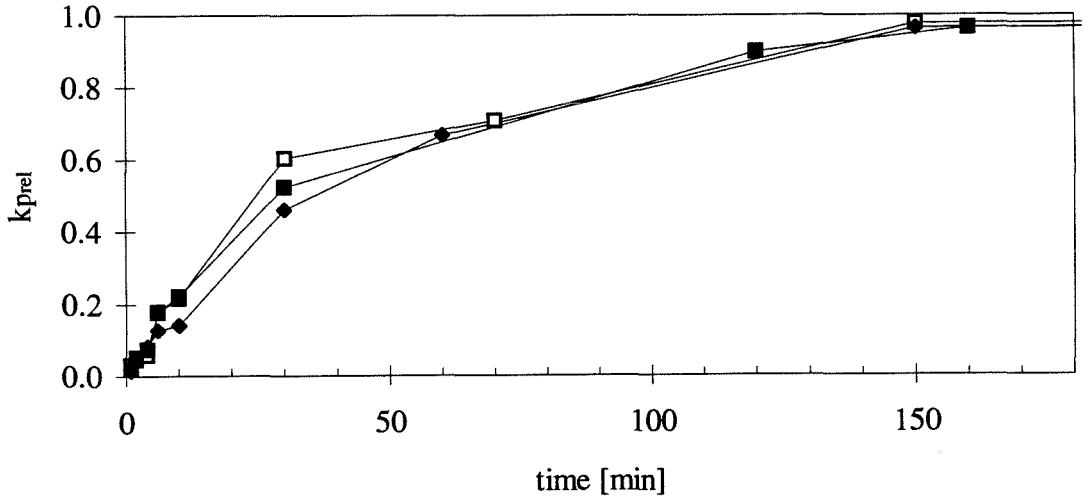

Figure 5.4. Adsorption kinetics of zinc onto silica with copper competition.
□, ■, ◆: 12 μM Zn^{2+} in 11 μM Cu^{2+} background.

5.2. FLUME EXPERIMENTS

5.2.1. Flow data

A total of 15 flume runs were performed in this work. Three of the runs were moving bedform runs (Runs 3, 4, 15). Of the remaining stationary bedform runs, all but two (Runs 1 and 2) were performed with artificially formed ripples. Furthermore, two of the runs were performed with the Nevada 70 (N70) sand (Runs 11,15), the rest with Ottawa 30 (O30) sand.

A summary of the experiment parameters in the flume runs is given in Table 5.2. For the convenience of the reader, the notation used in the table is listed below:

C_0	initial concentration of a specific metal ion in moles/volume solution after initial flume mixing
d	mean water depth
d'	effective water depth (total recirculating water volume/bed surface area)
f	friction factor = $8gr_hs/U^2$
f_b	bed friction factor (see explanation in text)
H	mean bedform height (trough to crest)
h_m	calculated piezometric pressure head (by Equation 3.7)
k	bedform wavenumber ($2\pi/\lambda$)
Q	recirculating water discharge in flume
Re	flow Reynolds number, $Re = 4Ur_h/\nu$
s	slope of water surface ≈ energy slope (uniform flow)
U	flow velocity of flume water over the bed = Q/(d·w), width w = 15.24 cm
u^*_b	normalized bedform velocity = u_b/u_m

u_b	measured bedform velocity (see explanation in text)
u_m	pore-water scaling velocity = kKh_m
t_p	pumping time scale = $(k^2Kh_m)^{-1}$
t_t	turnover time scale = λ/u_b
α	correction factor for parameter group 'Kh_m' = (fitted Kh_m)/(calculated Kh_m)
λ	mean bedform wavelength
Γ_p	adsorption equilibrium number (pumping model) = $t_{ads}k^2Kh_m$
Γ_t	adsorption equilibrium number (turnover model) = $t_{ads}u_b/\lambda$

The single basic fitting variable needed for comparison of the model of Chapter 3 to the observed flume results for bed uptake versus time is represented by the parameter α in Table 5.2.

As previously discussed in Section 3.2.1.1, the time normalization of the flux into the bed depends on the pore-water scaling velocity u_m. The pore-water scaling velocity is calculated from the following three parameters: bedform wavenumber $k = 2\pi/\lambda$, hydraulic permeability of the sediment K, and driving pressure head h_m (calculated from Equation 3.7). Of those parameters, only the wavenumber k can be measured accurately, at least for artificially formed ripples. However, there can be significant errors in the value of the hydraulic permeability K and the empirical formula for the piezometric pressure head h_m.

The two parameters K and h_m always appear grouped together in the model. Thus, a possible error in the pore-water pumping velocity can be associated with the parameter group 'Kh_m'. The value of Kh_m can be also derived from the data in flume experiments: if the conservative tracer lithium is used in the experiment, the pore-water scaling velocity u_m can be determined by fitting the pore-water advection model (without

adsorption) to the lithium data. The factor Kh_m can then be derived by dividing u_m by the bedform wavenumber k. *This method was used in all runs following* Run 4. *In the* absence of lithium (Runs 1 to 4), Kh_m can be found by fitting the model to the initial rate of exchange of pollutant between water column and sediment. The 'initial stage' can be defined as $t^*/(\theta R) < 1$. In the initial stage of the experiment, pollutant will be transported only into the bed. No pollutant will already have traveled far enough through the bed to be released again into the water column. Thus, the initial exchange of tracer between the water column and the bed does not depend on the partitioning of the tracer. Both methods yield the same value, but the use of the lithium data allows a better fit because of the larger number of data points that can be used for the fitting process.

The deviation between measured and calculated values of Kh_m is then expressed by the correction factor α, defined as the ratio of the fitted value of the group Kh_m divided by the calculated value for Kh_m. The same correction factor for Kh_m is applied to the mass exchange models for all metal ions in one run.

The value of the correction factor α is given in Table 5.2. Possible deviations between fitted end calculated values can arise from:

1. The empirical nature of the pressure head calculation formula (Equation 3.7). The formula is based on a relatively small number of pressure measurements over bedforms of one triangular shape, whereas the bedforms in this study have various different shapes. We do not know how h_m varies with bedform shape or wavelength/depth ratio.

2. Variations of the hydraulic permeability of the sediment between different runs. In permeability experiments, the hydraulic permeability of the sediment

was found to be very dependent on the packing of the sediment in the flume. Because the packing of the sediment was achieved by thumping on the side of the flume, it is likely that some differences between the actual hydraulic permeabilities in different runs exist.

Despite these possible sources of variation, the value of the correction factor α varied only between 1.0 and 2.0 (see Table 5.2), with the largest deviation occurring for Nevada 70 sand, which has a smaller hydraulic permeability. Thus, it can be assumed from the observations made in this work that the calculated value of kKh_m is a good approximation of the true pore-water Darcy velocity.

The bed friction factor f_b in the flume was calculated from the observed friction factor f for the overall flow and the flume wall friction factor f_w, which was measured as $f_w = 0.040$ (w is the width, d the depth of flow), by the relation for overall shear balance:

$$(2d + w) \cdot f = 2d \cdot f_{wall} + w \cdot f_b \text{ , thus} \tag{5.7}$$

$$f_b = \frac{(2d + w) \cdot f - 2d \cdot f_{wall}}{w}. \tag{5.8}$$

The friction factor is only given as a reference; it is not used in any calculation. There is also a relatively large error in the friction factor measurements because a small slope (about $5 \cdot 10^{-4}$) had to be measured over a short distance (about 3 m), resulting in an effective drop of water level elevation of only about 1.5 mm. Furthermore, due to end effects in the flume and changes in the water level over the bedforms, the mean water level at a certain point in the flume was difficult to determine, leading to possible additional errors.

Run	Bedforms	Sand	s ($\cdot 10^4$)	pH	Ion(s)	C_0 [μM]	H [cm]	λ [cm]	k [cm^{-1}]	d [cm]	d' [cm]	d'/λ
1	Ripples (n)	O30	4.0	7.1	Zn^{2+}	5	1.75	19.7	0.32	6.6	13.0	0.66
2	Ripples (n)	O30	4.0	7.0	Zn^{2+}	18	1.75	19.7	0.32	6.6	13.0	0.66
3	Ripples (n)	O30	8.7	6.9	Zn^{2+}	8.5	2.44	22.7	0.28	7.2	13.8	0.61
4	Ripples (n)	O30	40	6.8	Zn^{2+}	19	1.40	20.0	0.31	5.8	12.0	0.60
5	Ripples (a)	O30	5.9	7.0	Ca^{2+}, Li^{+}	30,30	3.18	21.9	0.29	9.0	16.1	0.73
6	Ripples (a)	O30	4.6	7.3	Zn^{2+}, Li^{+}, (Ca^{2+})	16,120,60	2.98	20.6	0.31	10.1	17.5	0.85
7	flat bed	O30	3.1	7.1	Ca^{2+}, Li^{+}	25,10	0.00	∞	0.00	4.9	10.9	-
8	Ripples (a)	O30	2.5	7.3	Zn^{2+}, Li^{+} (Ca^{2+})	24,100,100	3.57	24.0	0.26	11.5	19.3	0.80
9	Ripples (a)	O30	2.5	7.3	Zn^{2+}, Li^{+} (Ca^{2+})	all 0	3.57	24.0	0.26	11.5	19.3	0.80
10	Ripples (a)	O30	4.4	6.1	Zn^{2+}, Ca^{2+}, Li^{+}	18,37,55	3.18	18.6	0.34	10.5	18.0	0.97
11	Ripples (a)	N70	1.8	7.3	Zn^{2+}, Li^{+}	14,80	3.05	27.3	0.23	8.8	15.8	0.58
12	Ripples (a)	O30	5.3	7.3	Zn^{2+},Cu^{2+},Ca^{2+},Mg^{2+},Li	10,10,10,10,30	2.07	21.0	0.30	6.7	12.9	0.61
13	Ripples (a)	O30	5.3	7.1	Zn^{2+},Cu^{2+},Ca^{2+},Mg^{2+},Li	all 0	2.07	21.0	0.30	6.7	12.9	0.61
14	Ripples (a)	O30	5.3	6.0	Zn^{2+},Cu^{2+},Mg^{2+},Li^{+}	10,10,10,20	2.18	19.2	0.33	6.8	13.0	0.67
15	Ripples (n)	N70	20	7.0	Zn^{2+},Mg^{2+},Li^{+}	10,10,20	2.00	15.5	0.33	7.8	14.6	0.94

Table 5.2. Experimental parameters. Ions in parenthesis denote background ions. Ripples (n): naturally formed ripples. Ripples (a): artificially formed ripples. Temperature in all runs 21±1 °C.

Run	Q [cm^3/s]	U [cm/s]	Re ($\cdot 10^{-3}$)	h_m [cm H_2O]	α	u_m [cm/min]	f	f_b	u_b [cm/min]	u^*_b	t_p [min]	Γ_p	t_t [min]	Γ_t
1	1100	11.2	16.1	0.023	1.4	0.093	0.088	0.130		-	47	0.4	-	-
2	1100	11.2	16.1	0.011	1.0	0.029	0.088	0.130	-	-	99	0.2	-	-
3	2550	23.6	35.6	0.070	1.1	0.159	0.045	0.050	0.07	0.14	20	1.0	324	0.1
4	4080	46.9	63.0	0.280	-	0.760	0.047	0.052	10.2	4.6	4	4.8	1.9	10.
5	1985	14.7	24.7	0.033	1.0	0.086	0.088	0.145	-	-	40	0.5	-	-
6	1671	11.0	19.5	0.016	1.0	0.045	0.128	0.246	-	-	72	0.3	-	-
7	980	13.3	16.2	-	-	-	0.040	0.040	-	-		-	-	-
8	1480	8.6	16.1	0.010	1.1	0.023	0.131	0.271	-	-	164	0.1	-	-
9	1480	8.6	16.1	0.010	1.0	0.023	0.131	0.271	-	-	164	0.1	-	-
10	1507	9.6	17.3	0.013	1.0	0.040	0.165	0.340	-	-	74	0.3	-	-
11	990	7.5	12.5	0.017	2.0	0.019	0.108	0.188	-	-	463	0.04	-	-
12	1165	11.6	16.9	0.032	1.7	0.146	0.109	0.171	-	-	39	0.5	-	-
13	1165	11.6	16.9	0.032	1.6	0.146	0.109	0.171	-	-	39	0.5	-	-
14	1188	11.7	22.9	0.032	1.7	0.162	0.109	0.172	-	-	32	0.6	-	-
15	2375	20.3	41.4	0.053	-	0.042	0.144	0.252	0.29	1.1	72	0.3	53	0.4

Table 5.2. Experimental parameters (continued).

5.2.2. Bedform profiles

5.2.2.1. Stationary bedform profiles

The reported bedform height, wavelength and velocity given in Table 5.2 were determined by measuring the crest-to-crest spacing and the crest-to-trough height for all ripples through the sidewalls of the flume and averaging over these values. To verify the accuracy of the measurements of bedform height and wavelength, bedform profiles using a point gauge were taken in three of the runs with stationary, artificially formed ripples and one run with naturally formed ripples. It can be seen that the artificially formed ripples (Figures 5.5 through 5.7) are fairly regular with about equal spacing and relatively small variations in height. The origin is the upstream end of the sand bed. Figure 5.8 shows a section of the sediment bed in the flume with artificially formed ripples.

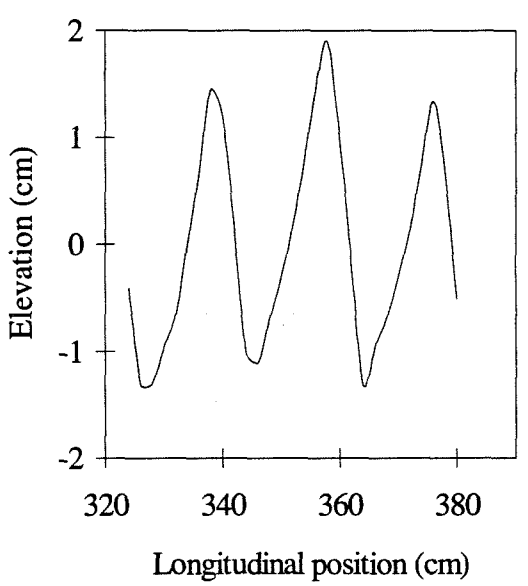

Figure 5.5. Section of bedform profile, Run 10. Artificially formed ripples, Ottawa 30 sand.

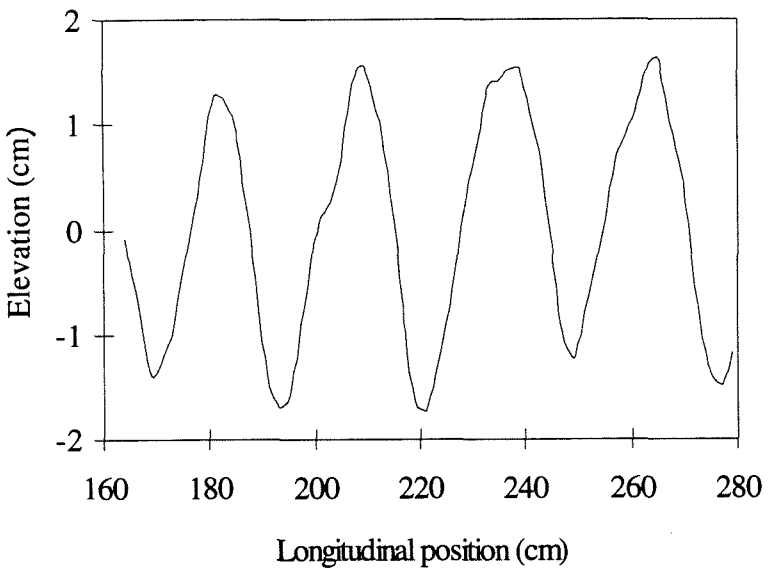

Figure 5.6. Section of bedform profile, Run 11. Artificially formed ripples, Ottawa 30 sand.

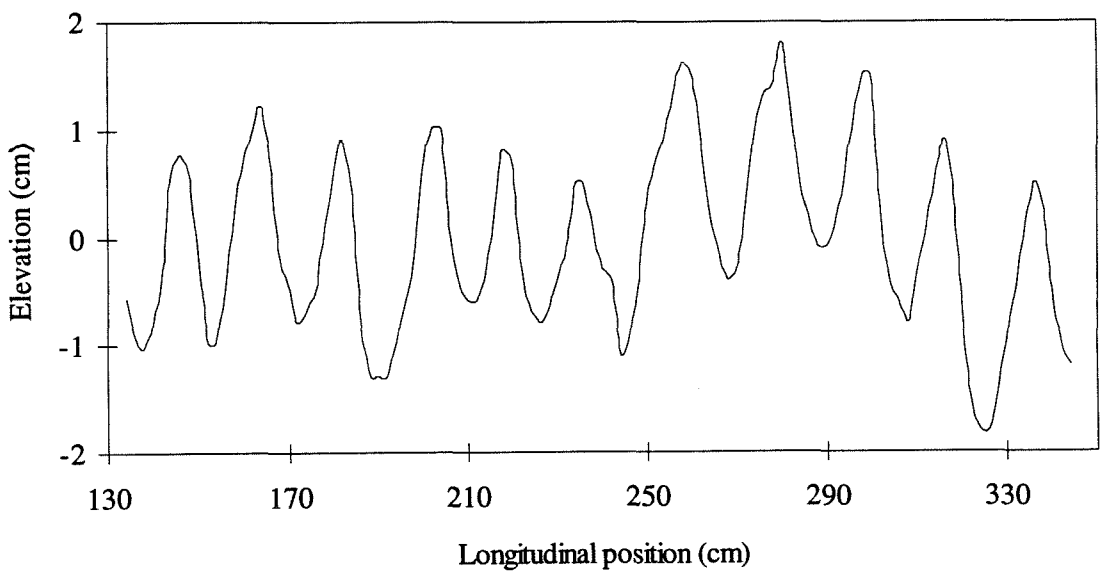

Figure 5.7. Section of bedform profile, Run 14. Artificially formed ripples, Ottawa 30 sand.

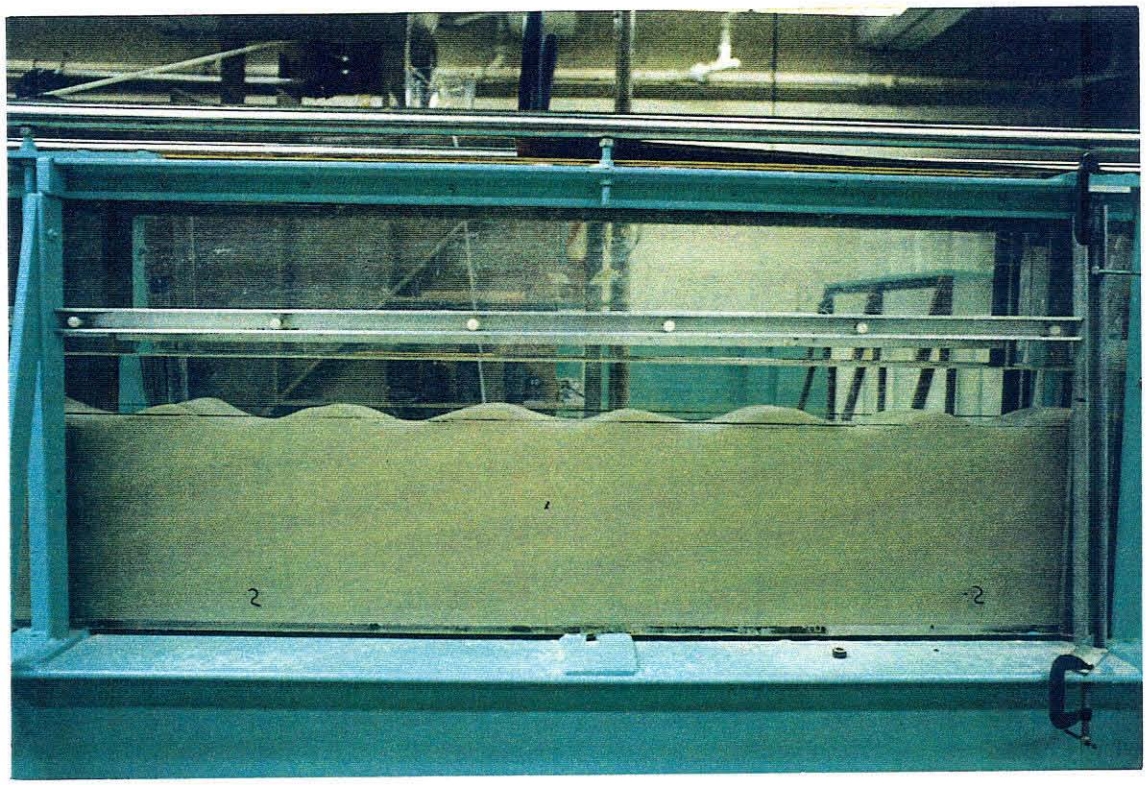

Figure 5.8. Photograph of artificially formed ripples. Flow is from left to right.

5.2.2.2. Moving and naturally formed bedform profiles

In the runs with moving or naturally formed ripples (Figure 5.9, Nevada 70 sand), the bedforms were much more irregular in wavelength and height. These variations were even more extreme for the coarser Ottawa 30 sand. Thus, accurate bedform parameters for naturally formed ripples were very difficult to determine.

Bedform wavelength and height varied by at least a factor of four between individual ripples. Furthermore, the average bedform height and length was varying with time over the course of an experiment. The large variations in bedform parameters are

caused by the small width of the flume and the shallow water depth used in the experiments. Naturally formed ripples would be more regular in a larger flume.

The bedform velocity for moving ripples was measured by observing the movement of a large number of bedforms through the sidewalls of the flume. The reported bedform velocity is the mean value of about 20 observations. There were large variations also in the velocity measurements, the bedform velocity of individual ripples varied by almost an order of magnitude. There was no clear correlation between deviations in bedform size and velocities.

Because of the extreme irregularity of the naturally formed ripples in this flume, the investigator chose to perform most experiments with artificially formed ripples. The shape of the artificially formed ripples is very similar to the shape of ripples observed in natural systems.

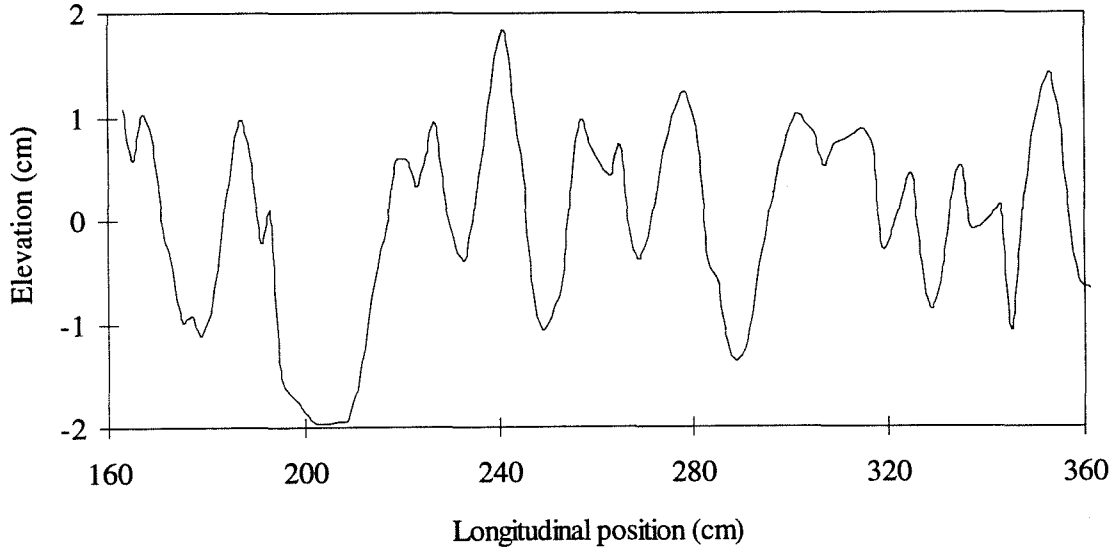

Figure 5.9. Section of bedform profile, Run 15. Naturally formed ripples, Nevada 70 sand.

5.2.3. Stationary bedforms

The figures in this section for runs with stationary ripples show the measured accumulated transport of the metal ions into the sediment bed versus time (symbols), shown as the fraction of the total mass of each ion contained within the sediment bed on the left-hand ordinate and the fraction contained in the overlying water column on the right-hand ordinate. To obtain the latter fraction, the measured concentration values in the adsorption runs were divided by the initial tracer concentration C_0, given in Table 5.2. In the desorption runs, measured concentration values were normalized by the initial concentration of the proceeding adsorption experiment.

Also shown are curves representing the result of the simulation calculation using the advection model with the retardation coefficients as indicated in the legend. Time is shown in nondimensionalized units (normalized by $1/(k^2Kh_m)$, see Section 3.2.1.1) on the lower abscissa. For reference purposes, the real experiment time (in hours) is shown on the upper abscissa. As an example of the raw data, the concentration measurements for zinc and lithium in the overlying water column as well as in the pore-water for Run 6 are shown in Appendix B.

The retardation coefficients shown in the legend are determined by fitting the retardation coefficient used the mass transfer model to the observed data points in the flume experiment. The retardation coefficients determined by this method are in good agreement with the retardation coefficients calculated from the batch adsorption experiments (see Section 5.1.1).

5.2.3.1. Adsorption experiments

In this section, the result of the flume adsorption experiments (experiments with initially clean bed and metal ions in the overlying water column, stationary ripples) are shown. Runs were performed at two pH values, about 6.2 and about 7.2. At higher pH value, some of the metal ions will precipitate and the experimental conditions will be significantly altered due to the presence of solids in the water column (see Section 4.2.2).

Lithium ions were used in all runs starting with Run 5 (when simultaneous analysis for more than one metal ion using the ICP-MS became possible), whereas Runs 1 through 4 were performed without a lithium tracer in solution. Because of the lack of a nonadsorbing tracer for Runs 1 - 4, the initial flux of zinc into the sediment was used to calibrate the dynamic pressure head used in the simulation model (see discussion in Section 5.2).

Runs 1 and 2 were performed under identical experimental conditions (bedform parameters and flow conditions), and the sand bed was not cleaned between these two runs. The scatter in the data points for Run 1 (Figure 5.10) can be explained by the low initial zinc concentration (C_0 = 5 μM), so that decreasing subsequent concentrations (less than 1 μM after 1 day) were at the low end of the concentration range that could be measured accurately by the flame atomic absorption spectrometer which was used for the analysis of concentrations in the first four runs. The zinc concentration in Run 2 (Figure 5.11) was then chosen about fourfold higher to increase measurement accuracy. It can be seen that the retardation coefficient for the experiment at low zinc concentration (R = 15 for C_0 = 5 μM) was slightly higher than the retardation coefficient at the higher concentration (R = 12 for C_0 = 18 μM). This effect is expected and can be explained by basic

surface adsorption models (see Chapter 3), which predict an increased partitioning of zinc to the surface with decreasing zinc concentration in solution (or increasing surface area, see Run 11).

As it can be seen in Table 5.2, the correction factor applied to the dynamic pressure head was larger for Run 1 ($\alpha = 1.4$) then for Run 2 ($\alpha = 1.0$). Because the sediment bed was not removed from the flume for washing between these two runs, changes in the bedform parameters cannot explain this difference. A possible reason for this discrepancy is potential settling of the sediment bed between the two runs, leading to reduced hydraulic permeability K in Run 2. This explanation is especially feasible because a period of almost three weeks expired between the end of Run 1 and the start of Run 2. Experimental techniques were also improved between these two runs.

Run 5 (Figure 5.12) was performed using calcium (instead of zinc) and lithium tracers. As expected from the batch experiments (see Table 5.1), the observed transfer of calcium into the sediment bed corresponded to a smaller partitioning of calcium ions to the surfaces compared to the partitioning of zinc ions at the same pH (for calcium expected R = 3, observed R = 5; for zinc expected R = 11, observed R = 12).

To investigate the effect of a high concentration of another bivalent metal ion on the mass exchange of zinc with the sediment bed, Runs 6 (Figure 5.13) and 8 (Figure 5.14) were performed with high calcium concentrations in solution (60 μM and 100 μM). However, no measurable difference in the zinc mass exchange to the runs performed with no calcium background concentrations (Runs 1 and 2) was observed in the experiments, indicating the higher calcium concentrations have no significant effect on the surface adsorption of zinc onto the sand surfaces in the sediment bed.

Runs 10 (Figure 5.15) and 14 (Figure 5.18) were performed at a lower pH (6.1 and 6.0). The effect of lower pH on the adsorption of zinc and calcium onto sand is apparent when comparing the results of zinc mass exchange in Run 10 (pH 6.0) and Run 6 (pH 7.3) and calcium mass exchange in Run 10 and Run 5 (pH 7.0): The retardation coefficient corresponding to the observed mass exchange in the flume run was reduced from R = 12 to R = 4 for zinc and from R = 5 to R = 2 for calcium. This trend is expected for (positively charged) metal ion partitioning to silica surfaces, and the observed retardation values agree well with the corresponding partitioning values observed in beaker experiments (see Table 5.1).

Nevada 70 sand was used in flume Run 11. Because the specific surface area of Nevada 70 sand is about 2.5 times larger than the specific surface area of Ottawa 30 sand, stronger partitioning of the adsorbing ions to the sand can be expected at same pH values. The observed retardation coefficient of zinc (R = 20) is indeed higher than in the experiments with Ottawa 30 sand (R = 12), in agreement with adsorption modeling.

In Run 12, five metal ions were used simultaneously. While the observed retardation of zinc (R = 12) was similar to previous experiments, the retardation of magnesium and calcium was somewhat smaller than expected from observations made in previous flume experiments (Run 5) and batch experiments. A possible explanation is reduced partitioning of calcium and magnesium to the sand due to either competition between these two ions or the presence of the zinc and copper ions in solution. The concentration decrease of copper in Run 12 was faster than can be explained by the advective transport model. However, at the pH in this run (pH 7.3), copper will form a solid (malachite, $Cu_2(OH)_2CO_3$) in solution (see Chapter 4). It is possible that solid formation lead to an additional loss of copper to the bed due to settling of malachite during

the higher aqueous copper concentrations during the initial phase of the run. In the later part of the run, the concentration decrease of copper in the overlying water can be expected by filtering (or very high retardation) of the copper (solid ?) in the sediment bed.

To verify the possible effect of solid formation on the mass exchange in Run 12, an experiment with copper in solution at a lower pH (pH 6.0) was performed in Run 14. At pH 6.0, copper will not yet form a solid. The mass exchange of copper with the sediment bed at pH 6.0 is in good agreement with the advection model (retardation coefficient R = 15).

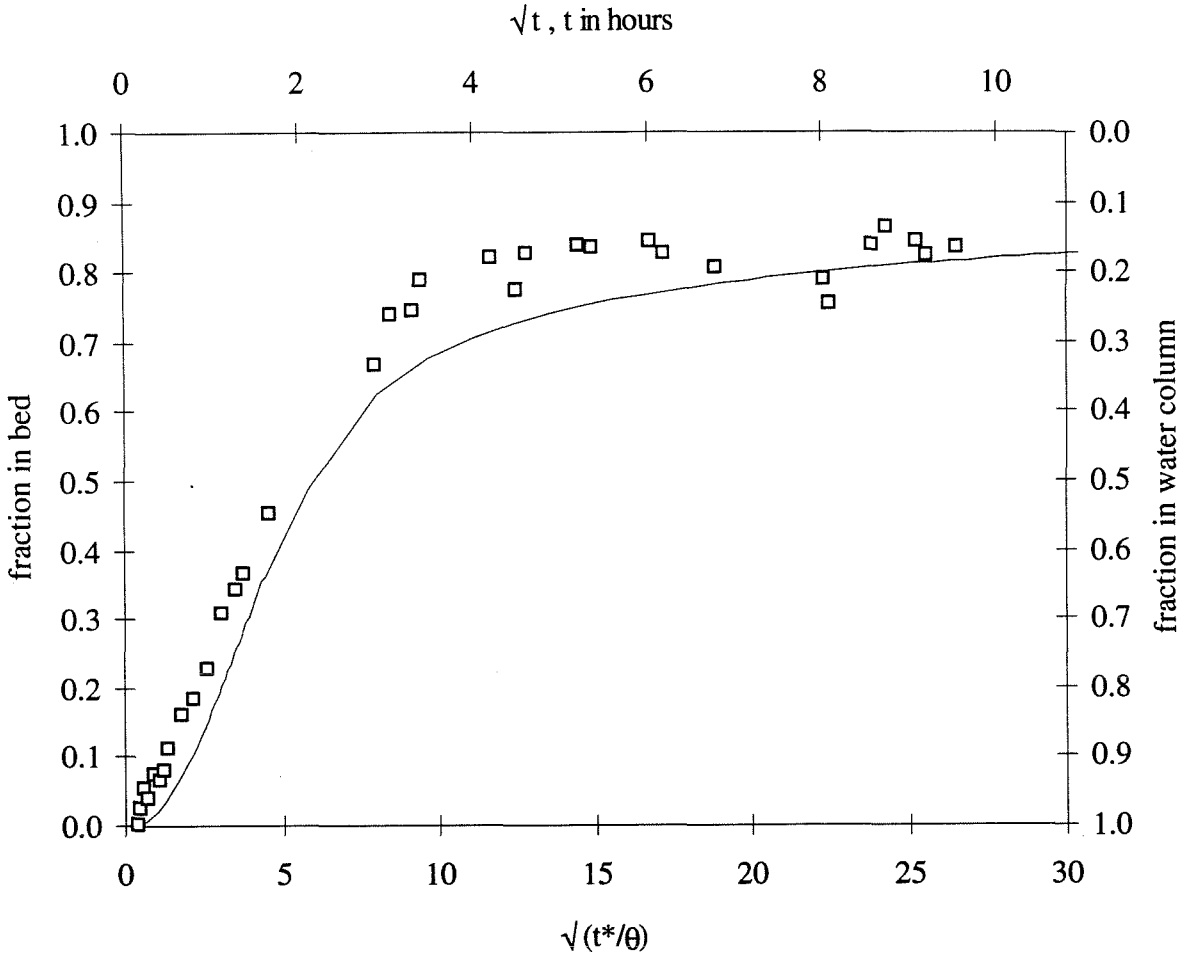

Figure 5.10. Transport of metal ions into sediment bed, Run 1. Stationary ripples, Ottawa 30 sand, pH 7.1.

□ Zn^{2+}

—— simulation Zn^{2+}, R=15.

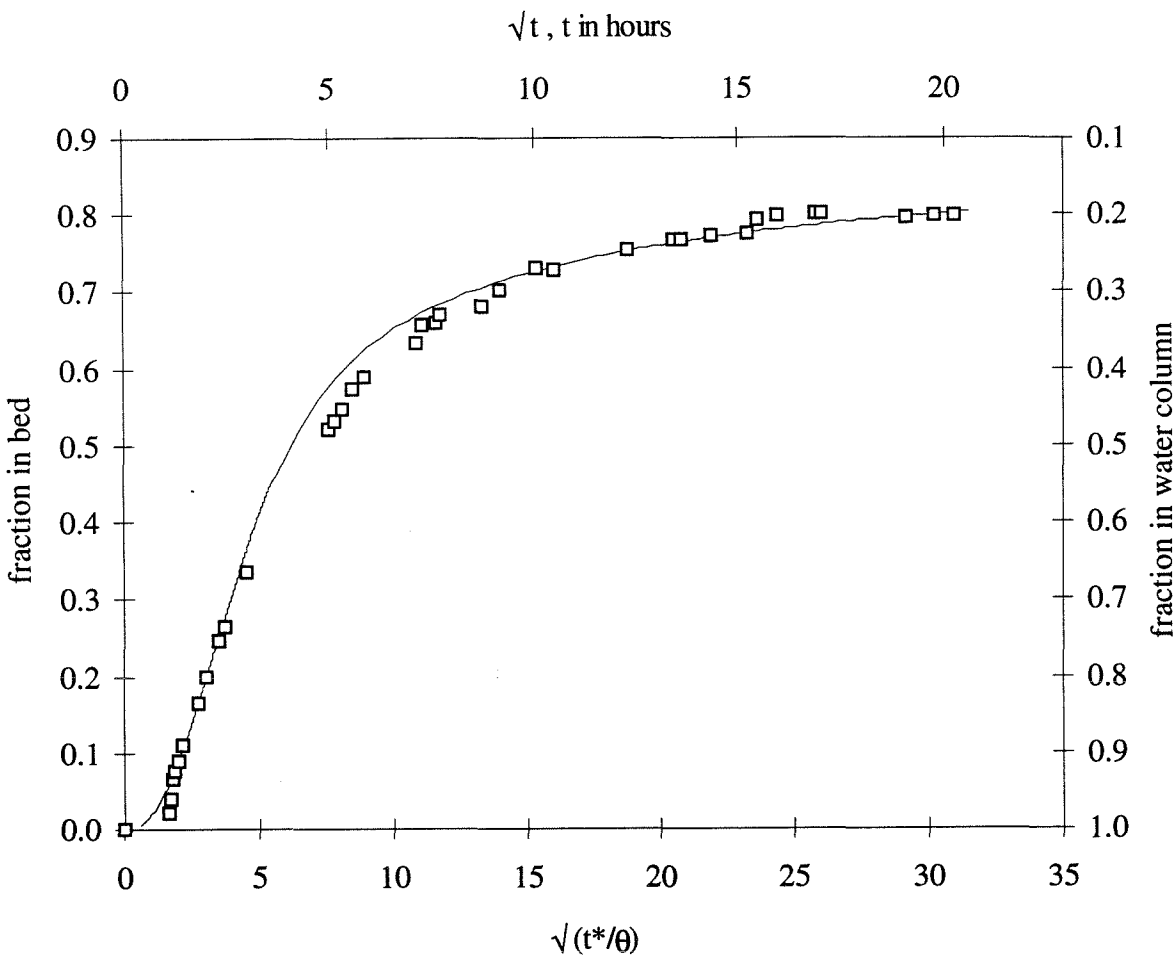

Figure 5.11. Transport of metal ions into sediment bed, Run 2. Stationary ripples, Ottawa 30 sand, pH 7.0.

□ Zn^{2+}

—— simulation Zn^{2+}, R=12.

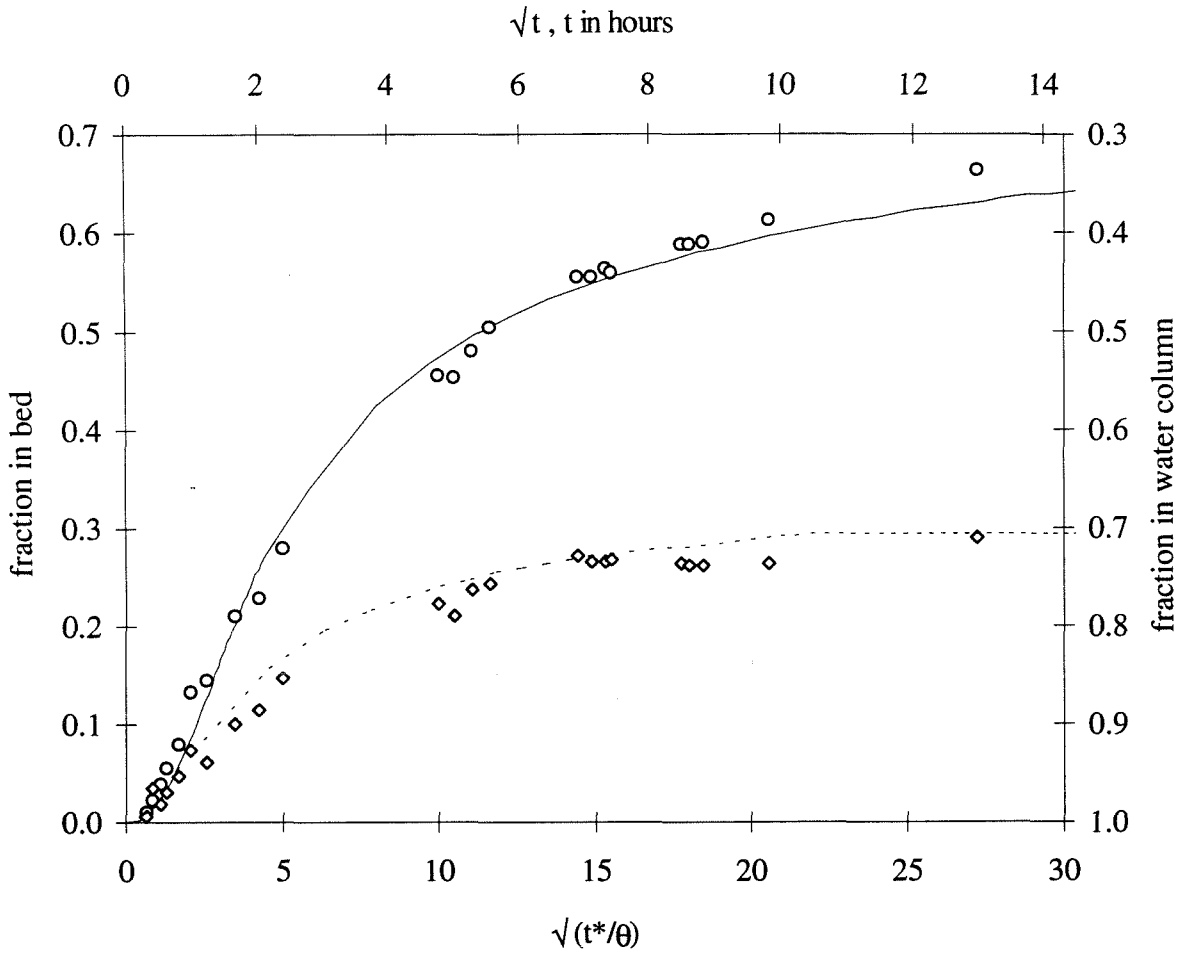

Figure 5.12. Transport of metal ions into sediment bed, Run 5. Stationary ripples, Ottawa 30 sand, pH 7.0.

O Ca^{2+}

✧ Li^{+}

—— simulation Ca^{2+}, R=5

– – – simulation Li^{+}, no adsorption.

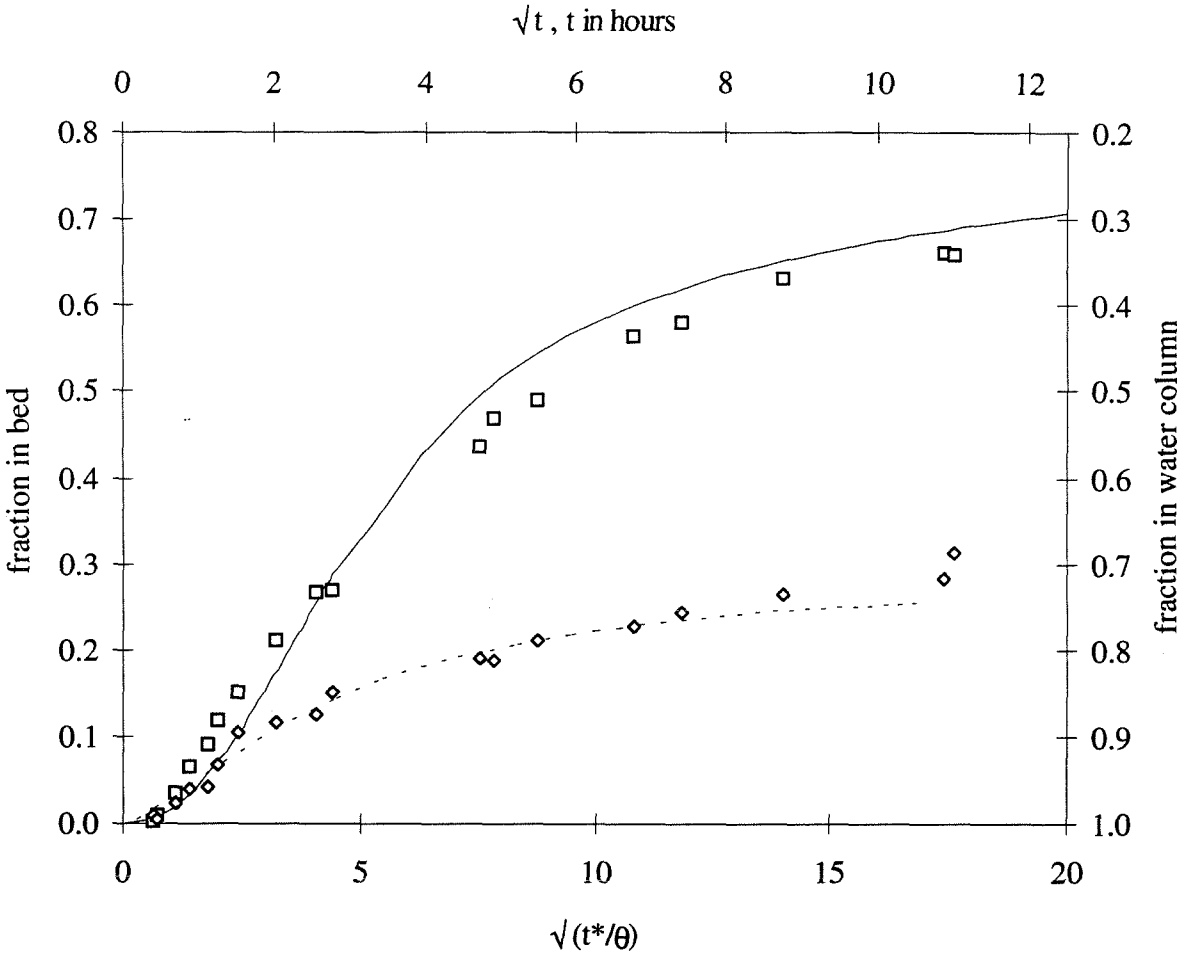

Figure 5.13. Transport of metal ions into sediment bed, Run 6. Stationary ripples, Ottawa 30 sand, pH 7.3.

□ Zn^{2+}

✧ Li^{+}

—— simulation Zn^{2+}, R=12

– – – simulation Li^{+}, no adsorption.

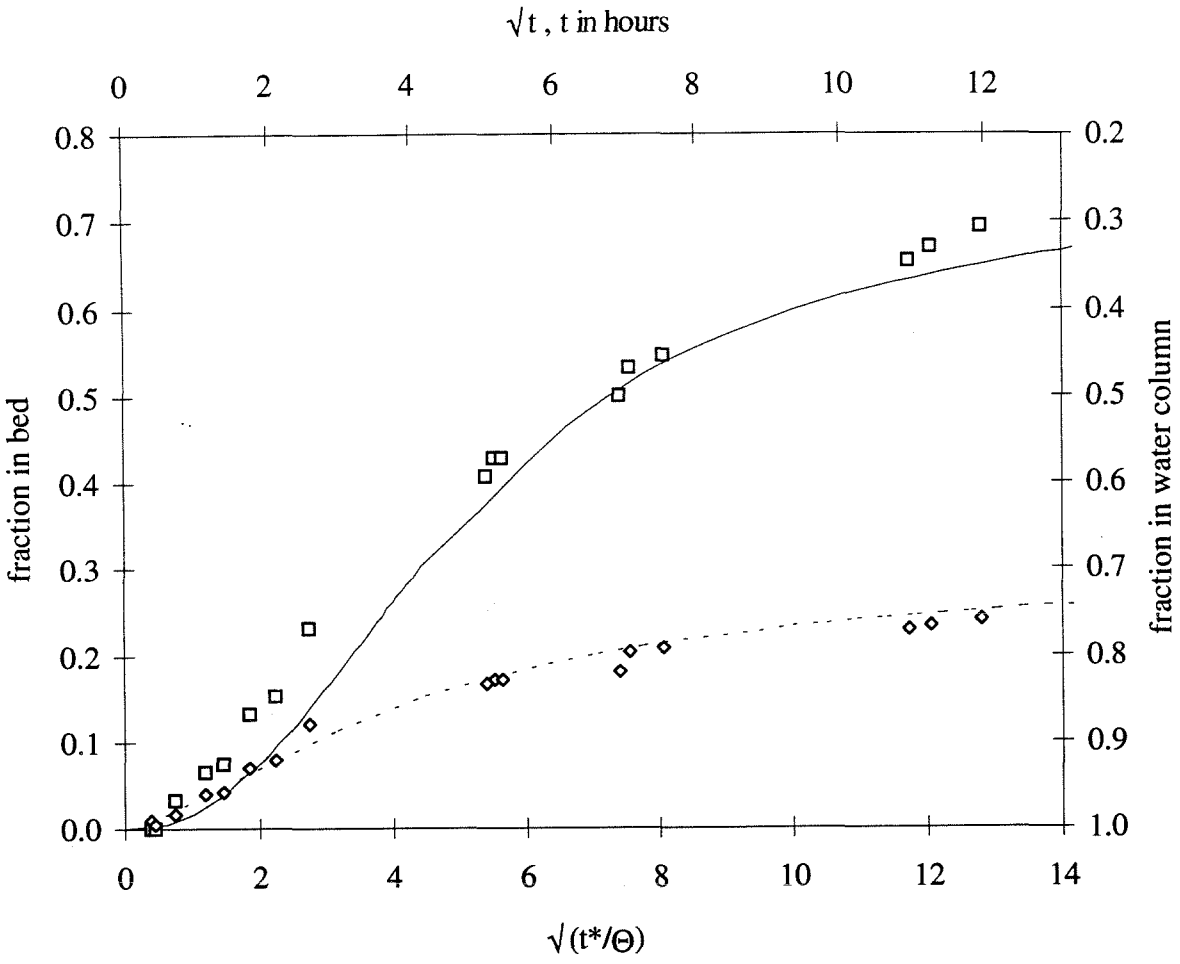

Figure 5.14. Transport of metal ions into sediment bed, Run 8. Stationary ripples, Ottawa 30 sand, pH 7.3.

□ Zn^{2+}

✧ Li^{+}

—— simulation Zn^{2+}, R=12

– – – simulation Li^{+}, no adsorption.

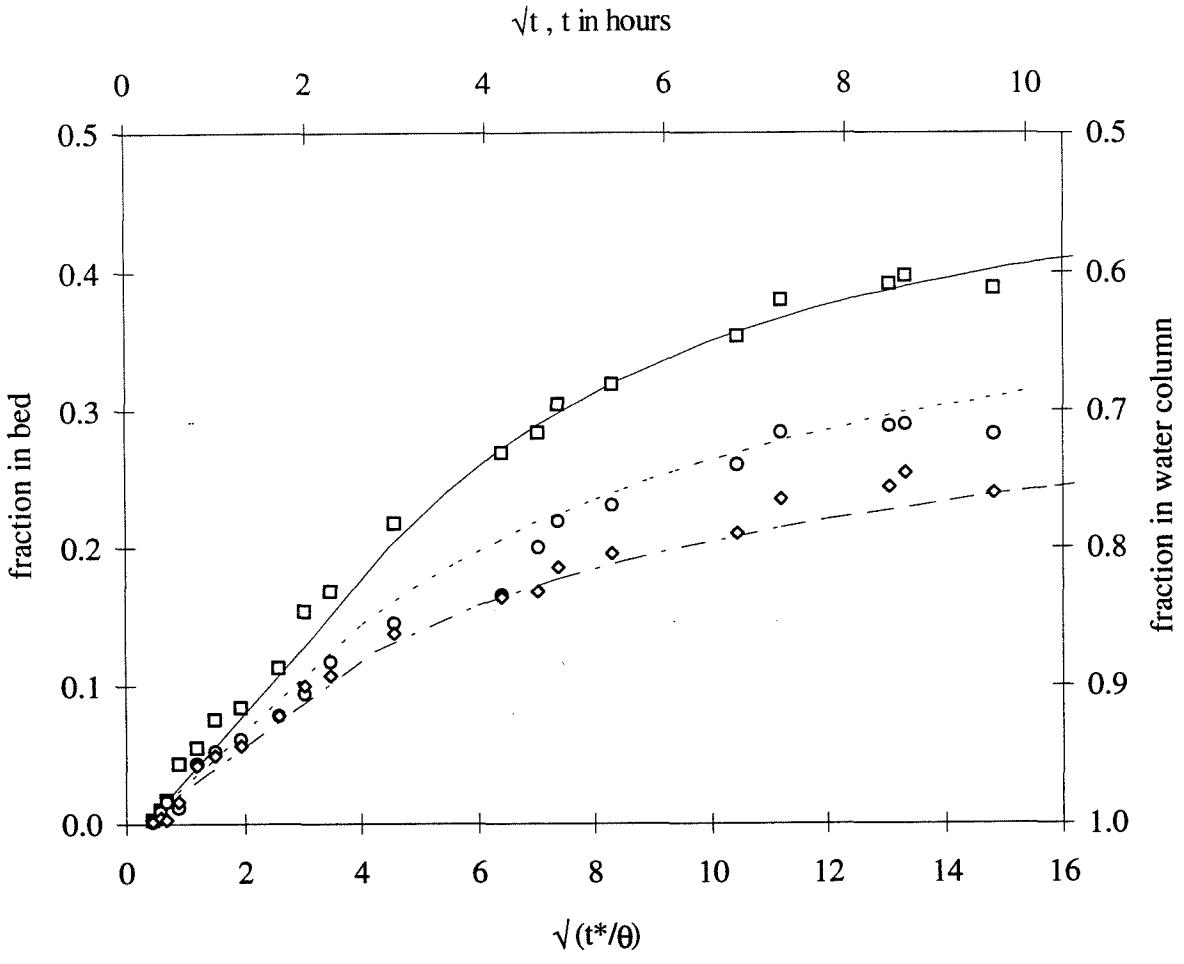

Figure 5.15. Transport of metal ions into sediment bed, Run 10. Stationary ripples, Ottawa 30 sand, pH 6.1.

□ Zn^{2+}

○ Ca^{2+}

✧ Li^{+}

—— simulation Zn^{2+}, R=3

– – – simulation Ca^{2+}, R=2

– – – simulation Li^{+}, no adsorption.

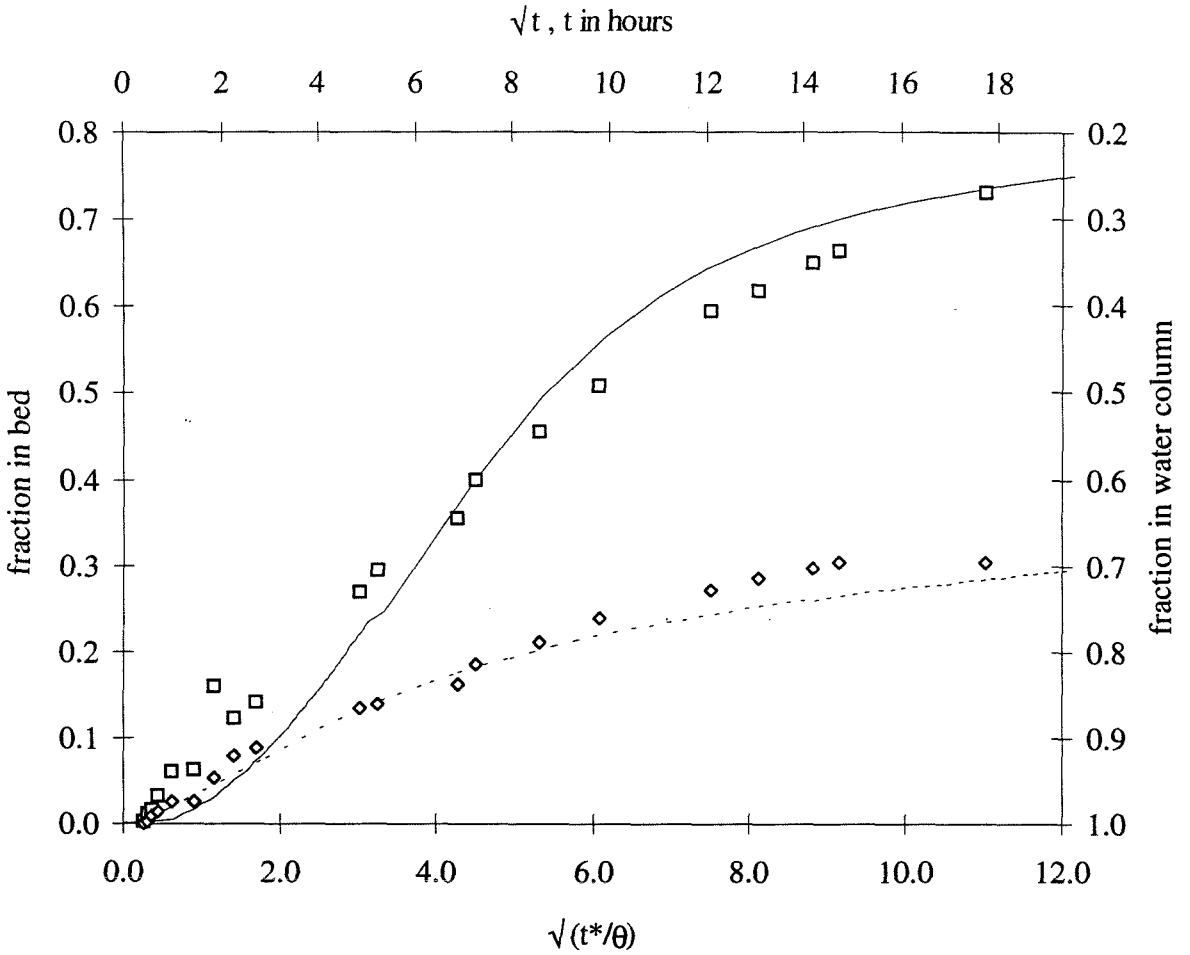

Figure 5.16. Transport of metal ions into sediment bed, Run 11. Stationary ripples, Nevada 70 sand, pH 7.3.

□ Zn^{2+}

✧ Li^{+}

—— simulation Zn^{2+}, R=20

– – – simulation Li^{2+}, no adsorption.

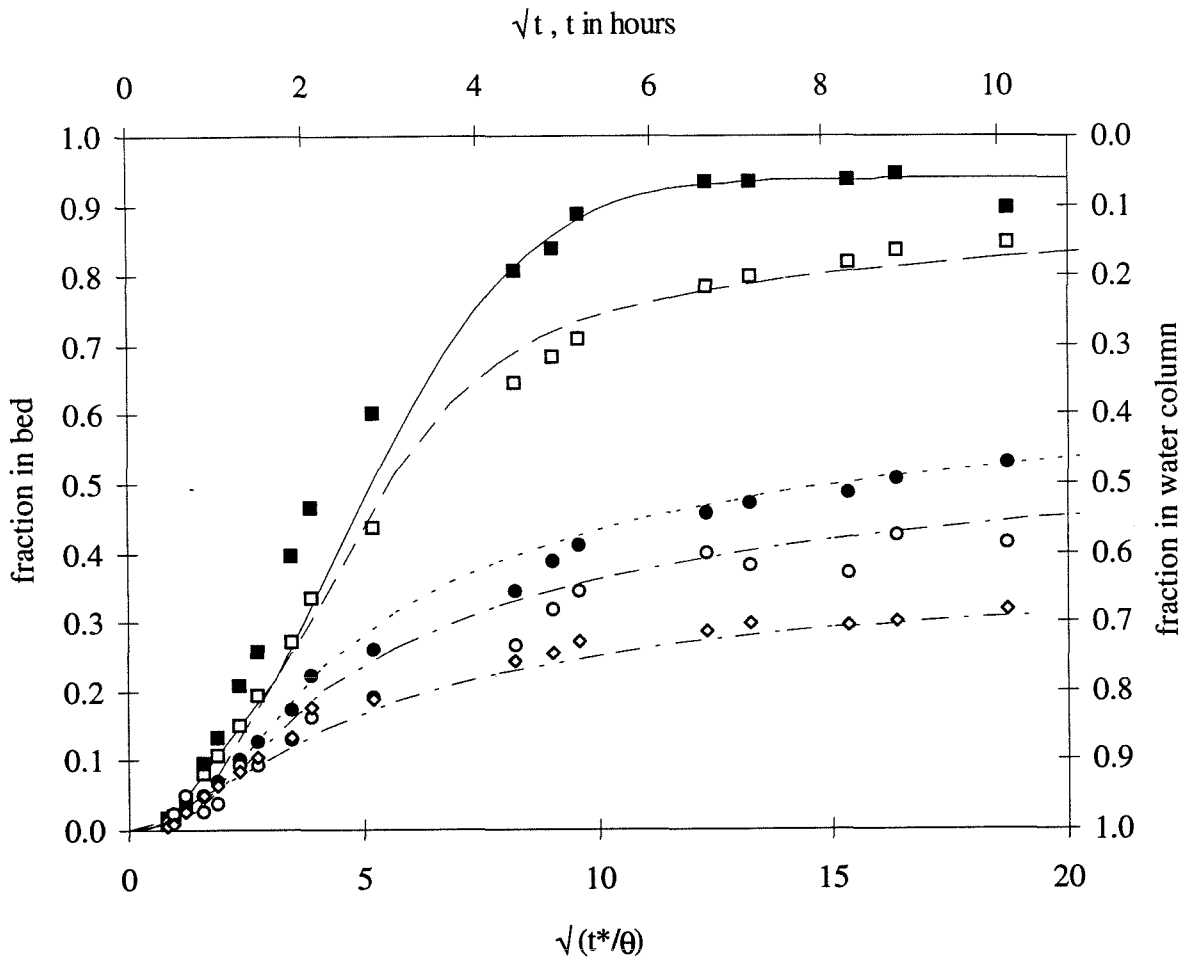

Figure 5.17. Transport of metal ions into sediment bed, Run 12. Stationary ripples, Ottawa 30 sand, pH 7.3.

■ Cu^{2+}

□ Zn^{2+}

● Mg^{2+}

○ Ca^{2+}

✧ Li^{+}

—— simulation Cu^{2+}, filtering

— — simulation Zn^{2+}, R=12

– – – simulation Mg^{2+}, R=3

— – — simulation Ca^{2+}, R=2

— – – – simulation Li^{+}, no adsorption.

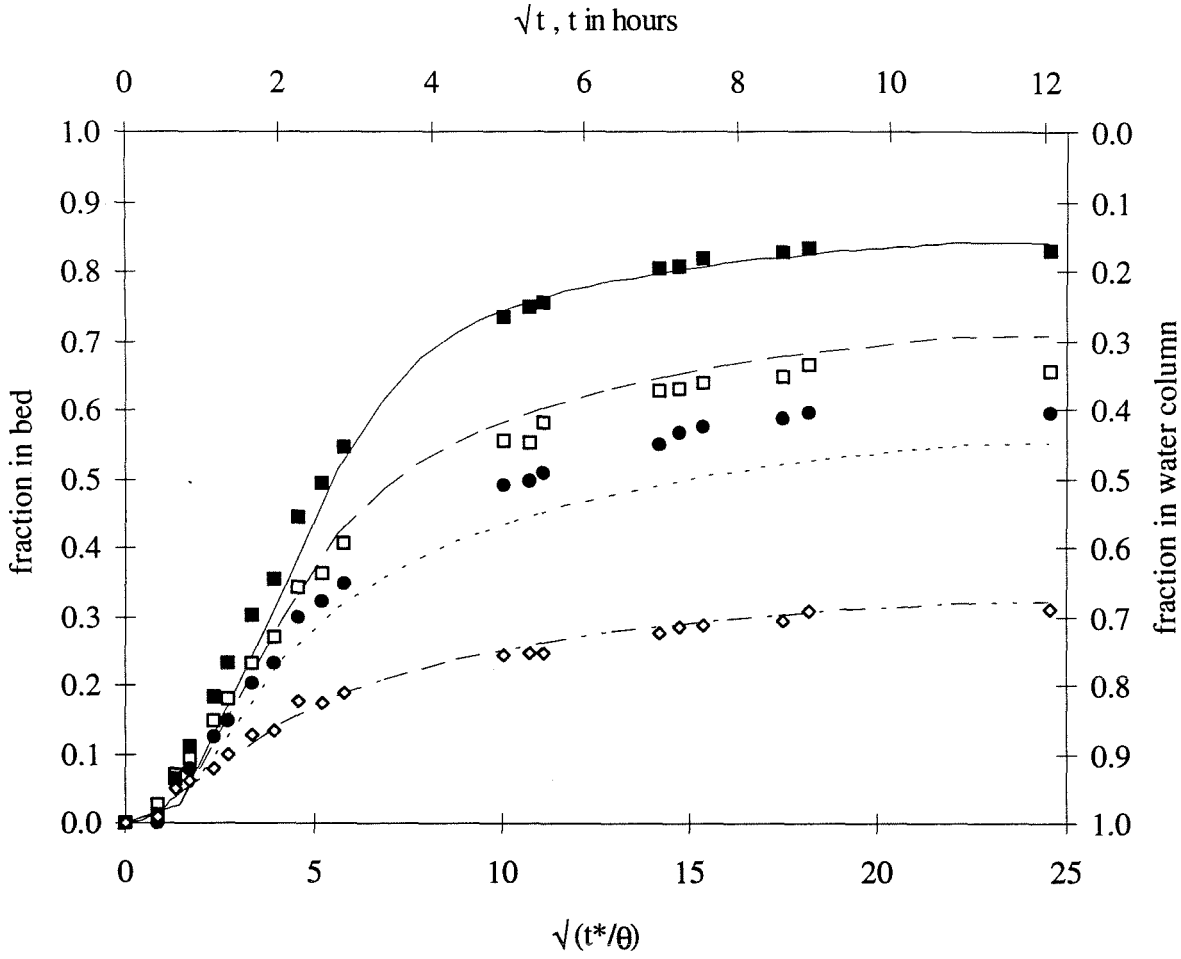

Figure 5.18. Transport of metal ions into sediment bed, Run 14. Stationary ripples, Ottawa 30 sand, pH 6.0.

■ Cu^{2+}

□ Zn^{2+}

● Mg^{2+}

✧ Li^{+}

—— simulation Cu^{2+}, R=15

— — simulation Zn^{2+}, R=7

– – – simulation Mg^{2+}, R=3

— – — – simulation Li^{+}, no adsorption.

The dominance of the pumping process over molecular diffusion can be demonstrated by using dimensional arguments for comparing the advective flux caused by pumping with flux into the bed caused by molecular diffusion: A typical molecular diffusion coefficient is $D = 10^{-5}$ cm^2/s. The time to reach a depth of $L = 1$ cm is approximately $t \cong L^2/D \cong 1$ cm/(10^{-5} cm^2/s) $\cong 10^5$ s, or 1600 minutes. An estimation of the average flux into the bed is thus about 1 cm/1600 min, or about 10^{-3} cm/min. In contrast, typical advective fluxes by pumping are $\bar{q} = u_m/\pi \cong 0.01$ - 0.1 cm/min. Even though the resulting dynamic pressure head is of a relatively small magnitude (between 0.1 and 10 cm), mass exchange by pore-water advection is dominating over molecular diffusion.

In the initial phase of the flume experiments ($t^*/\theta < 1$), the transfer of pollutants between stream water and sediment bed is dominated by the advective flux of solution into the sediment bed. At this stage, very little release of pollutant occurs because pollutant will not have traveled far enough along the streamlines to leave the bed. The partitioning of the pollutant to the sand surfaces has no effect on the advective flux of solutes into the bed, partitioning only effects the release of pollutants after transport through the sediment bed. Thus, the concentration decrease of the metal ions in the beginning of the experiments is independent of the adsorption characteristics of the ions.

At later times in the experiment ($t^*/\theta > 1$), the net transport of pollutants between sediment and water column becomes dependent on the retardation of the metal ions because nonadsorbing tracers (lithium) will be transported faster through the bed than the adsorbing bivalent metal ions and will be released from the bed earlier than the adsorbing tracers. Thus, the concentration decreases after the initial phase in the experiment in the water column will be dependent on the adsorption characteristics of the metal ions.

The pore-water pumping model describes the observed concentration changes in the water column well, the errors in the predicted concentrations are smaller than about 10 %. The only model parameter not entirely determined from measured values is the dynamic pressure head. The estimated pressure head determined from the empirical formula (see Chapter 3) was corrected by using the measured changes in lithium concentrations. However, the estimated pressure head predicted the observed value within a factor of two.

5.2.3.2. Desorption experiments

To investigate the reversibility of the surface adsorption of metal ions in the sediment bed, two experiments were performed with metal ions already in the sediment bed and no metal ions contained in the overlying water. In these runs, the overlying water was drained after completing an adsorption experiment and then replaced with fresh solution of same pH and ionic strength, but without any of the tracer metal ions in solution. The flume was the run again and the increase of tracer ion concentration in the overlying water was observed.

All experiment parameters (bedform parameters, water depth, flow velocity, correction factor α, retardation coefficients) in the desorption runs were kept identical to the corresponding previous adsorption experiments. Metal ion concentrations were normalized by the initial metal ion concentration C_0 in the proceeding adsorption run.

Run 9 (Figure 5.19) followed Run 8. It can be seen that the observed release of both zinc and lithium from the sediment bed is described very well by the advection model.

The observed release of lithium and the adsorbing metal ions (zinc, magnesium, calcium) from the bed in Run 13 (Figure 5.20, following Run 12) also is explained by the advection model. There is no measurable release of copper from the sediment bed in this experiment, in good agreement with the observed filtration of the copper in the previous run.

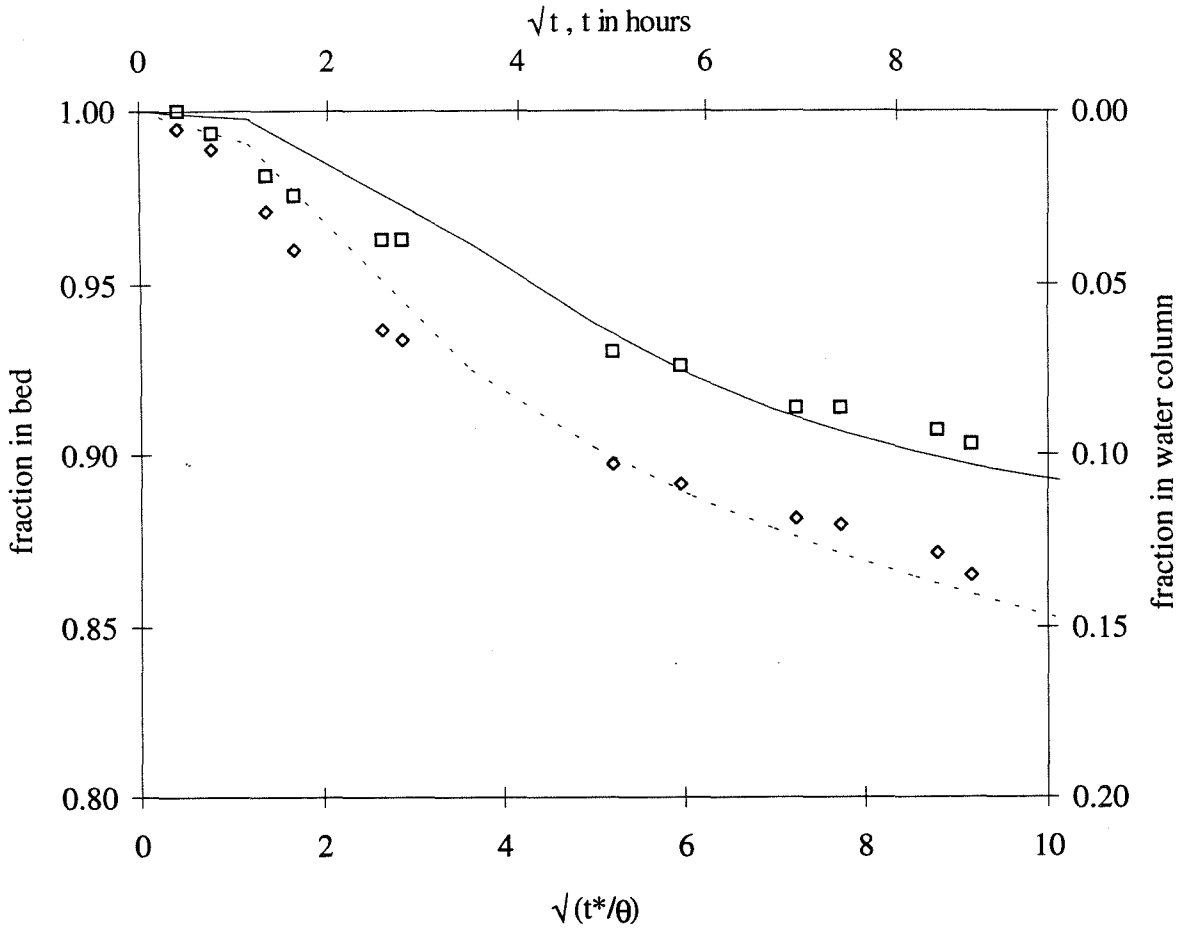

Figure 5.19. Transport of metal ions from sediment bed, Run 9. Stationary ripples, Ottawa 30 sand, pH 7.3.

□ Zn^{2+}

✧ Li^{+}

—— simulation Zn^{2+}, R=12

– – – simulation Li^{+}, no adsorption.

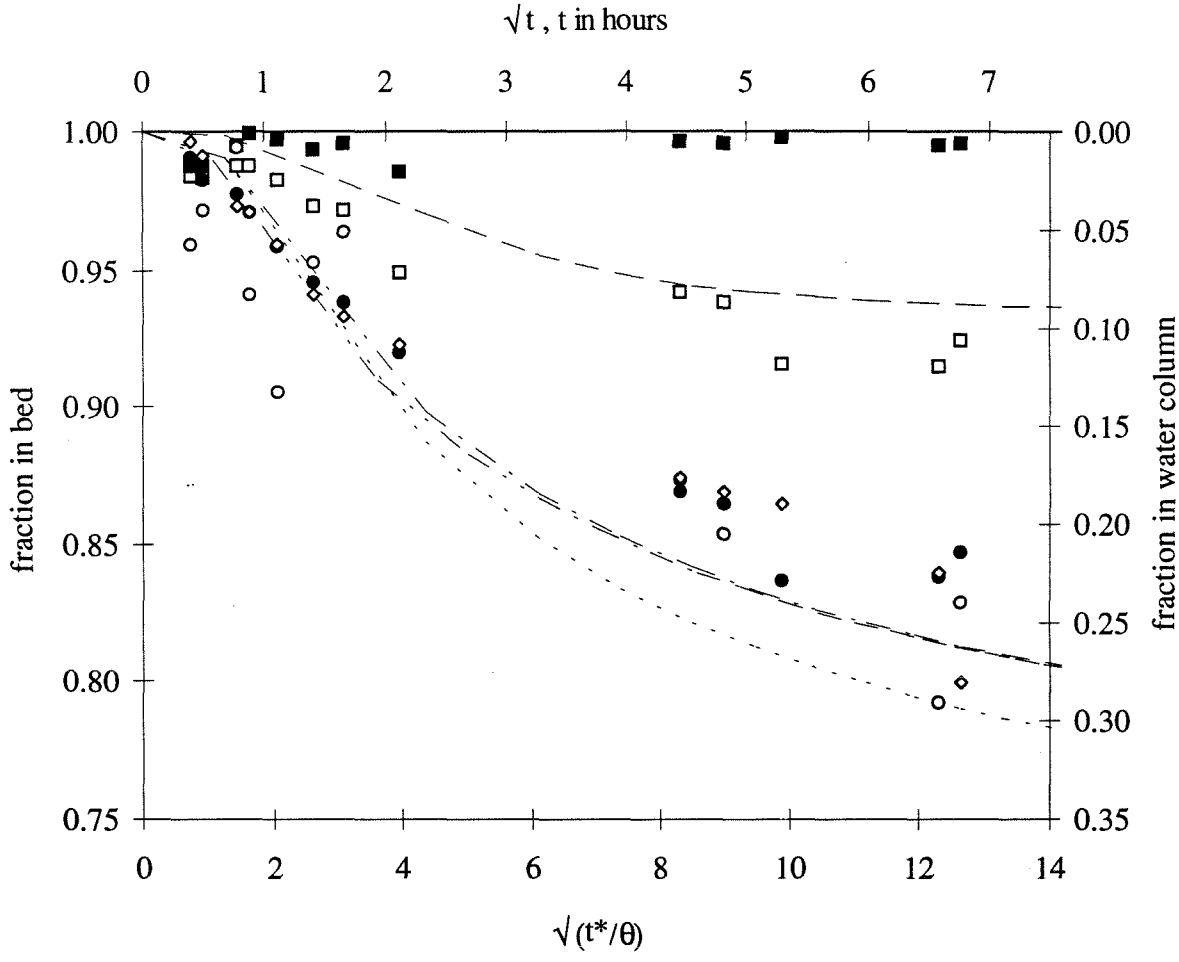

Figure 5.20. Transport of metal ions from sediment bed, Run 13. Stationary ripples, Ottawa 30 sand, pH 7.1.

■ Cu^{2+}

□ Zn^{2+}

● Mg^{2+}

○ Ca^{2+}

✧ Li^{+}

— — simulation Zn^{2+}, R=12

– – – simulation Mg^{2+}, R=3

– – – – simulation Ca^{2+}, R=2

– – – – simulation Li^{+}, no adsorption.

5.2.3.3. Pore-water concentration profiles

Time-dependent pore-water concentration profiles of the tracer ions for a number of flume runs are shown in Figures 5.21 to 5.29. Concentration profiles for different metal ions at one time are shown in Figures 5.30 to 5.34. The pore-water samples analyzed to investigate the concentration profiles were taken through ports which were located about halfway between the inlet and outlet sections of the flume. The sample volumes were taken at a distance of about 5 cm inwards from the flume wall. Pore-water samples were diluted one part flume water to six parts acidified water before analysis.

Using the pore-water concentration profiles, an approximate mass balance calculation can be performed for the flume runs. Because the advection fronts display a two-dimensional pattern and the pore-water samples are only taken at one point in the flume, the penetration depth of the tracers observed in the pore-water concentration profiles is not necessarily the average penetration depth of the sorbates in the flume. However, mass balance calculations show that the loss of metal ions in the overlying water can be explained by the penetration of the metal ions into the bed. The pore-water profiles were taken at approximately the same location relative to the bedforms in all cases, at about the midpoint between trough and crest on the upstream side of the bedforms. Thus, the penetration depths of the tracers can be compared not only between different metal ions in one run, but also between different runs.

The pore-water concentration profiles clearly show that advective pumping transports the metal ions much deeper into the sediment bed than molecular diffusion processes would. Also, the shape of concentration profiles are more like downward-moving fronts than solutions to the diffusion equation because of the relatively constant

concentration in the upper part of each profile. The concentration value of this upper constant part of the profile decreases gradually with time, especially for zinc, because the concentration of the overlying flume water is decreasing.

The measured pore-water concentrations in the upper part of the profiles show less of a variation for lithium than for the adsorbing tracers. It is possible that the mechanical disturbance caused by the insertion of the needle into the sand bed can cause some of the adsorbed metal ions to be 'scraped off' the surface, leading to a larger error in the pore-water concentration values for those ions.

It can be seen that the penetration depth increases with time and the metal ion concentrations in the upper, 'flat', part of the profile decrease with time (Figures 5.21 to 5.29). The penetration depth is always deepest for the nonadsorbing tracer lithium (Figures 5.30 to 5.34). The approximate maximum penetration depth of the metal ions is of the order of the wavelength of the ripples and, due to retardation, is reached first for nonadsorbing tracers and later for adsorbing ions.

The flume experiments show that the pore-water pumping process can drive pollutants deep into the sediment bed. After a period of about 100 pumping time scales, a nonadsorbing tracer will have penetrated into the bed to a depth equivalent to the wavelength of the ripples. Depending on their retardation coefficient, adsorbing pollutants will reach the deeper parts of the sediment bed later.

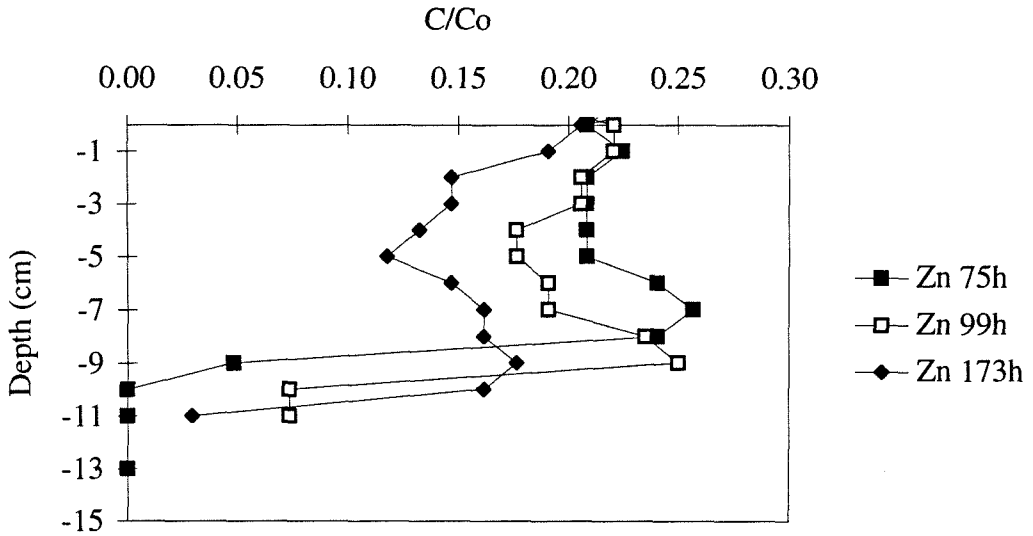

Figure 5.21. Pore-water concentration profile zinc, Run 1.

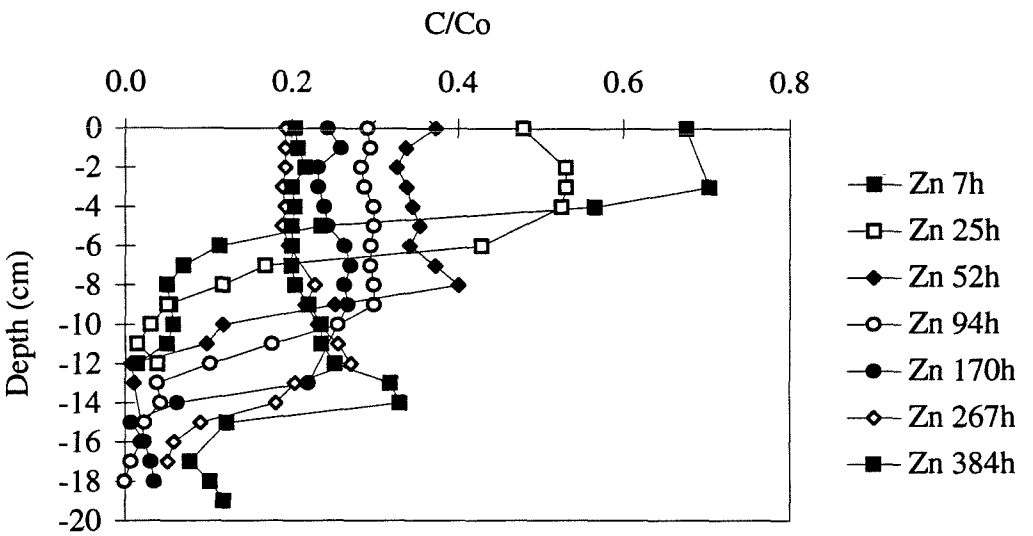

Figure 5.22. Pore-water concentration profile zinc, Run 2.

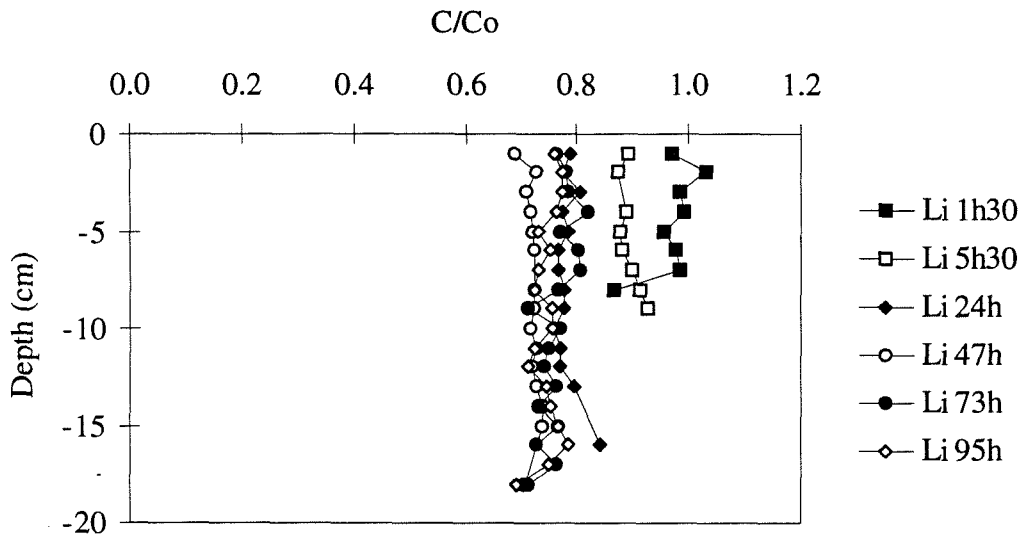

Figure 5.23. Pore-water concentration profile lithium, Run 5.

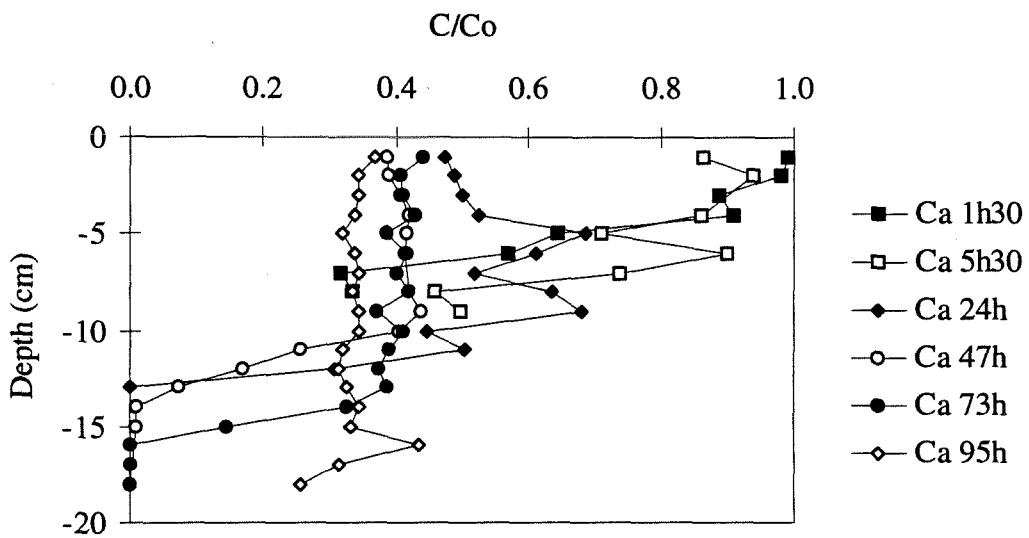

Figure 5.24. Pore-water concentration profile calcium, Run 5.

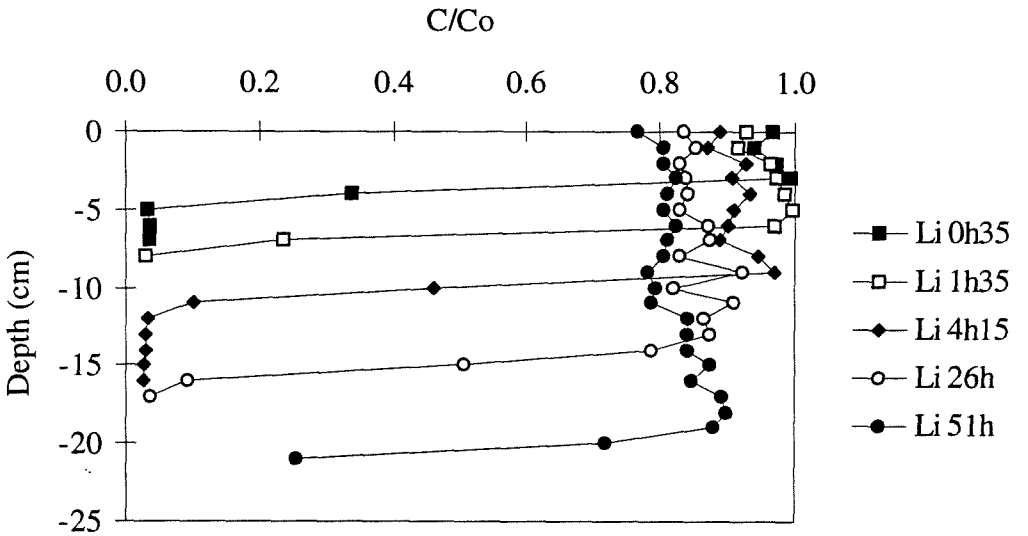

Figure 5.25. Pore-water concentration profile lithium, Run 6.

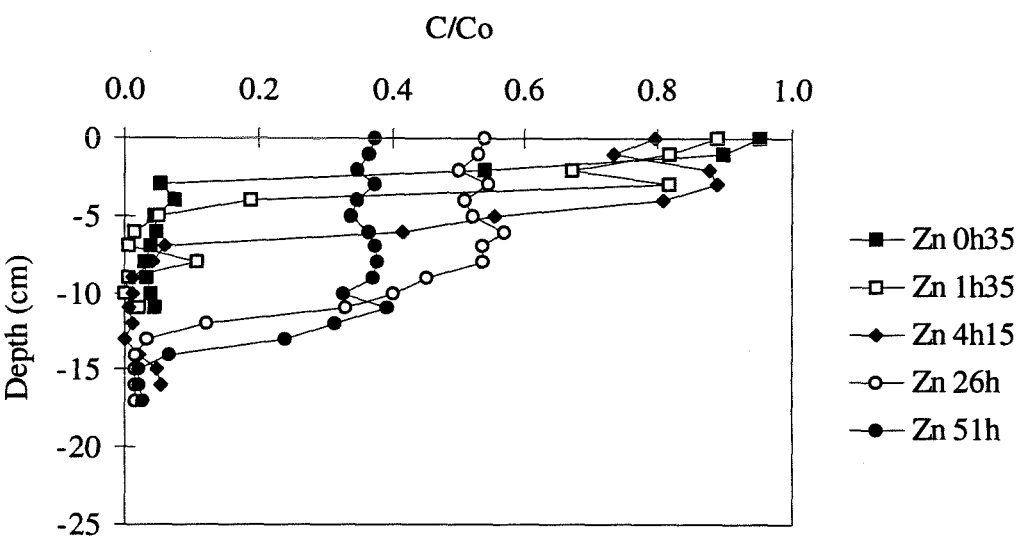

Figure 5.26. Pore-water concentration profile zinc, Run 6.

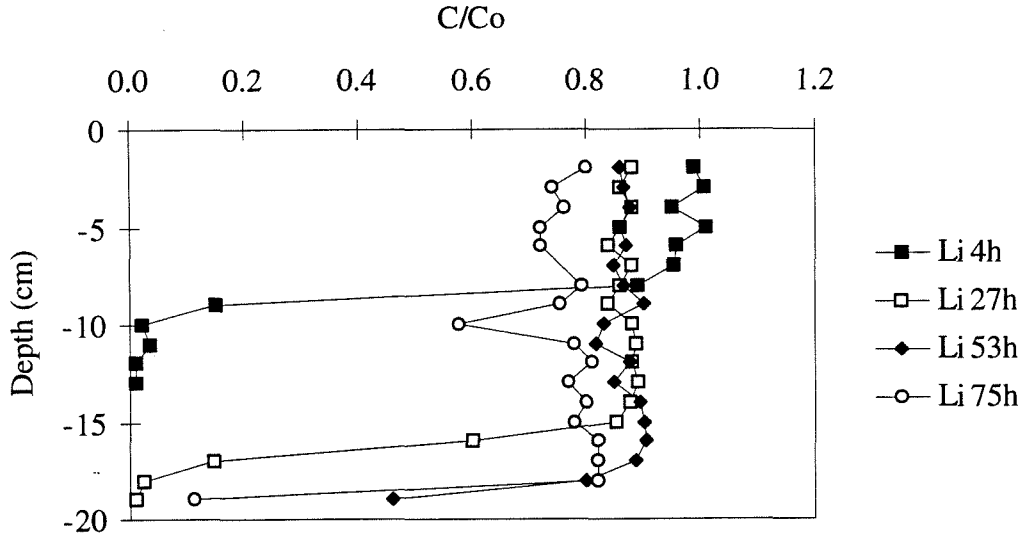

Figure 5.27. Pore-water concentration profile lithium, Run 10.

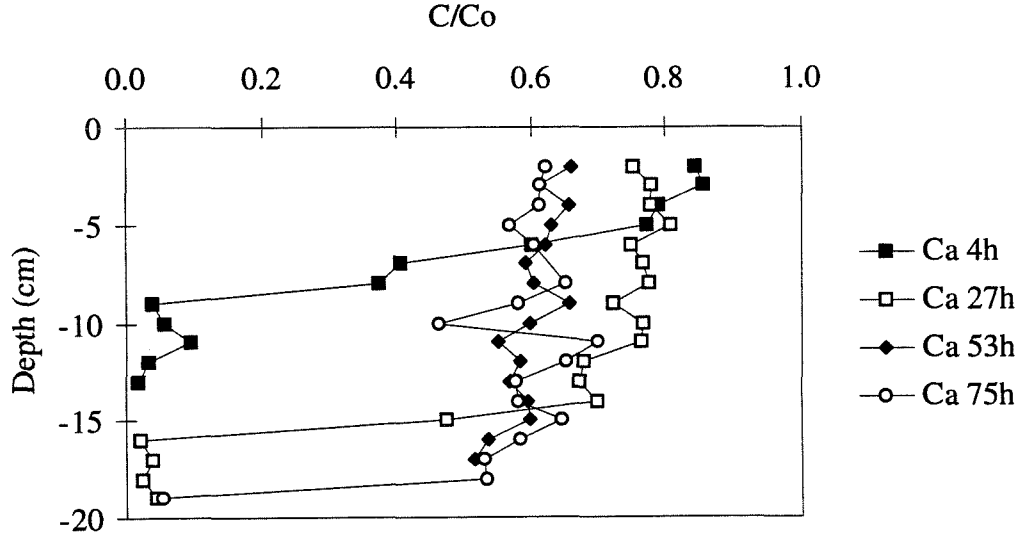

Figure 5.28. Pore-water concentration profile calcium, Run 10.

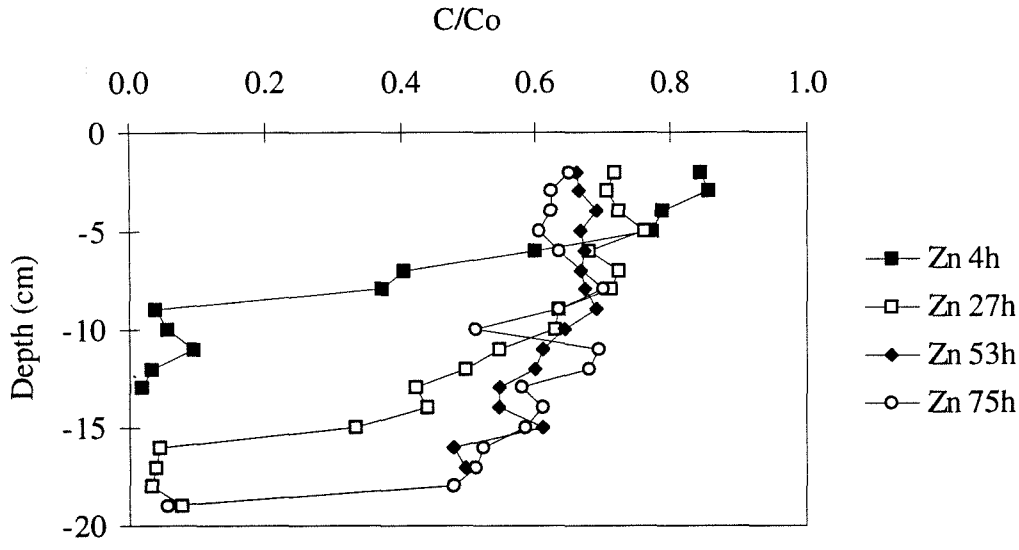

Figure 5.29. Pore-water concentration profile zinc, Run 10.

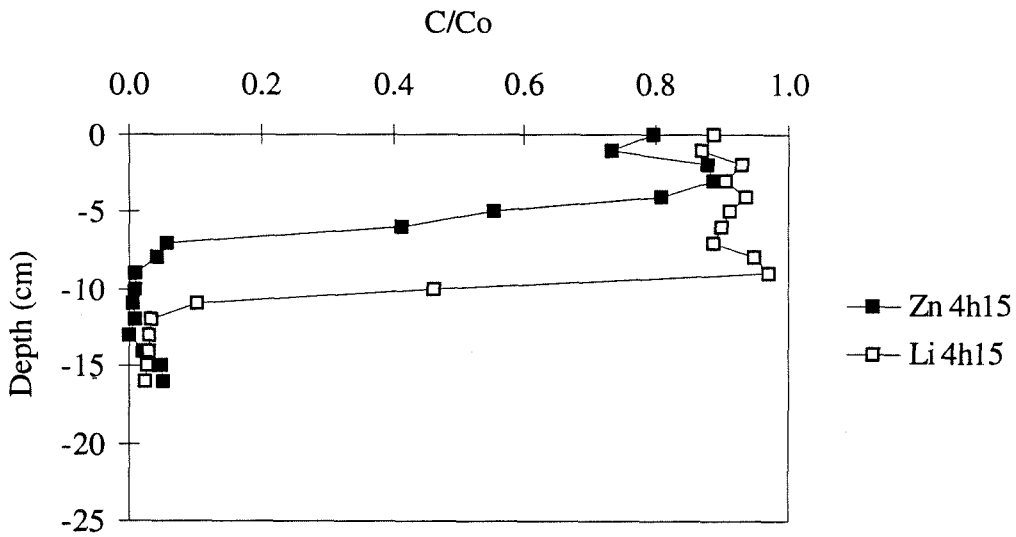

Figure 5.30. Pore-water concentration profile, Run 6, after 4 hours.

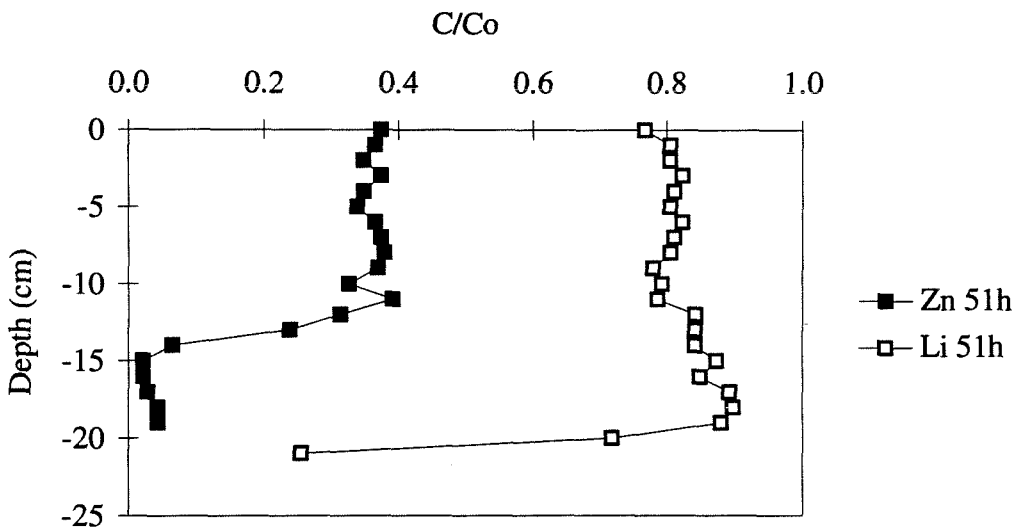

Figure 5.31. Pore-water concentration profile Run 6, after 51 hours.

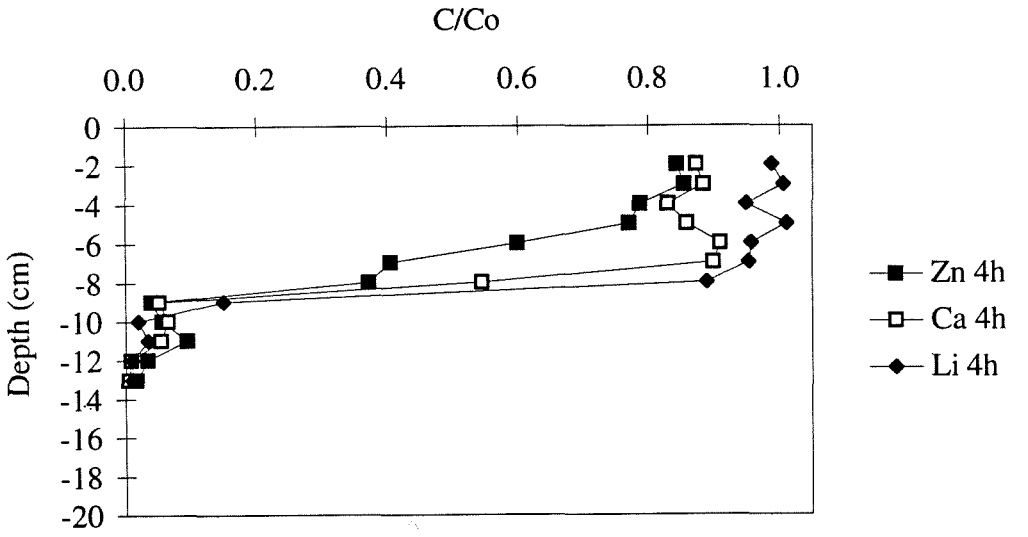

Figure 5.32. Pore-water concentration profile, Run 10, after 4 hours.

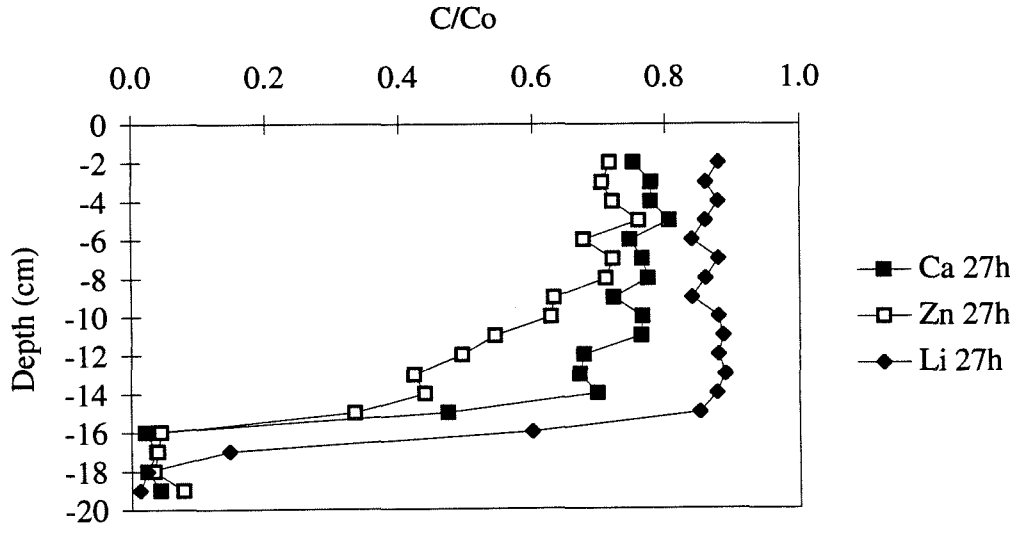

Figure 5.33. Pore-water concentration profile, Run 10, after 27 hours.

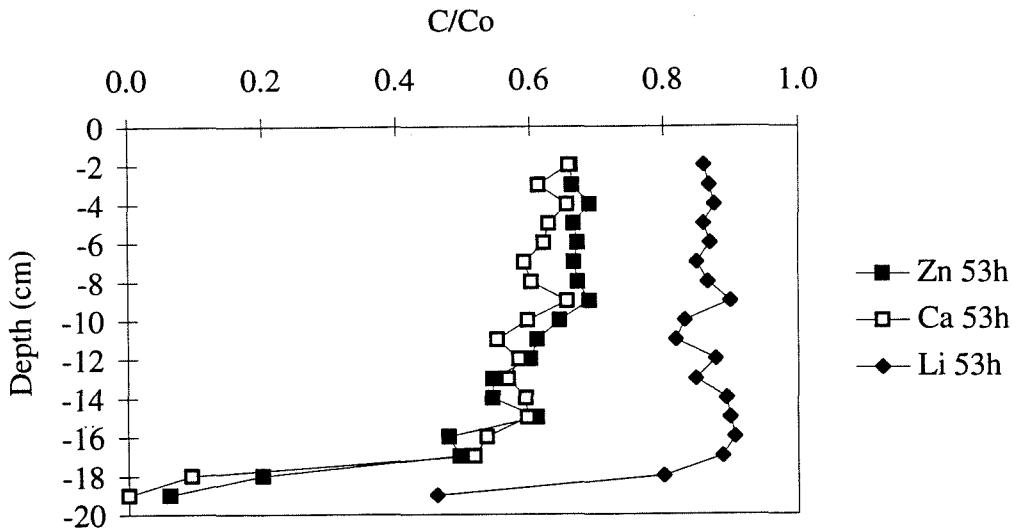

Figure 5.34. Pore-water concentration profile, Run 10, after 53 hours.

5.2.4. Moving bedforms

In this section, the results of the three runs with moving ripples are discussed. It is likely that effects of adsorption kinetics become important in the case of moving ripples. Naturally occurring bedforms are generally larger than the relatively small bedforms in the flume ($\lambda \cong 20$ cm). Because the time required for a bedform to propagate its one wavelength will be shorter in the flume than in a real river or stream and pore-water inside the bedform will be contained for a shorter time within the ripple, it is expected that kinetic effects are more important in the laboratory than in the field.

Run 3 (Figure 5.35) was a run with slowly-moving ripples ($u^*_{bed} = 0.14$). Even taking into account the effect of the partitioning of the zinc (R = 12), the partitioning-dependent parameter $u^*_{bed,R}$ is less than 2. The pumping model (with modified underflow to take bedform propagation into account) still fits the data very well, while the cover-up model cannot predict the observed mass exchange.

Runs 4 (Figure 5.36) and 15 (Figure 5.37) are runs with a much higher bedform velocity. In Run 4 ($u^*_{bed} = 4.6$), the exchange of metal ions with the bed can be explained only within a factor of 2 by the cover-up turnover model up to $t^*/(\theta R) \cong 100$, which is equivalent to about 60 bedform turnover time scales. However, at later times, the turnover model fails completely to explain the observed concentration decrease in the overlying water. This observation was also made by Elliott (1990). This indicates that the turnover model may approximately describe the initial process governing the exchange of pollutants between overlying water and sediment bed, but does not include mechanisms that dominate the pollutant exchange at later times. These processes could be passage of extremely deep troughs and pumping effects caused by the pressure field

moving with the bedforms. In the case of partitioning of the pollutant to the sediment, adsorption kinetics could cause additional deviations from the prediction.

In Run 4, the pollutant transport into the bed is approximately proportional to the square root of time. This indicates that the transport can be approximated by a pseudo-diffusion model. In order to fit the data points in Figure 5.36, the diffusion coefficient would have to be of the order of 10^{-2} cm^2/s, about three orders of magnitude higher than molecular diffusion coefficient (about 10^{-5} cm^2/s).

Run 15 (u^*_{bed} = 1.1) was performed with a bed of Nevada 70 sand. Despite a large number of washing cycles before running the experiment, a high concentration of fines was prevalent in the water column of Run 15 soon after starting the experiment. It is likely that the simulation model failed to describe the observed mass exchange between water column and bed because the metal ions adsorbed strongly to the fines in solution and not only to the sand grain surfaces in sediment bed. Subsequently, these fines could then be filtered out of the overlying water by the moving ripples. This explanation is supported by the result of a pore-water concentration profile (Figure 5.38), taken after completion of Run 15. In Figure 5.38 the metal ion concentrations are normalized by the final concentration of the metal ions in the overlying water after completion of the run to be able to better compare the depth penetration for the different metal ions. As the figure shows, the penetration depth into the bed for all three metal ions is only a few centimeters. The concentration profiles also show a rapid decrease of concentration with depth, indicating that bedform turnover was dominating over pore-water advection in this experiment. The partitioning of the metal ions to only the sand in the sediment bed is not strong enough to explain the small penetration depth of the ions.

The top five centimeters of the sediment (including pore-water) in the flume were sampled after conclusion of Run 15. The sample was acidified to desorb all metal ions potentially adsorbed to either the sand or the fines. The concentration of the metal ions in the acidified solution was measured, and a mass balance showed that the total amount of metal ions contained within the top 5 cm of the sediment bed does account fully for the loss of metal ions from the overlying water (about 30% of the initial amount of lithium, 80% of the zinc, 95% of the copper were contained within the sediment bed). This is only possible if significant adsorption to fines occurred in this experiment.

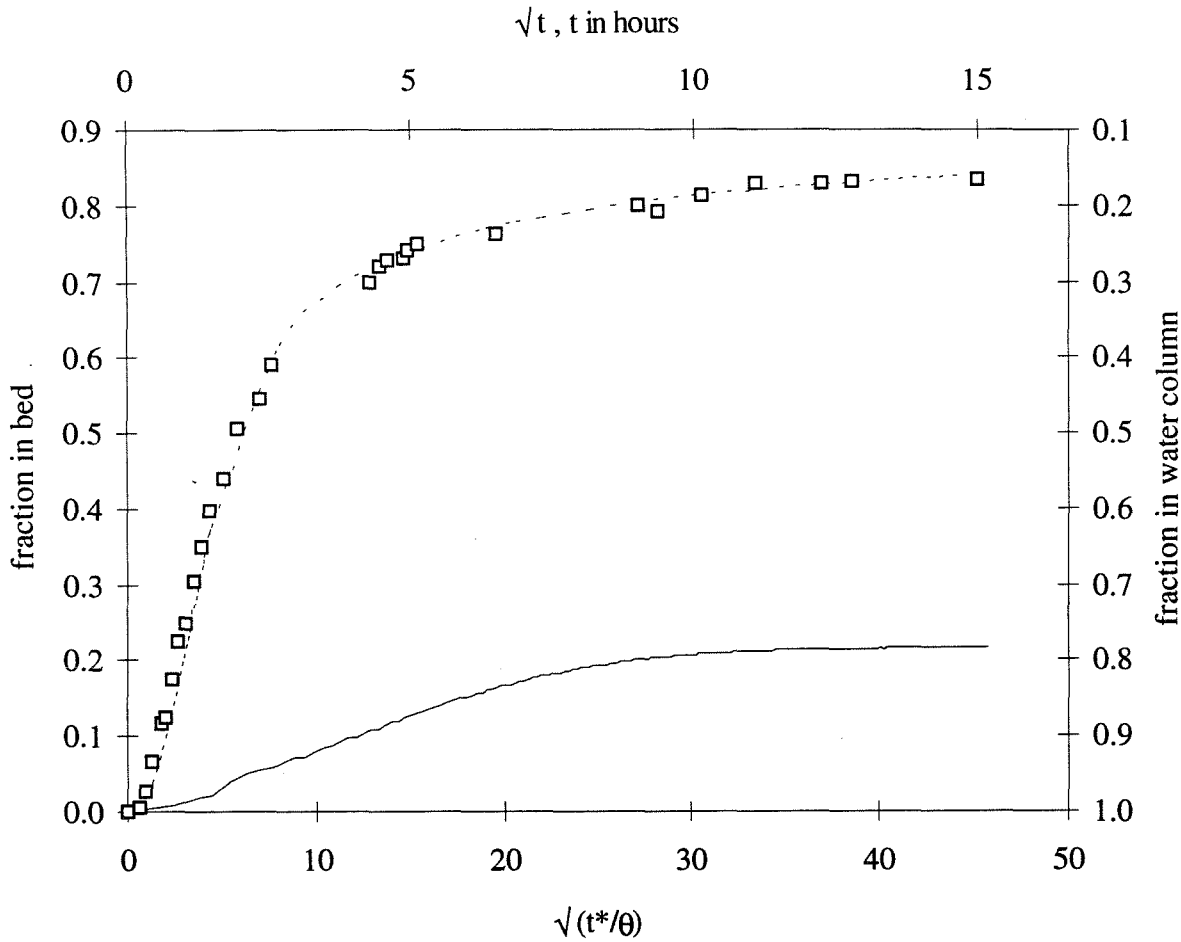

Figure 5.35. Transport of metal ions into sediment bed, Run 3. Moving ripples, Ottawa 30 sand, pH 6.9, $u^*_{bed} = 0.14$.

□ Zn^{2+}

– – – simulation Zn^{2+}, R=12, pumping model

—— simulation Zn^{2+}, R=12, cover-up model.

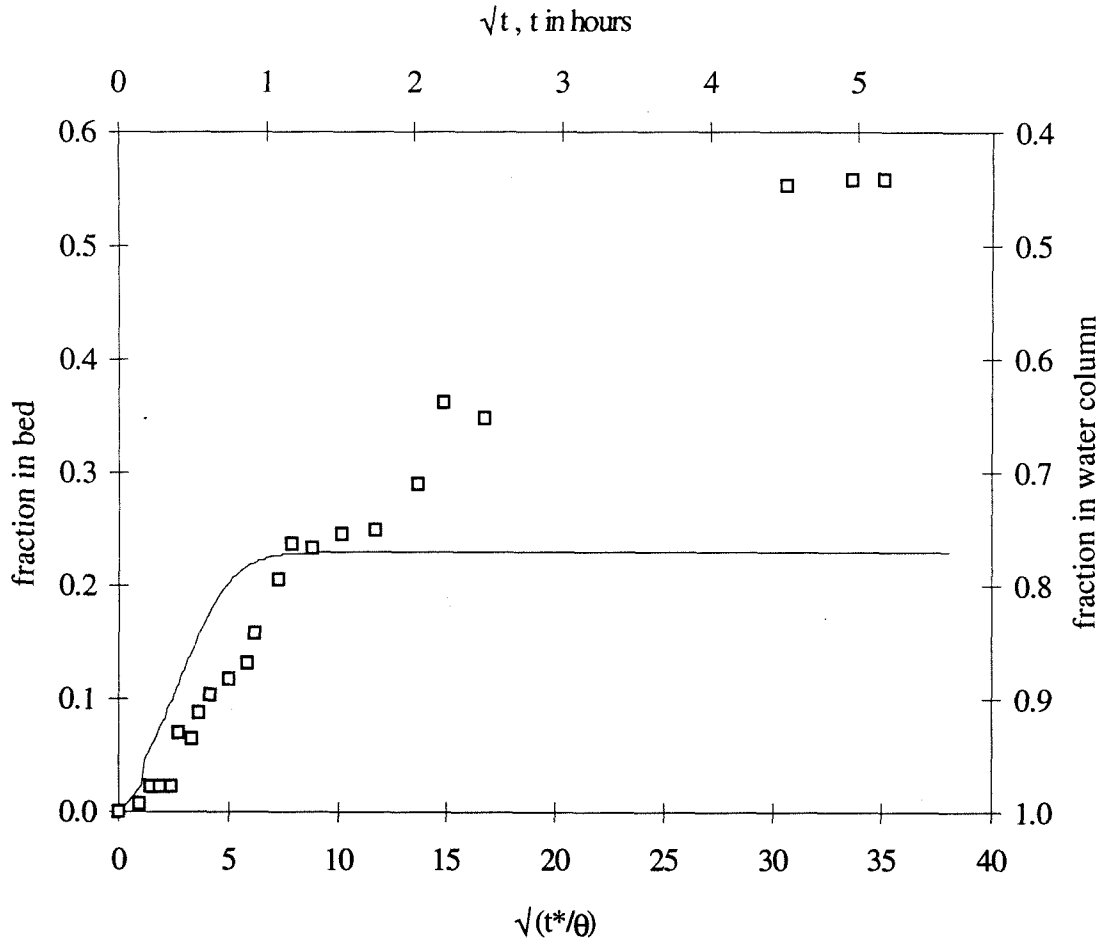

Figure 5.36. Transport of metal ions into sediment bed, Run 4. Moving ripples, Ottawa 30 sand, pH 6.8, $u^*_{bed} = 4.6$.

□ Zn^{2+}

—— simulation Zn^{2+}, R=12, cover-up model.

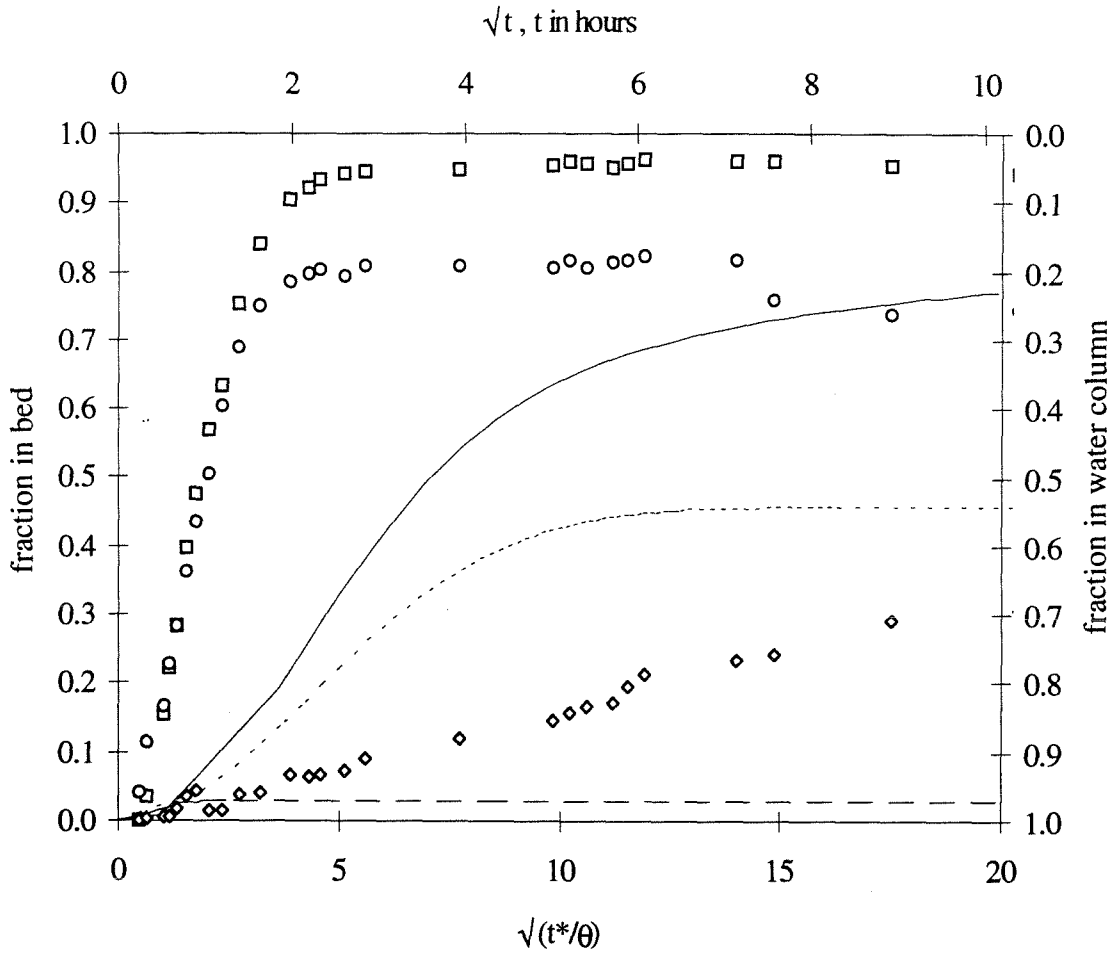

Figure 5.37. Transport of metal ions into sediment bed, Run 15. Moving ripples, Nevada 70 sand, pH 7.0, $u^*_{bed} = 1.1$.

□ Zn^{2+}

○ Ca^{2+}

✧ Li^{+}

—— R=20, pumping model

– – – R=20, cover-up model

— — cover-up model, no adsorption.

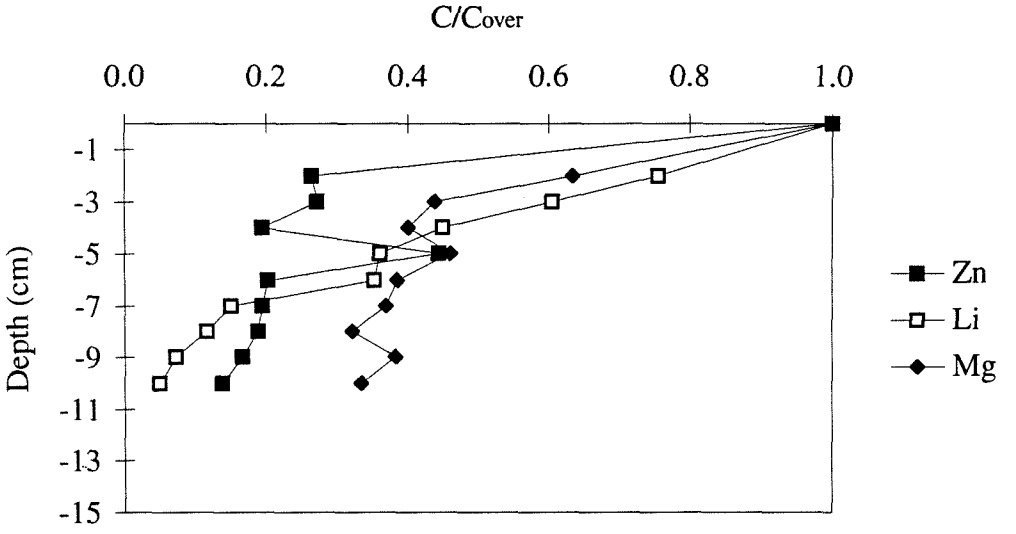

Figure 5.38. Penetration of metal ion tracers into sediment bed, Run 15, after completion of experiment.

5.2.5. Flat bed

The result of the flume run with a flat bed is shown in Figure 5.39. Since there are no bedforms, time can not be nondimensionalized in the usual manner. It can be seen in Figure 5.39 that the amount of metal ions in the bed approximately increases linearly with the square root of time. Furthermore, the transfer of the metal ions into the sediment bed is similar for both lithium (nonadsorbing) and calcium (adsorbing), and thus appears to be independent of the partitioning of the metal ion to the sediment. This indicates that the mass transfer can be modeled by a diffusion process. The effective diffusion coefficient can be easily estimated: After $\sqrt{t} = 10$, or $t = 100$ hours, about 25% of the metal ions are contained within the sediment bed. Assuming constant concentrations in the water column and the bed (see discussion in Chapter 3), the sediment bed is well mixed down to a penetration depth m/θ of the ions). The concentration of metal ions in the water column is given by $f = d'/(d'+m)$. With $d' = 10.7$ cm, the penetration depth m/θ is given by $m/\theta = d'(1-f)/(\theta f) = 11.1$ cm. Thus, the effective diffusion coefficient D is approximately $D = (11.1 \text{ cm})^2/(100 \text{ hrs}) = 1.2 \text{ cm}^2/\text{hr}$, or $3.4 \cdot 10^{-4} \text{ cm}^2/\text{s}$. This diffusion coefficient is at least an order of magnitude higher than the molecular diffusion coefficient for the metal ions (about $10^{-5} \text{ cm}^2/\text{s}$). The diffusion coefficient is very similar to the one observed by Elliott (1990) in his flat bed runs. Elliott also presents an analysis of possible causes for the increased exchange of solutes and concludes that pore-water exchange due to variations in the temporally averaged pressure at the bed surface seem to be the most likely cause.

To show that the bed exchange with a flat bed is smaller than exchange with a rippled bed, the result of the flat bed can be compared to a hypothetical run with similar hydraulic conditions (water depth, flow velocity) and ripples like, for example, in Run 2.

Using the pore-water pumping model, the predicted fraction in the bed for the pollutants after 100 hours assuming a rippled bed would be approximately 34% for lithium and 62% for calcium, significantly higher than the 25% observed in the flat bed run.

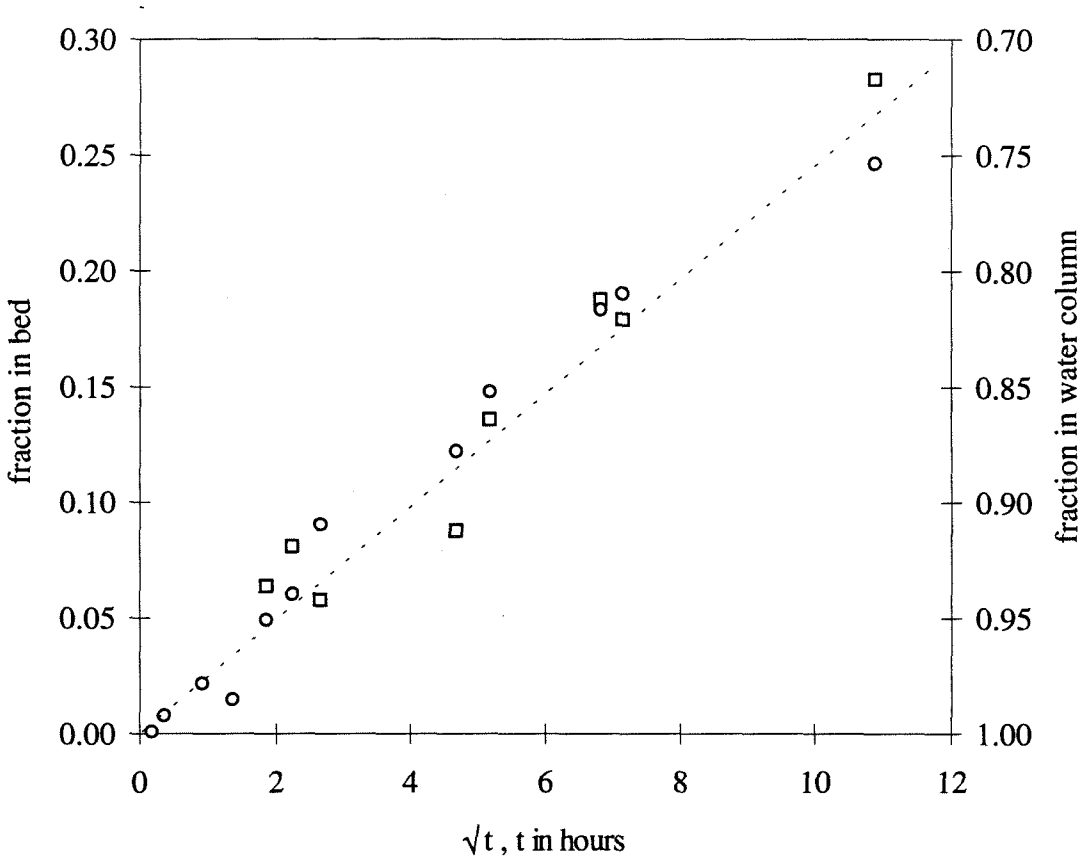

Figure 5.39. Transport of metal ions into sediment bed, Run 7. Flat bed, Ottawa 30 sand, pH 7.1.

□ Ca^{2+}

○ Li^{+}.

6. SUMMARY AND CONCLUSIONS

This chapter summarizes the experiments and results (Sections 6.1 and 6.2), discusses applications to natural rivers and pollutant transport models (Section 6.3), gives recommendations for future research (Section 6.4) and presents the main conclusions (Section 6.5).

6.1. SUMMARY OF EXPERIMENTS

The exchange of pollutants between overlying water and a permeable sediment bed was investigated using a 5 m long recirculating flume. The change of concentration in the water column was measured to determine the exchange of solution between sediment bed and overlying water. Pore-water samples were taken to investigate the variation of the pore-water concentration with depth in the sediment bed.

Experiments were performed using up to four different bivalent metal ions (copper, zinc, magnesium, calcium) and one monovalent metal ion (lithium) simultaneously. Lithium did not exhibit adsorption to the sediment bed of the flume and was used as an indicator for the exchange of water between the pores and the overlying water column. The bivalent metal ions partitioned to the sediment in different degrees and were used to investigate the influence of surface adsorption on the mass exchange between water column and sediment. The results of the experiments performed with the nonadsorbing lithium tracers are in excellent agreement with the results obtained by Elliott (1990) using dye tracers.

Flume experiments were performed for both stationary and moving ripples. Stationary ripples were both naturally and artificially formed. Two silica sands (mean grain

diameters 500 μm and 195 μm) with different hydraulic permeabilities and surface areas were used.

Partitioning values calculated from the observed mass transfer in the flume were compared to adsorption values in batch experiments to investigate the possibility to predict partitioning in a river bed from batch experiments.

6.2. FLUME EXPERIMENTS AND IMPORTANT MODEL PARAMETERS

6.2.1. Pore-water pumping model for stationary ripples

The mass exchange between sediment and the overlying water column for stationary ripples is modeled by pore-water advection, which is induced by pressure variations over the surface of the sediment bed. The pressure variations are caused by the disturbance of the shear flow above the bed by the ripples. Surface adsorption of a pollutant to the sediment is included in the model by assuming equilibrium partitioning of the pollutant to the sediment.

The pore-water pumping model for stationary ripples described observed mass exchange between sediment and overlying water in 11 flume experiments well; the deviations of the predicted concentration of metal ions in the water column were less than 10% from the observed values. The pumping model was found to be applicable for values of the normalized ripple velocity (see Table 6.2) $u^*_{b,R} < 0.5$. Generally, $u^*_{b,R}$ will be small if the dunes move slowly, the hydraulic permeability of the sediment is high or the driving piezometric pressure head is large. An example for mass exchange dominated by pumping is a stream with sandy ripples.

The formulas and typical values for piezometric pressure head, pore-water scaling velocity, pore-water pumping time scale and advective flux (per unit width) into the bed in terms of the stream flow velocity U, stream depth d, ripple height H, ripple wavelength λ and retardation coefficient R are given in Table 6.1. C_s is the concentration of the pollutant in the stream water.

The advective flux of pollutants into the bed is not effected by partitioning of the pollutant to the surfaces, but partitioning does effect the net mass exchange between overlying water and sediment bed for times $t^*/(\theta R) > 1$ because the rate and time of pollutant release from the bed depends on the adsorption characteristics.

Table 6.1. Formulas and typical scaling values for pore-water pumping model.

Parameter	**Formula**	**Typical range**
Piezometric pressure head	$h_m = \frac{0.21}{g} U^2 \left(\frac{H}{d}\right)^{\frac{3}{8}}$	0.1 - 1 cm
Pore-water scaling velocity	$u_m = \frac{0.42\pi}{g} \frac{K U^2}{R} \frac{1}{\lambda} \left(\frac{H}{d}\right)^{\frac{3}{8}}$	0.01 - 1 cm/min
Pumping time scale	$t_p = \frac{g}{0.84\pi^2} \frac{\lambda^2}{KU^2} \left(\frac{H}{d}\right)^{-\frac{3}{8}}$	0.1 - 100 hours
Advective flux into bed	$\bar{q}C_s = \frac{0.42}{g} \frac{KU^2}{\lambda} \left(\frac{H}{d}\right)^{\frac{3}{8}} C_s$	$\bar{q}$ = 0.01 - 1 cm/min
Adsorption equilibrium parameter	$\Gamma_p = t_{ads} k^2 K h_m$ $\Gamma_p >> 1$ no equilibrium $\Gamma_p << 1$ equilibrium	0.001 - 10

6.2.2. Turnover model for moving ripples

The mass exchange between water column and sediment for moving ripples could not be modeled well. The turnover model describes the observed streamwater/bed exchange of metal ions for about 50 turnover length scales within a factor of about 2, but completely fails to explain the concentration decrease in the overlying water column for later times. Thus, the cover-up model can only be used to estimate the initial flux of pollutant into the sediment bed and determine the magnitude of the mass exchange between overlying water and sediment bed caused by the ripple movement. Ripple turnover will be dominant for rapidly moving ripples, low hydraulic permeability of the sediment or small driving piezometric pressure head.

An example of turnover-dominated mass exchange is a river with large, rapidly moving, silty dunes. Model parameters and their typical values for the turnover model are listed in Table 6.2. It was found to be difficult to determine reliable values for ripple length, height, and propagation velocity due to large variations in these parameters in the flume experiments. The turnover process was not investigated in depth due to the complications caused by the flume size: kinetic considerations are much more important in the flume than in real systems because the short ripples propagate rapidly over their own length and do not allow the pore-water to equilibrate with the sediment inside the bedform. Also, due to the small depth-to-grain-size ratio in the flume, the ripple dimensions and ripple propagation speed are very irregular and thus very difficult to quantify and reproduce.

Table 6.2. Formulas and typical values for bedform turnover model.

Parameter	Formula	Typical range
Turnover time scale	$t_t = \frac{\lambda}{u_b}$	0.1 - 100 hours
Advective flux into bed		
a) pore-water in equilibrium with sediment	$\bar{q}C_s = \frac{u_b \theta H}{\lambda} C_s$	$\bar{q}$ = 0.001 - 0.1 cm/min
b) overlying water in equilibrium with sediment	$\bar{q}C_s = \frac{R u_b \theta H}{\lambda} C_s$	$\bar{q}$ = 0.001 - 1 cm/min
Normalized bedform velocity	$u^*_{b,R} = \frac{R\theta u_b}{Kkh_m}$	0 - 100
	$u^*_{b,R} >> 1$ turnover	
	$u^*_{b,R} << 1$ pumping	
Adsorption equilibrium parameter	$\Gamma_t = \frac{t_{ads} u_b}{\lambda}$	0.01 - 10
	$\Gamma_t >> 1$ no equilibrium	
	$\Gamma_t << 1$ equilibrium	

The initial flux of pollutant into the bed in the case of moving ripples depends on the ratio of adsorption and ripple-propagation time scales. There are essentially three regimes: for very rapidly moving ripples, it is possible that the adsorption time scale is longer than the ripple-propagation time scale. Then, adsorption equilibrium between solution and sediment will not be reached while the solution is contained within the ripples, and the uptake of metal ions into the bed will be controlled by kinetics.

If the two time scales are of about the same order of magnitude, stream water with metal ions from the overlying solution will be first covered up by the moving ripple and

then equilibrate with the sediment inside the ripple. Then, the initial flux of pollutant into the bed is given by the flux of solution into the bed as described in the cover-up model by $\bar{q}C_s \cong C_s\, u_b \theta H/\lambda$.

If the ripples are moving very slowly and the adsorption time scale is much shorter than the ripple-propagation time scale, it is possible that partitioning equilibrium exists between the surface of the sediment and the overlying water. In this case (very slowly moving, low permeability bottom sediments), pollutant will first adsorb to the sediment at the surface of the bed. The flux of pollutant into the bed is then given by both the flux of pollutant in solution and the flux of pollutant already sorbed to sediment which is subsequently covered by the propagating bedform. In this case, the initial flux of pollutant into the bed will be R times higher, $\bar{q}C_s \cong C_s\, R u_b \theta H/\lambda$.

After the time required for one ripple to progress by its own wavelength, the flux of pollutant into or out of the sediment will depend on kinetics and the concentration of pollutant in the water column and will require numerical modeling incorporating these factors. Also, advection of pollutants into the deeper regions of the bed will need to be considered for longer times (many bedform turnover times).

6.2.3. Batch experiments

Partitioning of the metal ions was investigated in batch scale adsorption experiments. Partitioning coefficients (or fraction adsorbed) and pH- dependence of the adsorption in batch experiments were found to agree within about 15% with the values calculated from the observed mass exchange in the flume experiments. For rivers with sandy bottom, is expected that the adsorption of a pollutant in the sediment bed of a natu-

ral stream can be predicted by carefully performing small scale laboratory adsorption experiments if the composition of the sediment samples is not modified during the sampling process. In case of an organic layer covering the sediment bed, additional processes could also be of importance.

The adsorption time scales of the metal ions used in the experiments were investigated in batch experiments. The assumption of adsorption equilibrium was found to be valid in the case of stationary ripples. In the case of moving ripples, kinetic effects of the metal ion adsorption onto sand can be of importance for short or fast-moving dunes. Appropriate parameters for the determination of kinetic equilibrium are given in Tables 6.1 and 6.2.

6.3. APPLICABILITY TO NATURAL STREAM SYSTEMS

The mass exchange models presented in this work can be used to investigate pollutant transfer between a sediment bed and an overlying water column in a sand-bed stream without calibration of parameters. Even though the laboratory experiments were performed under simplified conditions, the results of the study give insight into the relevance and magnitude of the mass exchange of adsorbing pollutants between stream and sediment bed.

To investigate the magnitude of mass exchange between stream water and sediment bed caused by pore-water pumping or turnover, only the physical dimensions of the ripples, the flow velocity and depth of the overlying water, and the hydraulic permeability and porosity of the sediment bed need to be known to estimate the flux of pollutant into and from the stream bed. For sandy sediments, it is possible to study the adsorption char-

acteristics of pollutants in batch experiments in the laboratory and then incorporate the results into the pore-water pumping model. Then, the importance of the processes investigated in this work can be examined by comparing the expected mass exchange to other processes that might occur in a natural stream: pore-water flow into and out of the banks of the stream, groundwater flow into or out of the stream, biologic processes and other effects.

The processes investigated in this work are most relevant for the investigation of short-time changes in pollutant concentration in a stream. However, short-time here means 'short' in terms of the pumping (or turnover) time scales, which can be of the order of days. Possible mass exchange due to long-term changes in the stream (for example, seasonal flow variations leading to changes in the morphology of the bed) are expected to outweigh the mass exchange caused by the ripples.

6.3.1. Use of the results in stream system models

The results obtained in this work allow improvement of existing pollutant transport models for porous sand-bed streams in active transport. Although it would be complicated to include a pore-water pumping submodel in a larger model describing a complete river system, the stream bed could still be modeled as a closed 'box' if equilibrium adsorption is assumed.

The terms describing the time-dependent fluxes into and out of the sediment bed in the case of pore-water pumping can be determined by the pumping model. The flux of pollutant into the bed is given in Table 6.1. However, it would be necessary to know the contamination history of the sediment (or the contamination status of the bed at a given

time) to accurately predict the outflow of pollutants from the stream bed. Then, the residence time function $\bar{R}_f$ must be incorporated to calculate the release of the pollutant from the bed.

The amount of tracer released from the bed at time = t that was transported into the bed at past time t-τ can be calculated from the derivative of the residence time function $\bar{R}_f$ at time τ (see discussion in Section 3.4.1). Assuming that the stream is well mixed in the cross section A, the general differential equation describing the pollutant concentration in the water column of the stream system is

$$\frac{\partial C(x,t)}{\partial t} + U\frac{\partial C(x,t)}{\partial x} = E\frac{\partial^2 C(x,t)}{\partial x^2} - \frac{\bar{q}}{d}C(x,t) + \frac{\bar{q}}{d}\int_{\tau=0}^{\tau=\infty}\left(-\frac{d\bar{R}_f}{d\tau}\right)C(x,t-\tau)d\tau \qquad (6.1)$$

where C is the cross-sectional average of the pollutant concentration in solution and E is the longitudinal dispersion coefficient. This differential equation has to be solved numerically to determine the value of pollutant concentration in the water column in space and time.

In the case of fast moving ripples or ripples with low hydraulic permeability, the turnover model can be used to estimate pollutant transfer into the bed. As can be seen in Tables 6.1 and 6.2, the flux of pollutant due to sediment turnover can be greater than the flux that would occur due to pore-water advection. However, the penetration depth of pollutant into the bed for moving ripples will usually be smaller than for pore-water pumping. For a pulse contamination, the pollutant is expected to be released faster from the bed than in the case of pumping because any part of a dune is again exposed to the overlying water after the dune has propagated by its own length. Irregularities in the dune height, wavelength and propagation speed will influence both transfer of pollutant into the bed and subsequent release from the sediment.

The turnover model for moving ripples did not describe the interfacial pollutant transfer well for long times, but it allows an estimation of the flux of pollutant into the bed in the case of a short-term spill (e.g., the length spill is short compared to the turnover time scale). Because turnover time scales in rivers can be rather long for large dunes (of the order of 10 - 100 hours), the model can still be applicable in real river systems if turnover is the dominant pollutant exchange process.

It is expected that the mass exchange between water column and sediment in a natural stream will be dominated by larger ripples because the amount of sediment exposed by ripple movement is proportional to the ripple height.

If chemical equilibrium can not be assumed, a two-dimensional, time-dependent model calculation of the adsorption of pollutant onto the sediment will probably have to be performed, leading to a much more complicated simulation model.

6.3.2. A simple example

For a short pulse of pollutant (e.g., the length of the pulse is small compared to the pore-water pumping time scale) in a sand-bed stream released at x = 0, the downstream decrease of pollutant concentration in the water column due to mass transfer into the bed can be approximated by investigating the flux of pollutant into the bed. Again assuming that the stream is nearly well-mixed in the cross-section A, the longitudinal dispersion equation can be written as

$$\frac{\partial C(x,t)}{\partial t} + U\frac{\partial C(x,t)}{\partial x} = E\frac{\partial^2 C(x,t)}{\partial x^2} - \frac{\bar{q}}{d}C(x,t) \qquad (6.2)$$

For the instant release of a mass M at t = 0, the solution to the differential equation is

$$C(x,t) = \underbrace{\frac{M/A}{\sqrt{4\pi Et}} e^{-\frac{(x-Ut)^2}{4Et}}}_{C_{disp}(x,t)} \underbrace{e^{-\frac{\bar{q}}{d}t}}_{\varphi(t)} \tag{6.3}$$

which can be written as

$$C(x,t) = C_{disp}(x,t) \cdot \varphi(t) \tag{6.4}$$

Here, $\varphi(t)$ then denotes the reduction factor in pollutant concentration due to the streambed exchange and can be shown in a plot of $\varphi(t) = C(x,t)/C_{disp}(x,t)$ versus time t.

For the example of a small sand-bed river with a depth of 0.5 m, a flow velocity of 0.3 m/s and ripples of 1 m length and 0.1 m height, the decrease of concentration in the flowing water (apart from longitudinal dispersion) with the downstream distance due to advective pumping is given in Figure 6.1. In this example, the driving piezometric pressure head h_m for bed pumping is calculated to be about 0.1 cm (see Equation 3.7). The value of the hydraulic permeability is taken as 0.1 cm/s, corresponding to a medium coarse sand bed. It can be seen that the pumping of pollutant into the bed significantly reduces the aqueous concentration in the water column: after about 100 hours, the concentration of pollutant in the water column is only about 30% of the value expected without bed exchange. The decrease in concentration would be even faster for a bed consisting of coarser sediments like gravel, and slower for a silty river bottom.

The pumping time scale, $1/(k^2Kh_m)$, in this example is approximately 7 hours, and the river water will have traveled about 6.5 km within this time. The longitudinal dispersion coefficient E can be approximated as E = 4 m^2/s (Fischer 1979). Using this value, the half-length of the pollutant cloud from a small source at a given time t can be estimated as $2\sigma = 2\sqrt{(2Et)}$. Then, at t = 100 hours, the front end length of the cloud (the

distance over which the pollutant concentration increases to its maximum) is about $2\sigma \cong$ 3.5 km. Thus, at a fixed point along the stream, the concentration of the pollutant increases from zero to its maximum value in about 3 hours. Because the pumping time scale (about 7 hours) is much longer than this value, the magnitude of the front end of the cloud will be exponentially decreased (due to one-way uptake into the bed) according to $\varphi(t)$ shown in Figure 6.1. On the other hand, the shape of the concentration rise curve will be unchanged because little pollutant is returned from the bed sooner than the rise time (because the rise time is less than the pumping time scale).

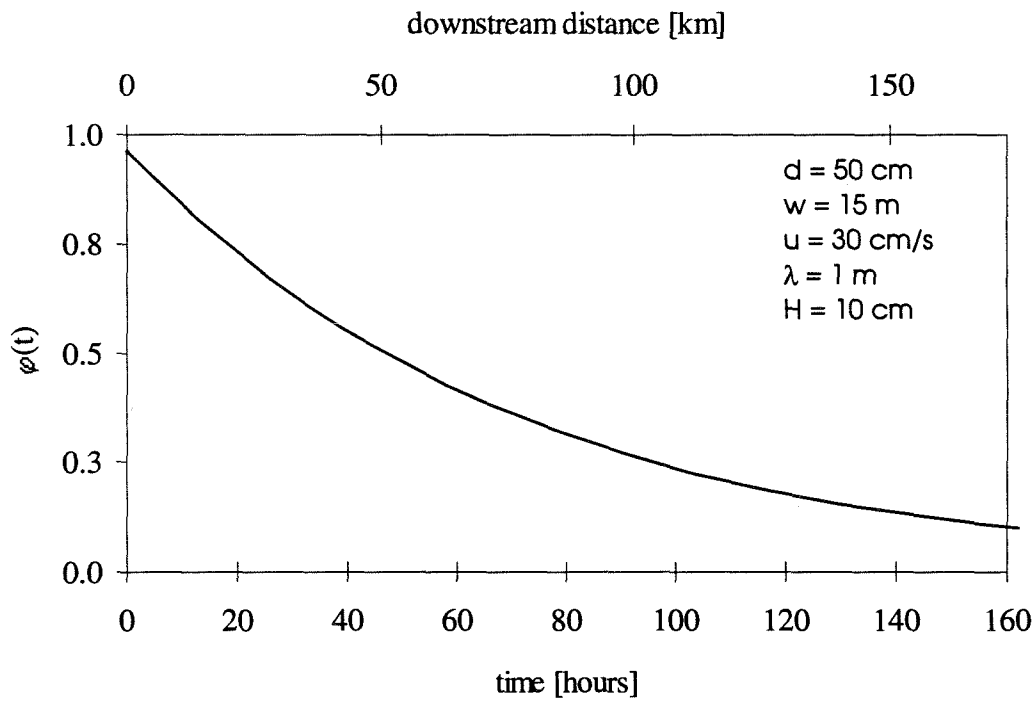

Figure 6.1. Additional decrease in pollutant concentration a in small sand-bed river due to pumping into the bed. Also shown is the distance traveled by the center of the cloud.

After the initial pulse has passed a fixed point in the bed, the leaching of pollutant from the sediment bed will produce a slowly changing, long lasting, low level contamination of the water. Thus, the time-dependent concentration passing at a fixed point x_0 along the river will also be affected by transfer of pollutant between water and bed: after the concentration peak will have passed x_0, the pollutant will be present in the river water much longer than expected if only dispersion is considered. The time scale for the decrease in the pollutant concentration by dispersion after 100 hours is again a few hours, but pollutant from the bed can be expected to transfer into the stream water for at least 25 or more pumping time scales (or over 100 hours), even longer for adsorbing tracers (see Section 3.4.1). Thus, the decrease of concentration in the water column (after the cloud center has passed a given point) will be dominated by the bed exchange, especially for long times when $\varphi(t)$ becomes small and a significant fraction of the pollutant has been pumped through the bed. The higher the retardation coefficient of the pollutant, the longer the leaching from the bed and the lower the tailing concentration of the pollutant will be. The pollutant can be advected into deep regions of the sediment bed to an approximate maximum penetration depth (which is only reached for very long times t^*) of the same order of magnitude as the wavelength of the ripples.

This example shows that pore-water pumping can be a very important process in a sand-bed stream and can have a strong effect on the concentration values of a pollutant in the water column. The pore-water pumping model will be mostly applicable to smaller rivers with beds consisting of medium or coarse, sandy sediment.

6.4. FUTURE RESEARCH

In this section, possible future research tasks are identified and discussed.

6.4.1. Piezometric pressure head over the ripples

The piezometric pressure head used in the model had to be calculated from an empirical formula based on relatively few experiments with ripples of only one size and shape. The effect of varying dune shape or the wavelength/depth ratio on the piezometric pressure head is not known. In order to more accurately determine the driving pressure head for the pore-water pumping model, additional experiments on a variety of ripples of different size and shapes will need to be performed. Especially for smaller ripples, the measurement of the piezometric pressure head will be extremely difficult because the maximum pressure difference across a dune will be of the order of 0.1 mm. In most applications in natural stream systems, the wavelength of dunes will be between about 20 cm and 10 m, and the dune height will be between 3 cm and 5 m. Data will need to be collected over a similar size range of dunes to assure a good prediction of the piezometric pressure head.

6.4.2. Surface coated sediments

Sediments in natural stream systems are generally coated by both metal oxide and organic coatings. These coatings can significantly alter the adsorption of pollutants onto surfaces compared to 'clean' sediment surfaces. Hence, future flume experiments should be conducted with more adsorptive media than silica sand to be more realistic for natural streams.

Preliminary experiments with humic acid coatings on sand showed that it can be difficult to obtain reproducible experimental conditions because of changes in the coating of the grains due to physical and chemical abrasion of the sediment by the cleaning process. The grain surfaces could be either coated artificially, or naturally coated sediments could be used. If the surfaces are coated artificially, the nature of the coating would probably be relatively well known, but the need of treating over 200 kg of sediment would be a challenge.

The surfaces of naturally coated sediments will be more difficult to classify. Furthermore, because the nature of the surface coating will likely change between experimental runs, the adsorption behavior of tracers would either have to be re-investigated for every experimental run, or 'fresh' sediment would have to be used for every experiment run.

As an alternative to metal oxide coating, it could be possible to use sediments with very high metal oxide content. The use of such sediments would allow the reuse of sediment in the experiments without the need to reapply surface coatings to the grains.

6.4.3. Particles: Clay and silt

Particulate matter is present in almost all natural stream systems in varying concentrations. It is expected that the presence of suspended particles in the water column will have a strong influence on the mass exchange of adsorbing tracers. Because of their large specific surface area, clay and silt particles could scavenge a large fraction of the pollutant in the water column. Then, the exchange of adsorbing tracers between the stream water and the bed will not only be determined by the adsorption characteristics of

the tracer, but also by the transport of the particles into and out of the bed. It would be necessary to first understand the transport of the particles between stream water and the bed. At a later stage, experiments could be conducted with both adsorbing tracers and suspended particles in the system and the two processes (adsorption to the bed sediment, adsorption to particles with subsequent transport into the bed) could be investigated simultaneously.

6.4.4. Organic tracers

Many pollutants in the environment are synthetic organic materials. It is therefore important to understand the transport of these organics in a natural stream system. Because organic pollutants generally adsorb to the coatings on the surfaces of natural sediments and adsorb only weakly to 'pure' surfaces, coated sediments will have to be used in order to investigate the behavior of synthetic organic pollutants in a sediment-water system. Furthermore, the volatility of some organic materials will need to be considered in such experiments, thus adding more complications.

6.4.5. Nonequilibrium adsorption

In this work, it has been shown that an equilibrium partitioning model can be used to describe the transport of metal ions into and out of a sand bed. However, if the adsorption kinetics are very slow, the assumption of equilibrium partitioning might not be applicable any more.

If the adsorption capacity of the surfaces is limited (small surface area, or high pollutant concentrations), the fraction of pollutant adsorbed to the surfaces depends on the amount of pollutant already on the surface. Then, equilibrium partitioning also can not be applied.

In these cases, it will be very difficult to develop a general model (similar to the residence-time model) describing the exchange of pollutant between water column and sediment bed, and it is likely that numerical simulations may need to be performed on a case-by-case basis.

6.4.6. Moving ripples or dunes

Mass exchange between stream water and sediment bed caused by ripple movement can be very important in the case of fast moving ripples, or in beds of low hydraulic permeability. The magnitude of the bedform propagation relative to the pore water pumping velocity is given by the normalized bedform velocity $u^*_{b,R}$. The relative bedforms velocity is partitioning-dependent because the ripples appear to be moving faster compared to the pore water pumping velocity if the pollutant partitions the sediment; in other words, the characteristic non-dimensional bedform velocity $u^*_{b,R}$ is proportional to R, the retardation coefficient.

Because of its size, the experimental apparatus used in this study is not very well suited to investigate the mass exchange of adsorbing pollutants due to moving ripples because ripple dimensions and propagation velocity are very irregular and therefore hard to classify. Furthermore, effects of adsorption kinetics are relatively very important because the time for ripples to propagate a distance equivalent their own length may be very short

(about 5 to 10 minutes), and adsorption equilibrium between pore-water and sediment inside the ripples is probably not reached within this short time. However, it is believed that in a natural stream, large dunes will be dominating the turnover mass exchange between water column and sediment because the amount of sediment exposed by their movement is the largest. Then, effects of adsorption kinetics are of much less importance because dunes are much longer and therefore require a much longer time to propagate their own length; equilibrium partitioning inside the bedforms can now be assumed. If the bedform velocity is very small, equilibrium partitioning might even exist between the sediment surface and the overlying water column.

Large dunes in natural sand-bed streams are often covered by faster moving ripples of smaller size. The importance of these smaller size ripples will also need to be investigated. Ripples observed in the flume were also sometimes covered by smaller ripples. These ripples, however, were so small ($H \cong 1/4$ - $1/2$ cm, $\lambda \cong 1$ - 4 cm) and irregular that they were found to be very difficult to characterize.

The investigation of moving ripples should be conducted in a bigger flume to produce larger, more naturally shaped ripples.

6.4.7. Field experiments

Because a number of different processes contribute to the concentration change of pollutants in a natural stream, it is usually difficult to observe the effects of each individual process in this setting. Concentration changes of a pollutant in the stream water will also be very small over short reaches of a stream (see Figure 6.1), so that accurate measurements of the mass transfer between the stream and the bed will be difficult. However,

pollutant exchange with the bed will certainly contribute significantly to the total mass balance for a stream and its channel and must be included in a model describing observed data in field studies. Laboratory experiments for single processes can be helpful to evaluate the relative importance of different processes in the field and assist in a proper model formulation.

6.5. CONCLUSIONS

1. The transfer of metal ions (copper, zinc, calcium, magnesium, and lithium) between stream water and a rippled sand bed in a laboratory flume with slowly moving or stationary ripples can be well predicted by a pumping model combining equilibrium partitioning and pressure-driven advection. The model agrees within 10% with the observed mass exchange in 11 flume experiments. The pumping process increases the exchange rate by several orders of magnitude over molecular processes.

2. The stronger the partitioning of the pollutant to the sediment in the bed, the larger the amount of pollutant that can be captured within the sediment bed and taken out of the flowing overlying water. Pollutants will then be slowly released from the bed over a long period of time (many pumping time scales) after the concentration in the water column has decreased. The flux of pollutant out of the bed will be longer lasting if partitioning to the sediment occurs.

3. The results from the laboratory flume experiments show that pressure-driven advection can transport pollutants from the stream water deep into the sediment bed. The wavelength of the ripples causing the pressure variation over the sediment bed

is a good approximation of the maximum penetration depth for long times. Stronger partitioning of the pollutant to the sediment results in a smaller penetration depth into the bed compared to nonadsorbing tracers at the same time.

4. For a sediment bed with rapidly moving ripples, the turnover model can be used to approximate the flux of tracer into the bed in the case of a short-term spill (e.g., the length spill is short compared to the turnover time scale). Predictions of the mass exchange increasingly deviated from the observed experimental data after about 50 bedform turnover times in the experimental run.

5. Appropriate scaling parameters have been defined to investigate the applicability of the pumping and turnover models. The normalized ripple velocity $u^*_{b,R} = (R\theta u_b)/(Kkh_m)$ can be used to determine the appropriate modeling approach. Based on three experiments, the pore-water pumping model (with modified underflow) can be used if $u^*_{b,R} < 0.5$, the turnover model applies if $u^*_{b,R} > 5$. In the intermediate regime, no general model could be developed because the two mass exchange processes depend on different parameters. Furthermore, some of these parameters also depend on the partitioning of the pollutants.

6. The validity of assuming kinetic adsorption equilibrium was investigated for both models. Equilibrium adsorption for the pore-water pumping model can be assumed if the adsorption time scale, t_{ads}, is short compared the pumping time scale, $t_p = 1/(k^2Kh_m)$. For the turnover model, kinetic equilibrium can be assumed if the adsorption time scale is short compared to the turnover time scale $t_t = \lambda/u_b$.

7. Partitioning experiments with the metal ions used in the flume experiments were performed in beakers. Results of the beaker experiments agreed within 15% with the observed partitioning of the metal ions in the flume for silica sand. It is possi-

ble to predict the partitioning of pollutants in the bed of rivers with porous sandy bottom by performing laboratory beaker experiments with sediment samples. However, care must be taken to assure that the sediment composition is not altered during the sampling.

8. Recommendations for future experiments include:
   - Precise measurements of the piezometric pressure head over differently sized and shaped ripples to improve the accuracy of mass transfer predictions using the pore-water pumping model.
   - Use of coated sediments, less uniformly sized sediments, and sediment mixtures including silt and clay.
   - Use of particulate matter and organic pollutants.
   - Investigation of the effects of chemical nonequilibrium on the mass exchange.
   - Further investigation of the mass exchange for moving ripples.
   - Field experiments.

REFERENCES

Ahrland, S., Grenthe, I. and Noren, B., 1960, **The Ion Exchange Properties of Silica Gel**, *Acta Chemica Scandinavica, 14,* 1059-1076

Ambrose, R.B., 1986, **User's Manual for the Chemical Transport and Fate Model TOXIWASP,** *U.S. Environmental Protection Agency, Report EPA-600/3-83-005*

ASCE, 1975, **Manuals and Reports on Engineering Practice, Sedimentation Engineering Handbook**, 54, 119

Bahr, J.M. and Rubin J., 1987, **Direct Comparison of Kinetic and Local Equilibrium Formulations for Solute Transport affected by Surface Reactions,** *Water Resources Research, 23(3),* 438-452

Basmadjian, D. and Quan, F., 1987, **Distribution of Chemicals in Rivers during Contamination and Recovery,** *Journal of Environmental Engineering, 114(6),* 1185-1201

Bear, J., 1972, **Dynamics of Fluids in Porous Media,** *Elsevier*

Bencala, K. E., 1984, **Interactions of Solutes and Streambed Sediment. 2. A Dynamic Analysis of Coupled Hydrologic and Chemical Processes that Determine Solute Transport,** *Water Resources Research 20(12),* 1804-1814

Bencala, K. E., McKnight, D. M. and Zellweger, G. W., 1990, **Characterization of Transport in an Acidic and Metal-Rich Mountain Stream based on a Lithium Tracer Injection and Simulations of Transient Storage,** *Water Resources Research 26(5),* 989-997

Bencala, K.E., 1993, **A Perspective on Stream-Catchment Conditions,** *Journal of the North American Benthological Society 12(1),* 44-47

Burns, L.A., Cline, D.M. and Lassiter, R.R., 1982, **Exposure Analysis Modelling System,** *U.S. Environmental Protection Agency, Report EPA-600/3-83-023*

Burris, D.R., Antworth, C.P., Stauffer, T.B. and MacIntyre, W.G., 1991, **Humic Acid-Modified Silica as a Model Aquifer Material,** *Environmental Toxicology and Chemistry, 10,* 433-440

Cerling, T.E., Morrison, S.J., Sobocinski, R.W. and Larsen, I.L., 1990, **Sediment-Water Interaction in a Small Stream: Adsorption of ^{137}Cs by Bed Load Sediments,** *Water Resources Research 26(6),* 1165-1176

Clark, S.W. and Cooke, S.R.B., 1968, **Adsorption of Calcium, Magnesium, and Sodium Ion by Quartz,** *Society of Mining Engineers AIME, 241,* 334-347

Clarke, G.K.C. and Waddington, E.D., 1991, **A Three-Dimensional Theory of Wind Pumping,** *Journal of Glaciology, 37(125),* 89-96

Davis, J.A. and Kent, D.B., 1990, **Surface Complexation Modeling in Aqueous Geochemistry,** *Reviews in Mineralogy, 23, Ch. 5,* 177-259

Davis, J.A. and Leckie, J.O., 1978, **Surface Ionization and Complexation at the Oxide/Water Interface,** *Journal of Colloid and Interface Science, 67(1),* 90-107

de Bruyn, P.L., 1955, **Flotation of Quartz by Cationic Collectors,** *Transactions AIME, 3,* 291-296

Donigan, A.S. and Crawford, N.H., 1976, **Modeling Nonpoint Pollution from the Land Surface,** *U.S. Environmental Protection Agency, Report EPA-600/3-76/083*

Donigan, A.S. and Davis, H.S., 1978, **User's Manual for Agricultural Runoff Model (ARM),** *U.S. Environmental Protection Agency, Report EPA-600/3-78/080*

Dugger, D.L., Stanton, J.H. et al., 1964, **The Exchange of Twenty Metal Ions with the Weakly Acidic Silanol Group of Silica Gel,** *The Journal of Physical Chemistry 68(4),* 757-760

Dzombak, D.A. and Morel, F.M.M., 1987, **Adsorption of Inorganic Pollutants in Aquatic Systems,** *Journal of Hydraulic Engineering, 113(4),* 430-475

Dzombak, D.A. and Morel, F.M.M., 1990, **Surface Complexation Modeling, Hydrous Ferric Oxide,** *John Wiley & Sons*

Edwards, M. and Benjamin, M.M., 1989, **Adsorptive Filtration using Coated Sand: A New Approach for Treatment of Metal-Bearing Wastes,** *Journal of the Water Pollution Control Federation, 61,* 1523-1533

Elliott, A.H., 1990, **Transfer of Solutes into and out of Streambeds,** *Ph.D. Thesis, California Institute of Technology*, available as Report KH-R-52, W. M. Keck Laboratory, 138-78 Caltech, Pasadena, CA 91125

Fehlman, H.M., 1985, **Resistance Components and Velocity Distributions of Open Channel Flow over Bedforms,** *Master's Thesis, Colorado State University, Fort Collins*

Fic, M. and Isenbeck-Schröter, M., 1989, **Batch Studies for the Investigation of the Mobility of the Heavy Metals Cd, Cr, Cu and Zn,** *Journal of Contaminant Hydrology, 4,* 69-78

Fischer, H., List, E.J.L., Koh, R.C.Y., Imberger, J. and Brooks, N.H. , 1979, **Mixing in Inland and Coastal Waters,** *Academic Press*

Fuller, C.C. and Davis, J.A., 1987, **Processes and Kinetics of Cd^{2+} Sorption by a Calcareous Aquifer Sand,** *Geochimica et Cosmochimica Acta, 51,* 1491-1502

Grimm, N.B. and Fisher, S.G., 1984, **Exchange Between Interstitial and Surface Water: Implications for Stream Metabolism and Nutrient Recycling,** *Hydrobiologia, 111,* 219-228

Gyr, A. and Schmid, A., 1989, **The Different Ripple Formation Mechanism,** *Journal of Hydraulic Research, 27(1),* 61-74

Haque, M.I. and Mahmood, K., 1985, **Geometry of Ripples and Dunes,** *Journal of Hydraulic Engineering, 111(1),* 48-63

Harvey, J.D. and Bencala, K.E., 1993, **The Effect of Streambed Topography on Surface-Subsurface Water Exchange in Mountain Catchments,** *Water Resources Research 29(1),* 89-98

Ho, R.T. and Gelhar, L.W., 1983, **Turbulent Flow over Undular Permeable Bedforms,** *Journal of Hydraulic Engineering, 109(5),* 741-757

Honeyman, B.D. and Santschi, P.H., 1988, **Metals in Aquatic Systems,** *Environmental Science and Technology, 22(8),* 862-871

Hüttel, M., Klöser, S., Forster, F. and Ziebis, W., 1994, **The Impact of Biological Sediment Topography on Interfacial Particle Flux,** Abstract in 1994 Ocean Sciences Meeting, Supplement to *EOS, Transactions, American Geophysical Union, 75(3),* 230

Iler, R.K., 1979, **The Chemistry of Silica,** *John Wiley & Sons*

Jackman, A.P., Walters, R.A. and Kennedy, V.C., 1984, **Transport and Concentration Controls for Chloride, Strontium, Potassium and Lead in Uvas Creek, a Small Cobble-Bed Stream in Santa Clara County, California,** *Journal of Hydrology, 75,* 111-141

James, R.O. and Parks, G.A., **Characterization of Aqueous Colloids by Their Electrical Double-Layer and Intrinsic Surface Chemical Potentials,** *Surface and Colloid Science, 12,* 119-217

James, R.V. and Rubin, J., 1979, **Applicability of the Local Equilibrium Assumption to Transport Through Soils of Solutes affected by Ion Exchange,** *Chemical modelling in aqueous systems, ACS Symposium 0097-6156 93, Ch. 11,* 225-235

Kotronarou, A., 1989, **Research on Model Sorbate for Ottawa Sand,** *Internal report, Environmental Engineering Sciences, Caltech*

Kudo, A. and Gloyna, E. F., 1971, **Transport of ^{137}Cs - II: Interaction with Bed Sediments,** *Water Research, 5,* 71-79

Kuwabara, J.S., Leland, H.V. and Bencala, K.E., 1984, **Copper Transport along a Sierra Nevada Stream,** *Journal of Environmental Engineering, 110(3),* 646-655

Lyklema, J., 1980, **Colloid Stability as a dynamic Phenomenon,** *Pure and Applied Chemistry, 52,* 1221-1227

MacIntyre, W.G., 1991, **A Comparison of Sorption Coefficients determined by Batch, Column, and Box Methods on a Low Organic Carbon Aquifer Material,** *Ground Water, 29(6),* 908-921

McIlroy, L.M.,., 1986, **Partitioning of Heavy Metals to Suspended Solids of the Flint River, Michigan,** *Environmental Toxicology and Chemistry, 5(7), 609-622*

Mikami, N., 1983, **Kinetic Study of the Adsorption-Desorption of the Uranyl Ion on a γ-Al_2O_3 Surface using the Pressure-Jump Technique,** *The Journal of Physical Chemistry 87(26),* 5479-5481

Msaky, J.J. and Cavet, R., 1990, **Adsorption Behavior of Copper and Zinc in Soils: Influence of pH on Adsorption Characteristics,** *Soil Science, 150(20),* 513-522

Nagaoka, H. and Ohgaki, S., 1990, **Mass Transfer Mechanism in a Porous River Bed,** *Water Resources, 24(4),* 417-425

O'Connor, D. J. , 1988, **Models of Sorptive Toxic Substances in Freshwater Systems. III: Streams and Rivers,** *Journ. of Environmental Engineering, 114(3),* 552-574

Onishi, Y. and Wise, S.E., 1982, **User's Manual for the Instream Sediment-Contaminant Model, SERATRA,** *U.S. Environmental Protection Agency, Report EPA-600/3-82-0550*

Onishi, Y., 1981, **Sediment-Contaminant Transport Model,** *Journal of the Hydraulics Division, Proc. ASCE, 107 (HY9),* 1089-1107

Papelis, C.,1988, **HYDRAQL: A Program for the Computation of Chemical Equilibrium Composition of Aqueous Batch Systems Including Surface-Complexation Modeling of Ion Adsorption at the Oxide/Solution Interface,** *Stanford University*

Parker, J.C. and Valocchi, A.J., 1986, **Constraints on the Validity of Equilibrium and First-Order Kinetic Transport Models in Structured Soils,** *Water Resources Research, 22(3),* 399-407

Reece, D. E., Felkey, J.R. and Wai, C.M., 1978, **Heavy Metal Pollution in the Sediments of the Cour d'Alene River, Idaho,** *Environmental Geology, 2(5),* 289-293

Richardson, C.P. and Parr, A. D., 1988, **Modified Fickian Model for Solute Uptake by Runoff,** *Journal of Environmental Engineering, 114(4),* 792-810

Salim, R. and Bloh, K., 1989, **Effect of Competition on the Adsorption of some Ions (Copper, Zinc, Zirconium, Selenium and Strontium) on River-Mud,** *Journal of Environmental Science and Health, A24(7),* 809-822

Savant, S.A., Reible, D.D. and Thibodeaux, L.J., 1987, **Convective Transport within Stable River Sediments,** *Water Resources Research, 23(9),* 1763-1768

Schindler, P.W., Fürst, B., Dick, R. and Wolf, P.U., 1976, **Ligand Properties of Surface Silanol Groups,** *Journal of Colloid and Interface Science, 55(2),* 469-475

Schnoor, J.L., Sato, C., McKechnie, D. and Sahoo, D., 1987, **Process, Coefficients, and Models for Simulating Toxic Organics and Heavy Metals in Surface Waters,** *U.S. Environmental Protection Agency, Report EPA-600/3-87-015*

Shen, H.W., Fehlman, H.M. and Mendoza, C., 1990, **Bed Form Resistance in Open Channel Flows,** *Journal of Hydraulic Engineering, 116(6),* 799-815

Shukla, U.C. and Mittal, S.B., 1979, **Characterization of Zinc Adsorption in some Soils of India,** *Soil Science Soc. Am. J., 43,* 905-908

Smith, K.S., Ranville, J.F. and Macalady, D.L., 1989, **Predictive Modeling of Copper, Cadmium, and Zinc Partitioning Between Streamwater and Bed Sediment from a Stream receiving Acid Mine Drainage, St. Kevin Gulch, Colorado,** *USGS Toxic Substances Hydrology Program, Water Resources Invest. Report 91-4034,* 380-386

Smith, R.M. and Martell, A.E., 1976, **Critical Stability Constants - Vol. 4: Inorganic Complexes,** *Plenum Press*

Smith, R.M. and Martell, A.E., 1976, **Critical Stability Constants - Vol. 6: Second Supplement,** *Plenum Press*

Stahl, R.S. and James, B.R., 1991, **Zinc Sorption by Iron-Oxide-Coated Sand as a Function of pH,** *Soil Science Soc. Am. J., 55,* 1287-1290

Stahl, R.S. and James, B.R., 1991, **Zinc Sorption by Manganese-Oxide-Coated Sand as a Function of pH,** *Soil Science Soc. Am. J., 55,* 1291-1294

Stumm, W. and Morgan, J.J., 1981, **Aquatic Chemistry,** *John Wiley & Sons*

Stumm, W., 1987, **Aquatic Surface Chemistry,** *John Wiley & Sons*

Subramanian, V., van Grieken, R. and van't Dack, L., 1987, **Heavy Metals Distribution in the Sediments of Ganges and Brahmaputra Rivers,** *Environmental Geology Water Science, 9(2),* 93-103

The Chemical Society, 1964, **Stability Constants of Metal-Ion Complexes,** *Burling House*

The Chemical Society, 1971, **Stability Constants of Metal-Ion Complexes - Supplement 1,** *Burling House*

Turner, A., Millward, G.E., Bale, A.J. and Morris, A.W., 1993, **Application of the K_D Concept to the Study of Trace Metal Removal and Desorption during Estuarine Mixing,** *Estuarine, Coastal and Shelf Science, 36,* 1-13

Valocchi, A.J., 1988, **Theoretical Analysis of Deviations from Local Equilibrium during Sorbing Solute Transport through Idealized Stratified Aquifers,** *Journal of Contaminant Hydrology, 2,* 191-207

Vanoni, V.A., 1974, **Factors Determining Bed Forms of Alluvial Streams,** *Journal of the Hydraulics Division, Proc. ASCE, 100, HY 3,* 363-377

Vittal, N., 1977, **Resistance of Two-dimensional Triangular Roughness,** *Journal of Hydraulic Research, 15(1),* 19-33

Webb, J. E. and Theodor, J. L., 1972, **Wave-Induced Circulation in Submerged Sands,** *Journal of the Marine Biological Association UK, 52,* 903-914

Wu, S. and Gschwend, P.M., 1986, **Sorption Kinetics of Hydrophobic Organic Compounds to Natural Sediments and Soils,** *Environmental Science and Technology, 20,* 717-725

Yasunaga, T. and Ikeda, T., 1986, **Adsorption-Desorption Kinetics at the Metal-Oxide-Solution Interface Studied by Relaxation-Methods,** *Geochemical Processes at Mineral Surfaces, ACS, Ch. 12,* 231-253

Young, J.R., 1981, **A Study of the Adsorption of Ni(II) onto an Amorphous Silica Surface by Chemical and NMR Methods,** *Ph.D. Thesis, California Institute of Technology*

APPENDIX A: TITRATION DATA

In all titration experiments: solution volume 500 mℓ, sand mass 300g.

Table A.1. Titration data: Zinc adsorption onto Ottawa 30 sand.

Sample	pH	C [μM]	f_a	Zn adsorbed [nmoles/g]	Σ [nmoles/cm^2]	k_p [cm^3/g]
1	2.6	5.4	0.00	0.00	0.0	0.00
2	3.7	5.4	0.00	0.00	0.0	0.00
3	4.2	5.3	0.17	0.20	0.0	0.04
4	4.8	5.0	0.44	0.70	0.1	0.14
5	5.3	4.5	0.65	1.51	0.2	0.33
6	6.1	3.6	0.82	3.01	0.4	0.83
7	6.8	2.7	0.90	4.52	0.6	1.67
8	7.0	1.7	0.95	6.12	0.9	3.51
9	7.3	1.5	0.96	6.53	0.9	4.33
10	7.6	1.0	0.98	7.33	1.0	7.16
11	7.5	1.2	0.97	7.03	1.0	5.83
12	7.7	0.7	0.98	7.83	1.1	10.83
13	7.8	0.8	0.98	7.73	1.1	9.87
14	8.7	0.4	0.99	8.33	1.2	19.76

Table A.2. Titration data, repeat 1: Zinc adsorption onto Ottawa 30 sand.

Sample	pH	C [μM]	f_a	Zn ads. [nmoles/g]	Σ [nmoles/cm^2]	k_p [cm^3/g]
1	2.3	18.7	0.00	0.00	0.0	0.00
2	3.0	18.6	0.01	0.04	0.0	0.00
3	3.3	18.6	0.02	0.05	0.0	0.00
4	4.0	18.6	0.05	0.19	0.0	0.01
5	4.8	18.5	0.10	0.35	0.1	0.02
6	6.8	11.5	0.85	11.85	1.7	1.03
7	7.2	7.0	0.94	19.37	2.8	2.75

Table A.3. Titration data, repeat 2: Zinc adsorption onto Ottawa 30 sand.

Sample	pH	C [μM]	f_a	Zn ads. [nmoles/g]	Σ [nmoles/cm^2]	k_p [cm^3/g]
1	3.1	15.1	0.00	0.00	0.0	0.00
2	3.6	14.8	0.20	0.65	0.1	0.04
3	4.3	14.6	0.25	0.90	0.1	0.06
4	5.0	14.5	0.30	1.12	0.2	0.08
5	6.3	12.1	0.70	5.11	0.7	0.42
6	7.0	8.7	0.87	10.82	1.5	1.25
7	7.1	7.1	0.91	13.40	1.9	1.89
8	7.6	4.2	0.96	18.28	2.6	4.38

Table A.4. Titration data, repeat 3: Zinc adsorption onto Ottawa 30 sand.

Sample	pH	C [μM]	f_a	Zn ads. [nmoles/g]	Σ [nmoles/cm^2]	k_p [cm^3/g]
1	3.0	10.8	0.00	0.00	0.0	0.00
2	3.6	10.7	0.05	0.11	0.0	0.01
3	4.2	10.5	0.18	0.42	0.1	0.04
4	4.9	10.1	0.39	1.17	0.2	0.12
5	5.3	9.2	0.60	2.55	0.4	0.28
6	6.2	6.0	0.88	7.96	1.1	1.33
7	7.0	3.6	0.95	12.00	1.7	3.36
8	7.4	2.5	0.97	13.85	2.0	5.65
9	7.7	2.1	0.97	14.44	2.1	6.87
10	7.6	1.9	0.98	14.70	2.1	7.57
11	7.8	1.7	0.98	15.18	2.2	9.17

APPENDIX B: SAMPLE FLUME DATA - RUN 6

Table B.1. Zinc concentration in water column: Run 6.

t [min]	t [hrs]	$\sqrt{(t/hrs)}$	C [μM]				C^*	$1-C/C^*$
			#1	#2	#3	average		
2	0.0	0.2	19.3	11.2	18.0			
6	0.1	0.3	15.0	16.3	17.3			
9	0.2	0.4	16.3	15.5	15.9	16.3	0.99	0.01
12	0.2	0.4	16.1	16.2		16.2	0.98	0.02
29	0.5	0.7	15.8	15.7		15.7	0.96	0.04
47	0.8	0.9	15.3	15.3		15.3	0.93	0.07
76	1.3	1.1	14.7	14.9		14.8	0.91	0.09
95	1.6	1.3	14.5	14.3		14.4	0.88	0.12
140	2.3	1.5	13.9	13.9		13.9	0.85	0.15
247	4.1	2.0	13.0	12.8		12.9	0.79	0.21
392	6.5	2.6	11.8	12.2		12.0	0.73	0.27
460	7.7	2.8	12.0	11.8		11.9	0.73	0.27
1340	22.3	4.7	9.0	9.4		9.2	0.56	0.44
1455	24.3	4.9	8.9	8.5		8.7	0.53	0.47
1814	30.2	5.5	8.2	8.5		8.3	0.51	0.49
2775	46.3	6.8	7.1	7.1		7.1	0.44	0.56
3300	55.0	7.4	6.8	6.9		6.9	0.42	0.58
4640	77.3	8.8	5.9	6.1		6.0	0.37	0.63
7140	119.0	10.9	5.3	5.7		5.5	0.34	0.66
7310	121.8	11.0	5.5	5.6		5.6	0.34	0.66

Table B.2. Lithium concentration in water column: Run 6.

t [min]	t [hrs]	$\sqrt{(t/hrs)}$	C [μM]				C^*	$1-C/C^*$
			#1	#2	#3	average		
2	0.0	0.2	77.5	114.6	126.0	106.0		
6	0.1	0.3	107.3	116.2	125.0	116.2		
9	0.2	0.4	113.4	115.7	118.3	115.8	0.99	0.01
12	0.2	0.4	115.4	115.0		115.2	0.99	0.01
29	0.5	0.7	113.8	112.8		113.3	0.98	0.02
47	0.8	0.9	111.2	111.6		111.4	0.96	0.04
76	1.3	1.1	110.1	112.0		111.1	0.96	0.04
95	1.6	1.3	108.5	107.4		107.9	0.93	0.07
140	2.3	1.5	103.2	104.1		103.7	0.89	0.11
247	4.1	2.0	102.5	102.5		102.5	0.89	0.11
392	6.5	2.6	101.1	101.3		101.2	0.87	0.13
460	7.7	2.8	97.6	99.2		98.4	0.85	0.15
1340	22.3	4.7	93.4	94.4		93.9	0.81	0.19
1455	24.3	4.9	95.0	93.0		94.0	0.81	0.19
1814	30.2	5.5	91.4	91.3		91.3	0.79	0.21
2775	46.3	6.8	88.3	90.5		89.4	0.77	0.23
3300	55.0	7.4	87.2	87.8		87.5	0.76	0.24
4640	77.3	8.8	84.6	86.1		85.4	0.74	0.26
7140	119.0	10.9	82.7	83.6		83.2	0.72	0.28
7310	121.8	11.0	78.9	80.5		79.7	0.69	0.31

Table B.3. Metal ion concentrations in pore water: Run 6 at 35 minutes.

Port	depth [cm]	C_{Zn} [μM]	C_{Li} [μM]	C/C_0 Zn	C/C_0 Li
M	0	19.4	146.0	0.95	0.97
N	-1	18.3	142.0	0.90	0.94
O	-2	11.0	147.0	0.54	0.97
P	-3	1.1	150.0	0.05	0.99
Q	-4	1.5	51.0	0.07	0.34
R	-5	0.9	4.8	0.04	0.03
S	-6	1.0	5.4	0.05	0.04
T	-7	0.8	5.2	0.04	0.03
U	-8	0.6	5.4	0.03	0.04
V	-9	0.7	5.5	0.03	0.04
W	-10	0.8	5.4	0.04	0.04
X	-11	0.9	5.2	0.04	0.03

Table B.4. Metal ion concentrations in pore water: Run 6 at 95 minutes.

Port	depth [cm]	C_{Zn} [μM]	C_{Li} [μM]	C/C_0 Zn	C/C_0 Li
M	0	17.4	153.0	0.89	0.93
N	-1	16.0	151.0	0.82	0.92
O	-2	13.1	158.8	0.67	0.96
P	-3	16.0	160.0	0.82	0.97
Q	-4	3.7	162.0	0.19	0.98
R	-5	1.0	164.0	0.05	1.00
S	-6	0.3	159.7	0.02	0.97
T	-7	0.1	38.9	0.01	0.24
U	-8	2.1	4.9	0.11	0.03
V	-9	0.1	5.1	0.01	0.03
W	-10	0.0	5.4	0.00	0.03
X	-11	0.4	5.2	0.02	0.03

Table B.5. Metal ion concentrations in pore water: Run 6 at 255 minutes.

Port	depth [cm]	C_{Zn} [μM]	C_{Li} [μM]	C/C_0 Zn	C/C_0 Li
M	0	15.0	150.0	0.80	0.89
N	-1	13.8	147.0	0.73	0.87
O	-2	16.5	157.0	0.88	0.93
P	-3	16.7	153.0	0.89	0.91
Q	-4	15.2	158.0	0.81	0.94
R	-5	10.4	154.0	0.55	0.91
S	-6	7.8	152.0	0.41	0.90
T	-7	1.1	150.0	0.06	0.89
U	-8	0.8	160.0	0.04	0.95
V	-9	0.2	164.0	0.01	0.97
W	-10	0.2	78.0	0.01	0.46
X	-11	0.1	17.3	0.01	0.10
Y	-12	0.2	5.4	0.01	0.03
Z	-13	0.0	5.1	0.00	0.03
ZA	-14	0.4	5.3	0.02	0.03
ZB	-15	0.9	4.7	0.05	0.03
ZC	-16	1.0	4.3	0.05	0.03

Table B.6. Metal ion concentrations in pore water: Run 6 at 26 hours.

Port	depth [cm]	C_{Zn} [μM]	C_{Li} [μM]	C/C_0 Zn	C/C_0 Li
M	0	11.0	135.7	0.54	0.83
N	-1	10.8	138.9	0.53	0.85
O	-2	10.2	135.0	0.50	0.83
P	-3	11.1	136.4	0.54	0.84
Q	-4	10.4	136.9	0.51	0.84
R	-5	10.6	135.0	0.52	0.83
S	-6	11.6	141.8	0.57	0.87
T	-7	10.9	142.0	0.53	0.87
U	-8	10.9	135.0	0.53	0.83
V	-9	9.2	150.0	0.45	0.92
W	-10	8.2	133.3	0.40	0.82
X	-11	6.7	148.0	0.33	0.91
Y	-12	2.5	141.0	0.12	0.87
Z	-13	0.7	142.0	0.03	0.87
ZA	-14	0.3	128.0	0.01	0.79
Z	-15	0.3	82.1	0.01	0.50
ZC	-16	0.3	15.0	0.02	0.09
ZD	-17	0.3	5.7	0.01	0.04
ZE	-18	0.4	4.9	0.02	0.03
ZF	-19	0.7	5.2	0.03	0.03
ZG	-20	2.0	5.7	0.10	0.04
ZH	-21	6.0	9.3	0.29	0.06

Table B.7. Metal ion concentrations in pore water: Run 6 at 51 hours.

Port	depth [cm]	C_{Zn} [μM]	C_{Li} [μM]	C/C_0 Zn	C/C_0 Li
M	0	8.6	123.0	0.37	0.77
N	-1	8.4	129.0	0.37	0.81
O	-2	8.0	129.0	0.35	0.81
P	-3	8.6	132.0	0.37	0.82
Q	-4	8.0	130.0	0.35	0.81
R	-5	7.8	129.0	0.34	0.81
S	-6	8.4	132.0	0.37	0.82
T	-7	8.6	130.0	0.37	0.81
U	-8	8.7	129.0	0.38	0.81
V	-9	8.5	125.0	0.37	0.78
W	-10	7.5	127.0	0.33	0.79
X	-11	9.0	126.0	0.39	0.79
Y	-12	7.2	135.0	0.31	0.84
Z	-13	5.5	135.0	0.24	0.84
ZA	-14	1.5	135.0	0.07	0.84
Z	-15	0.5	140.0	0.02	0.87
ZC	-16	0.5	136.0	0.02	0.85
ZD	-17	0.7	143.0	0.03	0.89
ZE	-18	1.0	144.0	0.04	0.90
ZF	-19	1.0	141.0	0.04	0.88
ZG	-20	1.2	115.0	0.05	0.72
ZH	-21	2.7	41.0	0.12	0.26

APPENDIX C: NONDIMENSIONAL RESIDENCE TIME FUNCTION

Table C.8. Nondimensional residence time function for sinusoidal pressure distribution, no underflow.

$\frac{t^*}{\theta R}$	$\bar{R}_f\left(\frac{t^*}{\theta R}\right)$	$-\frac{d\bar{R}_f\left(\frac{t^*}{\theta R}\right)}{d\left(\frac{t^*}{\theta R}\right)}$	$\frac{t^*}{\theta R}$	$\bar{R}_f\left(\frac{t^*}{\theta R}\right)$	$-\frac{d\bar{R}_f\left(\frac{t^*}{\theta R}\right)}{d\left(\frac{t^*}{\theta R}\right)}$	$\frac{t^*}{\theta R}$	$\bar{R}_f\left(\frac{t^*}{\theta R}\right)$	$-\frac{d\bar{R}_f\left(\frac{t^*}{\theta R}\right)}{d\left(\frac{t^*}{\theta R}\right)}$
0.1	0.999	$2.49\cdot10^{-2}$	3.8	0.532	$8.63\cdot10^{-2}$	40	$7.48\cdot10^{-2}$	$1.78\cdot10^{-3}$
0.2	0.995	$4.89\cdot10^{-2}$	4.0	0.515	$8.13\cdot10^{-2}$	50	$6.04\cdot10^{-2}$	$1.16\cdot10^{-3}$
0.3	0.989	$7.15\cdot10^{-2}$	4.4	0.484	$7.24\cdot10^{-2}$	60	$5.07\cdot10^{-2}$	$8.17\cdot10^{-4}$
0.4	0.981	$9.20\cdot10^{-2}$	4.8	0.457	$6.48\cdot10^{-2}$	70	$4.36\cdot10^{-2}$	$6.06\cdot10^{-4}$
0.5	0.971	0.110	5.2	0.432	$5.83\cdot10^{-2}$	80	$3.83\cdot10^{-2}$	$4.67\cdot10^{-4}$
0.6	0.959	0.125	5.6	0.410	$5.26\cdot10^{-2}$	90	$3.41\cdot10^{-2}$	$3.71\cdot10^{-4}$
0.7	0.946	0.138	6.0	0.390	$4.77\cdot10^{-2}$	100	$3.08\cdot10^{-2}$	$3.02\cdot10^{-4}$
0.8	0.931	0.148	6.5	0.368	$4.25\cdot10^{-2}$	125	$2.47\cdot10^{-2}$	$1.95\cdot10^{-4}$
0.9	0.916	0.156	7.0	0.347	$3.80\cdot10^{-2}$	150	$2.07\cdot10^{-2}$	$1.36\cdot10^{-4}$
1.0	0.900	0.161	7.5	0.329	$3.42\cdot10^{-2}$	175	$1.77\cdot10^{-2}$	$1.00\cdot10^{-4}$
1.2	0.868	0.166	8.0	0.313	$3.10\cdot10^{-2}$	200	$1.56\cdot10^{-2}$	$7.70\cdot10^{-5}$
1.4	0.834	0.166	8.5	0.298	$2.82\cdot10^{-2}$	250	$1.25\cdot10^{-2}$	$4.95\cdot10^{-5}$
1.6	0.801	0.162	9.0	0.285	$2.57\cdot10^{-2}$	300	$1.04\cdot10^{-2}$	$3.44\cdot10^{-5}$
1.8	0.770	0.156	9.5	0.273	$2.35\cdot10^{-2}$	350	$8.92\cdot10^{-3}$	$2.54\cdot10^{-5}$
2.0	0.739	0.149	10	0.261	$2.16\cdot10^{-2}$	400	$7.81\cdot10^{-3}$	$1.94\cdot10^{-5}$
2.2	0.710	0.141	12	0.224	$1.59\cdot10^{-2}$	450	$6.95\cdot10^{-3}$	$1.54\cdot10^{-5}$
2.4	0.683	0.133	14	0.196	$1.22\cdot10^{-2}$	500	$6.26\cdot10^{-3}$	$1.25\cdot10^{-5}$
2.6	0.657	0.125	16	0.174	$9.67\cdot10^{-3}$	600	$5.22\cdot10^{-3}$	$8.67\cdot10^{-6}$
2.8	0.633	0.118	18	0.157	$7.84\cdot10^{-3}$	700	$4.48\cdot10^{-3}$	$6.38\cdot10^{-6}$
3.0	0.610	0.110	20	0.143	$6.48\cdot10^{-3}$	800	$3.92\cdot10^{-3}$	$4.88\cdot10^{-6}$
3.2	0.588	0.104	25	0.116	$4.31\cdot10^{-3}$	900	$3.48\cdot10^{-3}$	$3.86\cdot10^{-6}$
3.4	0.568	$9.75\cdot10^{-2}$	30	$9.82\cdot10^{-2}$	$3.07\cdot10^{-3}$	1000	$3.14\cdot10^{-3}$	$3.13\cdot10^{-6}$
3.6	0.549	$9.17\cdot10^{-2}$	35	$8.49\cdot10^{-2}$	$2.29\cdot10^{-3}$	8000	$3.93\cdot10^{-4}$	$4.91\cdot10^{-8}$